



UNIVERSITÀ DI PARMA

Dipartimento di Ingegneria e Architettura (DIA)

Corso di Laurea Magistrale in Ingegneria Civile

Fractiles Based Sampling Procedure: a new probabilistic approach to evaluate the design resistance of a structural element

Procedura di campionamento basata sui frattili: un nuovo approccio probabilistico per valutare la resistenza di progetto di un elemento strutturale

Relatore:

Prof.ssa Ing. Beatrice Belletti

Correlatori:

Prof. Ing. Alfred Strauss (Boku University, Vienna)

Ing. Francesca Vecchi

Laureando:

Mattia Pancrazio Cosma

A.A. 2017/2018

Do something, that people say, you will not be able to do
[M.P- Cosma]

RINGRAZIAMENTI

Sarò banale, ma le prime persone che mi sento di ringraziare sono i miei genitori, la mia mamma ed il mio papà. Sino ad oggi, non mi hanno mai voltato le spalle e credendo sempre in me, hanno coltivato in ogni modo la passione che nutro per lo studio, per la ricerca e per la voglia di scoprire cose nuove, consentendomi di raggiungere obiettivi molto importanti, come questo ed altri traguardi.

Grazie papà, per avermi insegnato sin da piccolo cosa significa sacrificio e lavoro; grazie a ciò, possiedo ora uno spiccato senso del dovere che mi aiuta ogni giorno a fare un passo in più.

Un ringraziamento va anche a mio fratello, il quale nonostante il rapporto amore/odio, fa quello che dico.

Infine, per completare il quadro familiare, non posso che dire grazie alla mia cagnolina, anche se non potrà leggere; entrata nella mia vita tre anni fa, è stata in grado di aumentare la mia sensibilità verso il genere umano e forse placare i miei animi ribelli. Nel lungo periodo senza di lei, mi sono sentito perso.

Un sentito ringraziamento va alla Prof.ssa Belletti, che grazie alle sue conoscenze internazionali mi ha dato l'opportunità di vivere un'esperienza indimenticabile, che segnerà il resto della mia vita.

Grazie ad Alfred ed a tutto il personale della Boku University di Vienna, che mi ha accolto calorosamente. Un enorme ringraziamento a Francesca, prima dottoranda, poi amica sempre pronta a tirarti fuori dai momenti più bui. A lei va un grosso in bocca al lupo per la sua futura carriera.

Grazie agli amici di una vita, Angelo, Ciro, Marini, Carmine, Biddo sempre pronti a regalare momenti di spensieratezza. Grazie anche ai "Mamma la capu", vicini nonostante la lontananza ed a tutte le persone che nonostante gli anni, continuano a starmi vicine, come Vanessa.

Grazie a tutte le splendide amicizie che sono nate nel piccolo mondo universitario. Grazie agli amici del "Caro Pampanin", Tommaso, Stefano e Nicola con cui ho pienamente condiviso questi ultimi momenti.

Grazie a Genna, amico d'infanzia, che non mi ha mai abbandonato, grazie a Paolo & Sabina ed a tutto lo staff della Pizzeria "La Vela", dove ho avuto il piacere di lavorare in questi ultimi due anni e dove sono nate bellissime amicizie come quelle con Roberta & Raffaella.

Grazie a Barbara, ormai diventata una seconda mamma, ed a tutta la tifoseria della Junior Pallavicino.

Grazie a te, che andata via così presto, non hai avuto modo di vedere tutto questo; sono sicuro che saresti stata fiera di me.

This page is intentionally left white

SUMMARY

1. INTRODUCTION	7
1.1. Levels of approximation	8
1.2. Safety Formats	9
1.2.1. Partial Safety Factor Format (PSF).....	10
1.2.2. Probabilistic Safety Format.....	12
1.2.2.1. Estimation Of Coefficient Of Variation (ECOV)	12
1.2.2.2. Aim of this work: Fractiles Based Sampling Procedure	15
1.3. Work organization.....	16
2. EXPERIMENTAL TESTS FOR STOCHATISTIC MODEL DEVELOPMENT	18
2.1. Compressive Test.....	19
2.2. Three-point bending fracture tests	19
2.2.1. Statistical mechanical parameters values.....	21
3. SIMULATION TECHNIQUES.....	22
3.1. PARC	22
3.1.1. Basic Hypotheses	23
3.1.2. Strain Field for Concrete.....	23
3.1.3. Strain Field for Steel	24
3.1.4. Cyclic Uniaxial Constitutive Relationship of Concrete	25
3.1.5. Cyclic Uniaxial Constitutive of Embedded mild steel bars	26
3.1.6. Tension-stiffening by Model Code 2010	27
3.1.7. PARC CL 2.0	29
4. CASE STUDY MODEL.....	30
4.1. Experimental test and check of the model prediction	32
5. FULLY PROBABILISTIC APPROACH.....	34
5.1. Basic Probabilistic Concepts and main Probability Distribution Functions	36
5.1.1. Normal Distribution	37
5.1.2. Log-Normal Distribution	38
5.1.3. Gumbel Distribution	39
5.2. Monte Carlo type simulation.....	42
5.3. Latin Hyperbolic Sampling.....	43
5.3.1. FReET Software.....	47
5.3.2. Design Resistances Evaluation	51
5.3.2.1. Log-Normal design resistance at Peak Load.....	53
5.3.2.2. Log-Normal design resistance at various fixed displacement	53
5.3.2.3. Log-Normal design resistance at 2.5% stirrups deformation reached	54
6. FRACTILES BASED SAMPLING PROCEDURE.....	57

6.1. Validation of the Leading Parameter	58
6.1.1. Validation based on Input-Output Comparison	58
6.1.2. Validation based on sensitivity analyses.....	61
6.1.2.1. Load Levels definition	65
6.1.2.2. Sensitivity studies in deformation and load capacities	68
6.1.2.3. Sensitivity studies in crack pattern developments	72
6.1.3. Validation based on Target Correlation Matrix	82
6.1.4. Validation based on FBSP	84
6.1.4.1. Compressive strength leading parameter	84
6.1.4.2. Tensile strength leading parameter	86
6.1.4.3. Fracture energy leading parameter.....	88
7. COMPARISON	93
8. FBSP BASED ON MODEL CODE INFORMATION	95
8.1. Compressive strength leading parameter	95
8.1.1. PDF of mechanical parameters comparison.....	97
8.2. Tensile strength leading parameter	99
8.2.1. PDF of mechanical parameters comparison.....	100
8.3. Fracture energy leading parameter.....	103
9. APPENDIX: PROBABILISTIC STRUCTURAL RESPONSES OF DIFFERENT RC PANELS	105
9.1. Model and failure mechanism prediction with real experimental mechanical parameters...	108
9.2. Failure mechanism prediction with new mechanical parameters values	113
9.3. Probabilistic structural responses	118
9.3.1. Fully Probabilistic	118
9.3.2. Fractiles Based Sampling Procedure.....	120
9.3.2.1. CA2 panel	121
9.3.2.2. CA4 panel	123
9.3.2.3. CB4 panel.....	125
9.3.3. Probabilistic structural responses by using different aggregate interlocking models....	127
10. CONCLUSION.....	131
11. REFERENCES.....	134

1. INTRODUCTION

Engineering systems, components and devices are not perfect. A perfect design is something remaining operational and reaches the objective of the system without failure during a preselected life, i.e. it represents the deterministic view of an engineering system. This is an ideal, impractical, and economically infeasible view. Even if technical knowledge is not a limiting factor in designing, manufacturing, constructing and operating the final system, the cost of development, testing, materials and engineering analysis may far exceed economic prospects for such a system. Therefore, practical and economical limitations dictate the use of not-so-perfect designs. However, designers, manufacturers and end users, try to minimize the occurrence and recurrence of failures. The failure of a general engineering system or in this specific case of a structural element is related to the presence of uncertainties, which in the analysis and design of these systems has always been recognized. Uncertainties are involved in every part of the system: structure, load, environment and material parameters. Values such as the resistance of the materials or the magnitude of the applied loads could be different from the assigned values during the design of the system. Specifically, the following types of uncertainties can be identified in general:

- natural randomness of actions, material properties and geometric data;
- statistical uncertainties provided by a limited size of available data;
- inadequacy of the adopted structural model due to simplifications of the real conditions;
- human error in design or construction;

As it is known, the design of a structure essentially involves two phases; in the first phase, the evaluation of the stress state (internal action) which occurs in the structural element should be evaluated; in this phase, uncertainties related to the external loads come into play. In the second phase, the resistance of the structural element should be evaluated; herein uncertainties related to the mechanical resistance of the materials come into play. Finally, the design is completed by demonstrating that the design resistance is greater than the external loads. This work is focused on the evaluation of the design resistance, therefore only uncertainties related to the materials were investigated.

Traditional approaches simplify the problem by considering the uncertain parameters to be deterministic and take into account them through the use of partial safety factors in the limit states. Such approaches do not guarantee the required reliability and do not provide information on the influence of each parameter. Specifically, with this approach the designer could state that the structure is safe but it is not known how the level of safety reached.

1.1. Levels of approximation

With the aim to evaluate the design resistance of a structural element, different type of analyses could be performed. All these analyses are approximations of the reality, with different levels of accuracy. A Levels-of-Approximation (LoA) approach is a design strategy where the accuracy of the behavior estimation of a structural element response could be, if necessary, progressively refined through a better estimate of the physical parameters involved in the design equations or in the model ([11],[14]). The LoA approach is based on the use of rational theories that are based on physical models. Both behavior and strength of structural element are characterized through a series of parameters and a set of design equations. The parameters may be physical variables (such as crack widths), mechanical properties (such as tensile compressive strength) or geometrical parameters (such as the width of a beam).

*This figure is not available.
Please contact the Author.*

Figure 1. Different LoA

The difference occurring in the context of application of different LoA is clearly explained in the Figure 1. Changing from a low LoA to an high LoA, there is both an increase of accuracy in the evaluation of the behavior of a structural element (or in the estimate of a design resistance) and an increase of time devoted to analysis.

The first LoA has to provide simple and safe hypotheses for evaluating the physical parameters of design equations. It leads to safe (yet realistic) values of the behavior and strength of the structural element; this approach is usually sufficient only for preliminary design.

For higher LoA (II or III), the physical parameters of design equations are typically evaluated through simplified analytical formulas accounting for the internal forces and other geometrical and mechanical parameters. These LoA are still low time-consuming and are usually sufficient to cover most design cases.

Finally, in the best LoA are including the new numerical approaches that were developed during the recent years. These methods, known commonly as Finite Element Analysis leads to results closer to the reality.

In this work only the best LoA was applied to evaluate the design resistance; the demonstration that this one leads to higher value of design resistance is widely known in the literature, so this is not an aim of this work.

For each of this approach, regulations ([12],[13]) provide different methods with which uncertainties could be taken into account. The way in which uncertainties are taken into account, define a specific safety format.

1.2. Safety Formats

Within the LoA shown above, different safety formats are provided by the codes to evaluate the design resistance of a structural element, or more in general, of an entire engineering system. In this work, the following Safety Formats are taken into account:

- Partial Safety Factor (PSF);
- Probabilistic Safety Format;

1.2.1. Partial Safety Factor Format (PSF)

According to this method, the basic variables are deterministic quantities. In this way, this method takes into account uncertainties and variabilities originating from various causes, by using safety coefficients.

According to PSF, to evaluate the design resistance of a structural element (by using the best LoA), only one NLFEA should be led. Design mechanical properties of materials, derived from the characteristic mechanical properties, were used to lead the analysis. According to Model Code 2010 (fib,2013) the design mechanical properties are calculated as shown in the following equations.

$$f_{cd} = \frac{f_{ck}}{\gamma_{rd} \cdot \gamma_c} \quad (1)$$

where the characteristic concrete compressive strength was obtained by subtracting 8 MPa to the mean compressive strength estimated by laboratory tests.

The other concrete mechanical parameters (fracture energy, elastic modulus and tensile strength) were evaluated by using the correlation between concrete mechanical parameters, provided by Model Code 2010 (fib,2013).

$$f_{ctd} = \frac{0.7 \cdot \left[2.12 \cdot \ln(1 + 0.1 \cdot (f_{cm})) \right]}{\gamma_{rd} \cdot \gamma_c} \quad (2)$$

where the term in square brackets represent the mean value of the concrete tensile strength which multiplied for 0.7 leads to the characteristic concrete tensile strength.

$$G_f = \frac{73 \cdot f_{cd}^{0.18}}{\sqrt{2}} \quad (3)$$

$$E_c = 21500 \cdot \left(\frac{f_{cd}}{10} \right)^{1/3} \quad (4)$$

In the Eq.(1)-(2) γ_{rd} is the model uncertainty coefficient equal to 1.06, γ_c is the concrete partial safety coefficient equal to 1.5.

In the same way for the steel mechanical parameters (and also for tendons mechanical parameters):

$$f_{yd} = \frac{f_{yk}}{\gamma_{rd} \cdot \gamma_s} \quad (5)$$

where γ_s is the steel partial safety coefficient equal to 1.15.

The ultimate load R_u obtained from the analysis by inputting the design mechanical properties is already the design resistance R_d .

Notice that to verify the girder (for example the shear resistance), from this load should be evaluated the shear value (known the static scheme of the girder) and make a comparison between this load with the real applied load. This work is left to the designer; here is meant such design resistance of the girder the ultimate point load applied to the girder.

1.2.2. Probabilistic Safety Format

The main objective of a reliability analysis by using the probabilistic approach is a probabilistic assessment of the safety of the structure by estimating the failure probability (or the reliability index β). More in general, fixing the reliability index, the design resistance (such as the shear resistance of a girder) could be evaluated. How a probabilistic safety formats works, will be shown in the §5.

At this time, is important to highlight the difference between the probabilistic safety formats that are available. The application of the probabilistic safety format in its exact formulation (better known such as Fully Probabilistic) could be led by using:

- Monte-Carlo type simulation;
- Latin Hyperbolic Sampling;

Nowadays, codes provide an alternative simplified method to the Fully Probabilistic (FP), known as Estimation Of Coefficient Of Variation (ECOV, see §1.2.2.1).

1.2.2.1. Estimation Of Coefficient Of Variation (ECOV)

According to this method two non-linear analyses have been performed by inputting mean and characteristic mechanical properties of materials even if in the context of ECOV ([10]) application is not clearly how these mechanical parameters can be evaluated; a reasonable choose (commonly designer's choice) could be evaluate the mechanical concrete parameters (mean and characteristic) starting from the mean value of compressive strength and by using Model Code 2010 (*fib, 2013*) correlations but without the application of uncertainty coefficient or partial safety one. By using Eq.(6) the design resistance R_d is then calculated.

$$R_d = \frac{R_{u,m}}{\gamma_{rd} \cdot \gamma_r} \quad (6)$$

Where $R_{u,m}$ is the ultimate load obtained from the analysis by inputting mean mechanical properties, γ_{rd} is the model uncertainty coefficient equal to 1.06 and γ_r is calculated as reported in Eq.(7).

$$\gamma_{rd} = e^{\alpha_r \cdot \beta \cdot V_r} \quad (7)$$

By adopting a sensitivity index $\alpha_R = 0.8$ and a reliability index equal to 3.8.

According to this method, the coefficient of variation is evaluated by using Eq.(8).

$$V_r = \frac{1}{1.65} \ln\left(\frac{R_{u,m}}{R_{u,c}}\right) \quad (8)$$

where $R_{u,c}$ is the ultimate load obtained from the analysis by inputting characteristic mechanical properties.

Analysis with mean mechanical parameter	
Compressive strength	f_{cm}
Tensile strength	$f_{ctm} = \left[2.12 \cdot \ln(1 + 0.1 \cdot (f_{cm})) \right]$
Fracture energy	$G_{fm} = \frac{73 \cdot f_{cm}^{0.18}}{\sqrt{2}}$
Elastic modulus	$E_c = 21500 \cdot \left(\frac{f_{cm}}{10} \right)^{1/3}$
Analysis with characteristic mechanical parameter	
Compressive strength	$f_{ck} = f_{cm} - 8$
Tensile strength	$f_{ctk} = 0.7 \cdot \left[2.12 \cdot \ln(1 + 0.1 \cdot (f_{cm})) \right]$
Fracture energy	$G_f = \frac{73 \cdot f_{ck}^{0.18}}{\sqrt{2}}$
Elastic modulus	$E_c = 21500 \cdot \left(\frac{f_{ck}}{10} \right)^{1/3}$

Notice that the values of the mechanical parameters were evaluated as shown in §1.2.1 but without applying the partial safety coefficients.

For steel and tendons mechanical parameters, the characteristic value could be obtained by multiplying the mean value for a coefficient which was obtained by experimental test (0.9-0.92).

1.2.2.2. Aim of this work: Fractiles Based Sampling Procedure

In this work another simplified probabilistic method to evaluate the design resistance of a structural element will be proposed. The new method, called “Fractiles Based Sampling Procedure (FBSP)” will be widely explained in §6.

The reason of the new proposal and a comparison with the above mentioned formats will be shown in this work. To better explain the state of art and the goal of this work a flowchart is shown in Figure 2.

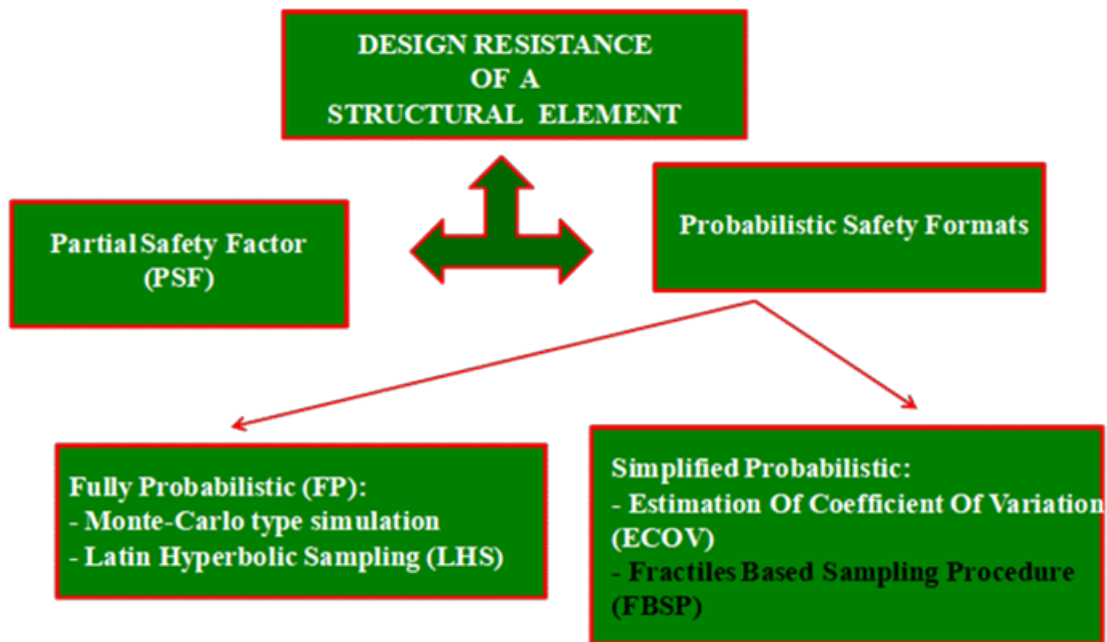


Figure 2. State of art and goal of this work

1.3. Work organization

This work is focused on the evaluation of the design resistance of a T-shaped prestressed concrete girder (see §4), by adopting different safety formats method. Specifically, the main goal of this work, is developing a new simplified probabilistic method to evaluate the design resistance of a structural element (Fractiles Based Sampling Procedure, FBSP). Contents of this work are arranged as follows:

- In §2 the experimental tests led with the aim to obtain statistical mechanical parameters values, required to the develop of the probabilistic safety method, are discussed. Therefore, mean values, standard deviations and model of probability function for concrete, steel and tendons mechanical parameters were estimated. These tests have been led at the Faculty of Civil Engineering, Brno University of Technology, Czech Republic in cooperation with BOKU University, Vienna and Austrian company Franz Oberndorfer GmbH & Co KG.
- In §3 the adopted simulation technique is illustrated. Specifically, this topic is focused on the description of the non-linear model (PARC) developed at the University of Parma, to take into account the non-linear behavior of the RC structures.
- In §4 a briefly explanation of the case study adopted to explain and demonstrate the application of FBSP is shown; herein the numerical model of the T-shaped girder, developed by using Abaqus software (authors give thanks to Dassault Systems for the granting license) is also presented.
- In §5 is reported a view on the probabilistic safety formats that are available; in particular, a focus on the fully probabilistic approach is made in this chapter. A briefly story of the Monte-Carlo type simulation is presented and the application of Latin Hyperbolic Sampling, whose results lead to the FBSP, is developed;
- In §6 is widely shown the new method proposed in this work. Starting from the definition of the leading parameter, central pint of this method, different studies are presented with the aim to evaluate which is the best leading parameter.

- In §7 a comparison between the design resistance obtained by FBSP and the same design resistance obtained by the other methods provided by codes and illustrated in §1 is shown.
- In §8 a modified application of FBSP is proposed; the application of this procedure could be usefully when few statistical values of the mechanical parameters are available. In the context of modified FBSP application, correlations between mechanical parameters reported in Model Code 2010 (fib,2013) were used. As it will be shown, from this application, were obtained surprising results;
- In §9 a probabilistic study on different RC panels is proposed; aim of this topic will be shown how the importance of mechanical parameter could change by changing the failure mechanism of the structural element.

2. EXPERIMENTAL TESTS FOR STOCHATISTIC MODEL DEVELOPMENT

As it will be shown in §5, the develop of a stochastic model requires the knowledge of probabilistic values of the material properties. Therefore, for each material property useful to describe the engineering system (basic variable), probability density function (PDF), mean value and covariance should be known. Specifically, the basic variables adopted to correctly develop the stochastic model shown in this work are: f_c = compressive strength of the concrete; f_t = tensile strength of the concrete; E_c = elastic modulus of concrete; G_f = fracture energy in tension of the concrete; E_s = elastic modulus of steel; f_{ys} = yielding stress of steel; f_{yt} = yielding stress of tendons; E_s = elastic modulus of tendons; P = precompression force of tendons.

While the definition of the probabilistic mechanical properties of steel (ductile material) is something which could be easily pursued, the same is not true regarding the definition of the probabilistic mechanical properties of concrete, which is a brittle material. Recent years have seen a significant increase in interest in the formulation of inverse methods to determine the quasi-brittle fracture behavior of concrete. Basically, two groups of inverse analysis techniques exist [2]:

- a) those that use the complete load-displacement diagram of one specimen size and shape;
- b) those that use the peak loads of specimens of various sizes and shapes;

In this topic experimental tests led to obtain probabilistic values of the concrete mechanical properties will be presented. In particular, the standardized compression test and the standardized three-point bending test of notched specimens were performed in the course of these investigations.

2.1. Compressive Test

A number equal to 160 cubic specimens with standard size were tested in accordance with EN12390-3 at Faculty of Civil Engineering, Brno University of Technology, Czech Republic in cooperation with IKI BOKU University, Vienna and Austrian company Franz Oberndorfer GmbH & Co KG. Statistical mechanical parameters of the compressive strength were evaluated by assessing *via* statistical consideration results obtained by all the 160 specimens and checked with a complex procedure, called Inverse Analysis ([31], [35]).

2.2. Three-point bending fracture tests

One of the typical tests for obtaining materials parameters, and the fracture parameters in particular, is the fracture test of specimens with a central edge notch in a three-point bending configuration (see Figure 3). The test results provide more than just the basic mechanical parameters such as modulus of elasticity; they also deliver fracture parameters that describe the behavior of the material during a fracture process as well as its crack propagation resistivity. Such parameters include the effective crack elongation, the effective fracture toughness, the effective toughness and the specific fracture energy. The volume density of the tested material can be also evaluated. As a by-product (by using broken parts), compressive strength values are obtained from compression tests of broken parts of specimens tested in bending.

*This figure is not available.
Please contact the Author.*

Figure 3. Three-point bending fracture tests

Beam specimens for the three-point bending tests were prepared with original dimensions of $120 \times 120 \times 360$ mm and were cast, cured and stored under conditions identical to those of the compression tests. With the aim to obtain good statistical evaluation parameters before testing, all original beams were bisected lengthwise, thus, the number of tested specimens was increased. As a result, 28 specimens with nominal dimensions of $58 \times 120 \times 360$ mm were tested. It should be noted that the modified size is not a standard specimen dimension.

Each specimen was provided with a central edge notch about 40 mm deep ($1/3$ the depth of the specimen). Each specimen was loaded continuously with a constant displacement increment (about 0.1 mm/min) in the centre of the span. Mid-span deflection was recorded using inductive sensors with an accuracy of 0.001 mm. Essential for the deflection measurement is the elimination of

deflection caused by the settlement of specimens at their supports, which may lead to less reliable measured data. The measurement result took the form of a load vs. mid-span deflection diagram (l - d diagram) which included both pre- and post-peak branches. The main target of the three-point bending fracture tests was to determine experimentally the variability of the fracture energy G_f .

The fracture energy G_f is obtained by integrating the function load vs. mid-span deflection (l - d diagram, Figure 4). Once evaluated the fracture energy for each specimen, with the well known statistical equations, mean value and standard deviation were assessed and the PDF was chosen by fitting the experimental tests (see Figure 16).

*This figure is not available.
Please contact the Author.*

Figure 4. Example of l - d diagram obtained by three-point bending test led on different specimens

2.2.1. Statistical mechanical parameters values

As shown in the above paragraphs, statistical concrete mechanical parameters were evaluated; with the same approach, steel and tendons mechanical parameters have been assessed. Results of the extended campaign test are shown in Table 1, for all the basic variables describing the engineering system shown in §4.

Table 1. Experimental mechanical parameters values.

Symbol	Mean	Cov[%]	PDF	Unit
Concrete mix (C50/60 B4 – 28 Days)				
f_c	77	16.4	GMB min EVI	MPa
f_t	3.9	20.6	GMB max EVI	MPa
E_c	34.8	20.6	WBL min(3par)	GPa
G_f	219.8	32.8	GMB max EVI	Jm ⁻²
Steel reinforcement (BSt 550B), Multilinear diagram				
E_s	200	2	Normal	GPa
f_{ys}	610	4	Normal	MPa
Tendons (Cables – St1570/1770), Bilinear with hardening				
E_t	195	2.5	Normal	GPa
f_{yt}	1670	2	Normal	MPa
Prestressing force				
P	0.0418	6	Normal	MN

3. SIMULATION TECHNIQUES

The development of FBSP, as it will be shown, is based on the FP results; specifically, application of the method is shown and demonstrated on a case study presented in §4. All the NLFEA led in this work were carried out by using Abaqus Software coupled with PARC_CL_2.0 (Belletti et al. 2017), a fixed cracked model developed at the University of Parma and implemented in Abaqus user subroutine UMAT, for which is able to take into account the non-linear behavior of reinforced concrete.

3.1. PARC

Describing the structure as an assembly of elements, subject to plane stress strain (such as, for example, the finite element membranes or multilayer "shell"), the behavior of reinforced concrete structures can be analyzed by non-linear analysis to finite elements. Today, this type of non-linear finite element analysis (NLFEA), is emerging as an alternative method for analytical calculation. While maintaining the same levels of security guaranteed by the latter, the non-linear simulations must be followed by appropriate checks of reliability of the results obtained. The choices made in the modeling field, such as the type and size of finite elements, the mechanical model chosen in order to consider the phenomena of inelastic or cracking phenomena, the type of constitutive law, and much more, greatly influence the results of the non-linear finite element analysis.

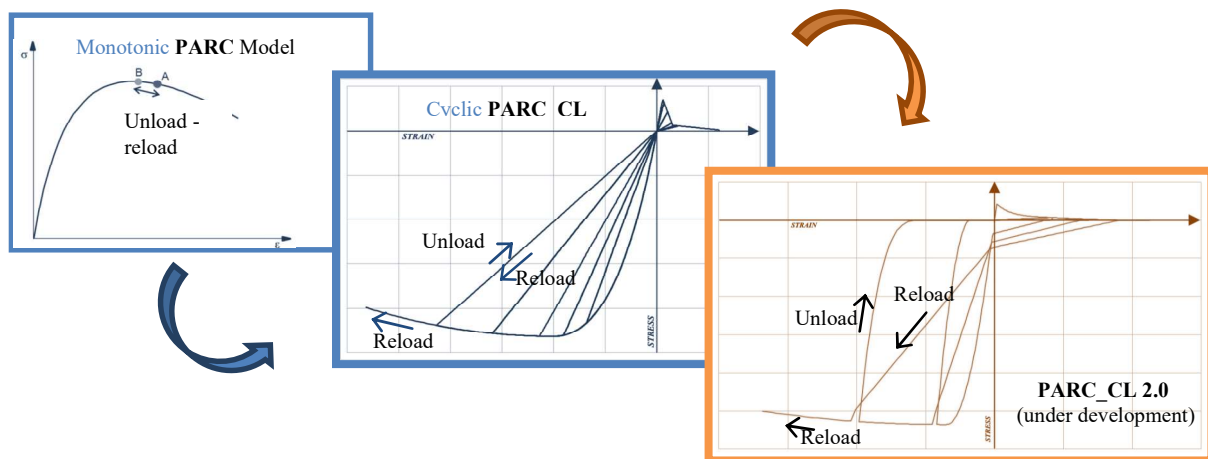


Figure 5. PARC evolution

For the study of the structural response of various types of construction, at the University of Parma, was proposed a model for the cracking loads monotonous, known as PARC, later extended in order to analyze structures subjected to cyclic loading-unloading-reloading secant (PARC_CL 1.0), as shown in Figure 5 . The reasons that led authors to the formulation of this new model derived from the observation that even in a structure subjected to monotonic loads, due to the redistribution of internal actions, the state of stress can take a cyclical pattern (think for example to the phenomenon of cracks opening and closing). The model provides a discharge PARC_CL 1.0 secant source and the cycles of loading / unloading, as expected, do not allow the passage from a state of traction to compression and vice versa.

Therefore this model, doesn't take into account to the component of irreversible plastic deformation in the structure when it is subjected to cyclical stress, does not lend itself to an accurate and realistic modeling. The search for a realistic modeling for structures subjected to seismic actions, leading to the need, for more complex models, in order to conduct nonlinear dynamic analyses. Therefore, in the present work, the model PAR_CL 2.0 has been used to conduct the analyses.

3.1.1. Basic Hypotheses

The proposed PARC_CL 2.0 model is based on a total strain fixed crack approach, in which at each integration point two reference systems are defined: the local x,y -coordinate system and the $1,2$ -coordinate system along the principal stress directions. The angle between the 1 -direction and the x -direction is denoted as ψ , whereas θ_i is the angle between the direction of the i th order of the bar and the x -direction. When the value of the principal tensile strain in concrete exceeds the concrete tensile limit strain $\varepsilon_{t,cr}$, for the first time, the first crack is formed, and for following loading stages, the $1,2$ -coordinate system is fixed. The crack spacing a_m is assumed as being constant, and its evaluation is conducted by “a priori” methods based on the transmission length l_t (Model Code 2010).

3.1.2. Strain Field for Concrete

The concrete behavior is assumed orthotropic both before and after cracking and the total strains at each integration point are calculated in the orthotropic $1,2$ -system:

$$\{\varepsilon_{1,2}\} = [T_\varepsilon(\psi)]\{\varepsilon_{x,y}\} \quad (8)$$

Where $[T_\varepsilon]$ is the transformation matrix and:

$$\{\varepsilon_{1,2}\} = \{\varepsilon_1 \quad \varepsilon_2 \quad \gamma_{12}\}^t \quad (9)$$

$$\{\varepsilon_{x,y}\} = \{\varepsilon_x \quad \varepsilon_y \quad \gamma_{xy}\}^t \quad (10)$$

where ε_x and ε_y are the normal strains in the x,y -directions and is the shear strain in the x,y -coordinates. ε_1 and ε_2 are the strains in the $1,2$ -direction, respectively, when a panel is subjected to biaxial loading and taking into account the Poisson ratio ν .

The uniaxial strains in the $1,2$ -coordinate system can be written as:

$$\bar{\varepsilon}_1 = \frac{1}{1-\nu^2} \varepsilon_1 + \frac{\nu}{1-\nu^2} \varepsilon_2 \quad (11)$$

$$\bar{\varepsilon}_2 = \frac{\nu}{1-\nu^2} \varepsilon_1 + \frac{1}{1-\nu^2} \varepsilon_2 \quad (12)$$

$$\bar{\gamma}_{12} = \gamma_{12} \quad (13)$$

When, after the first crack the Poisson's ratio is assumed to be zero, in (11) and (12), the biaxial strains are the same as the uniaxial strains.

3.1.3. Strain Field for Steel

The reinforcement is assumed smeared in concrete. Rotating the uniaxial strains of the concrete, in the $1,2$ -system, it is possible to obtain the uniaxial strains along each steel bars, as follow:

$$\bar{\varepsilon}_{x-i} = \bar{\varepsilon}_1 \cos^2 \alpha_i + \bar{\varepsilon}_2 \sin^2 \alpha_i - \bar{\gamma}_{12} \cos \alpha_i \sin \alpha_i \quad (14)$$

3.1.4. Cyclic Uniaxial Constitutive Relationship of Concrete

The uniaxial curves for concrete, are obtained substituting the uniaxial strains $\bar{\epsilon}$ in Eq.(15) for tension and in Eq.(16) for compression (according to [18]).

Tension:

$$\sigma = \begin{cases} E_c \cdot \bar{\epsilon} & 0 \leq \bar{\epsilon} < \epsilon_{t,el} \\ 0.9 \cdot f_t + 0.1 \cdot f_t \left(\frac{\bar{\epsilon} - \epsilon_{t,el}}{\epsilon_{t,cr} - \epsilon_{t,el}} \right) & \epsilon_{t,el} \leq \bar{\epsilon} < \epsilon_{t,cr} \\ f_t \left\{ \left[1 + \left(c_1 \cdot \frac{\bar{\epsilon} - \epsilon_{t,cr}}{\epsilon_{t,u}} \right)^3 \right] \cdot \exp \left(-c_2 \cdot \frac{\bar{\epsilon} - \epsilon_{t,cr}}{\epsilon_{t,u}} \right) - \frac{\bar{\epsilon} - \epsilon_{t,cr}}{\epsilon_{t,u}} \cdot (1 + c_1^3) \cdot \exp(-c_2) \right\} & \epsilon_{t,cr} \leq \bar{\epsilon} < \epsilon_{t,u} \\ 0 & \bar{\epsilon} \geq \epsilon_{t,u} \end{cases} \quad (15)$$

Compression:

$$\sigma = \begin{cases} E_c \cdot \bar{\epsilon} & \epsilon_{c,el} < \bar{\epsilon} \leq 0 \\ \frac{f'_c}{3} \cdot \left[1 + 4 \left(\frac{\bar{\epsilon} - \epsilon_{c,el}}{\epsilon_{c,cr} - \epsilon_{c,el}} \right) - 2 \left(\frac{\bar{\epsilon} - \epsilon_{c,el}}{\epsilon_{c,cr} - \epsilon_{c,el}} \right)^2 \right] & \epsilon_{c,crl} < \bar{\epsilon} < \epsilon_{c,el} \\ \frac{f'_c}{3} \cdot \left[1 - \left(\frac{\bar{\epsilon} - \epsilon_{c,cr}}{\epsilon_{c,u} - \epsilon_{c,cr}} \right)^2 \right] & \epsilon_{c,u} < \bar{\epsilon} < \epsilon_{c,cr} \\ 0 & \bar{\epsilon} \leq \epsilon_{c,u} \end{cases} \quad (16)$$

where:

$$\begin{aligned} \epsilon_{t,el} &= 0.9 \cdot f_t / E_c & \epsilon_{c,el} &= f'_c / (3 \cdot E_c) & \epsilon_{t,u} &= 5.136 \frac{G_F}{a_m \cdot f_t} & \epsilon_{c,u} &= \epsilon_{c,cr} - 1.5 \cdot \frac{G_c}{a_m \cdot f_c} \\ \epsilon_{t,cr} &= 0.00015 & \epsilon_{c,cr} &= 5 \cdot \epsilon_{c,el} & c_1 &= 3 & c_2 &= 6.93 \end{aligned}$$

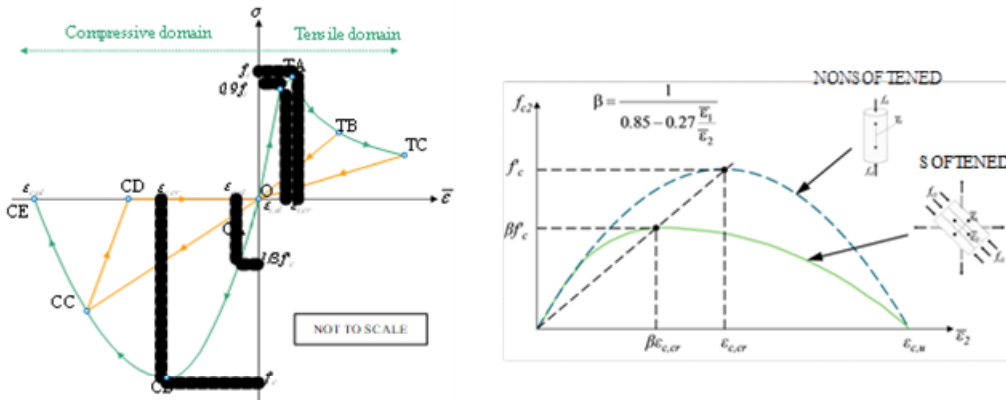


Figure 6. Concrete behavior

The value of G_F represents the fracture energy of concrete in tension and can be evaluated according to [11], while G_C represents the fracture energy of concrete in compression. The ratio between the fracture energy of concrete in compression and in tension is assumed equal to 250 according to [28]. Tension stiffening effect has not been taken into account in the model. The biaxial state of concrete in compression, due to transverse cracking, is also taken into account using the formulation proposed in [40]. Concrete-to-concrete interface phenomena are taken into account according to Gambarova's relation [15]. Gambarova's relation can be schematized with a bilinear curve, as in Figure 7.a, where the maximum value of the shear stress, τ^* is evaluated on the basis of the crack opening, w , and the crack sliding, v :

$$\tau^* = \bar{\tau} \left(1 - \sqrt{\frac{2w}{d_{\max}}} \right) \frac{a_3 + a_4 |v^*/w|^3}{1 + a_4 (v^*/w)^4} \frac{1}{w} v^* \quad (17)$$

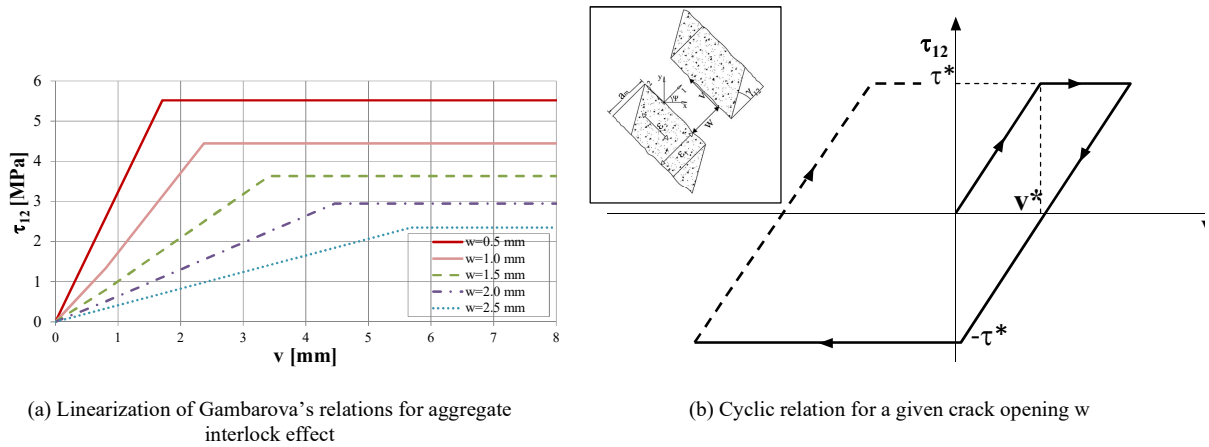


Figure 7. Implemented Gambarovova's model

where $\bar{\tau} = 0.27f'_c$; $v^* = f'_c w / a_5 + a_6$; $a_3 = 2.45 / \bar{\tau}$; $a_4 = 2.44(1 - 4 / \bar{\tau})$; $a_5 = 0.366f'_c + 3.333$; $a_6 = f'_c / 110$ and d_{\max} is the maximum aggregate diameter. The Gambarova's relation is extended to obtain a cyclic curve: it is assumed that the unloading path has the same stiffness of the initial path Figure 7.b. The aggregate interlock effect is neglected for crack opening values higher than half the maximum aggregate diameter d_{\max} .

3.1.5. Cyclic Uniaxial Constitutive of Embedded mild steel bars

The Menegotto-Pinto model [26] is employed in this study to represent the hysteretic stress-strain behavior of reinforcing steel. The proposed model takes into account the bars yielding, strain hardening branch, Bauschinger effect and the elastic modulus degradation under load reversal. The

benefits of such relationship are related to the simplicity of formulation and the possibility of considering residual plastic strains during load cycles, Figure 7. A curved transition from a straight line asymptote with slope E_0 to another asymptote with slope E_1 is shown in Eq.(18). The stress σ_0 and the strain ε_0 defined the intersection point of the two asymptotes of the branch considered (point A in Figure 8). Similarly, σ_r and ε_r are the stress and strain at the point where the unloading branch begins (point B in Figure 8). As shown in Figure 8 $(\sigma_0, \varepsilon_0)$ and $(\sigma_r, \varepsilon_r)$ are updated after each strain reversal. R is the parameter that influences the shape of the transient curve and allows a representation of the Bauschinger effect, calculated according to Eq.(18), where ξ is updated following the strain reversal and its value does not change when reloading occurs after partial unloading. According to [16], in this version was assumed that $R_0=20$, $a_1=18.45$ and $a_2=0.001$.

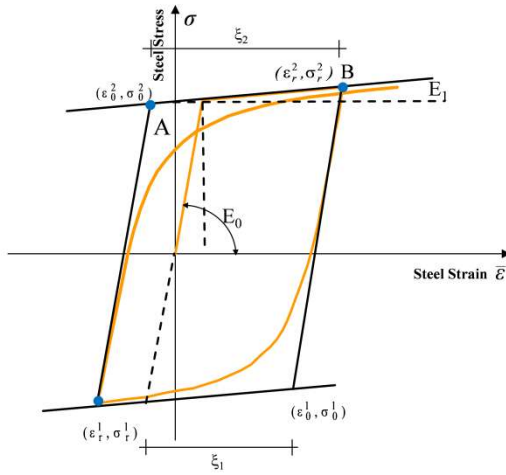


Figure 8. Hysteretic model for steel reinforcement

$$\sigma^* = b\varepsilon^* + \frac{(1-b)\varepsilon^*}{(1 + \varepsilon^{*R})^{1/R}} \quad (18)$$

$$\varepsilon^* = \frac{\bar{\varepsilon} - \varepsilon_r}{\varepsilon_0 - \varepsilon_r}$$

$$\sigma^* = \frac{\sigma - \sigma_r}{\sigma_0 - \sigma_r}$$

$$b = \frac{E_1}{E_0}$$

$$R = R_0 - \frac{a_1 \cdot \xi}{a_2 + \xi} \quad (19)$$

3.1.6. Tension-stiffening by Model Code 2010

In the Model Code 2010, the bond is expressed only in function of the slip. The model aims at the evolution of the stress and strain distribution along the crack spacing under repeated loading. For any given average re-bar strain and length of reinforcing bar between adjacent cracks, the profile of strain and stress along the reinforcement can be computed based on the bond stress distribution along the reinforcing bar. The crack pattern is supposed to be fully developed (stabilized cracking phase), i.e., concrete and steel slip along the whole crack spacing generating bond stresses. Such stresses transfer a fraction of the load from the embedded bar to the uniformly loaded effective concrete area.

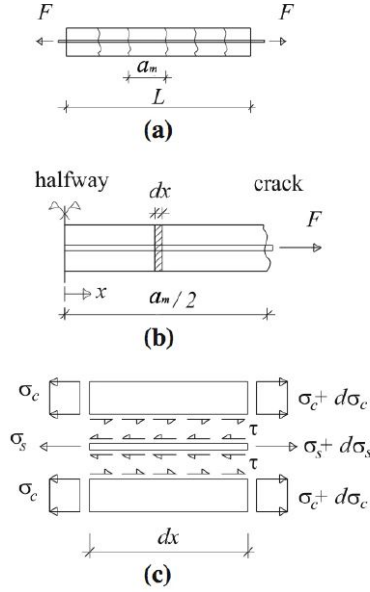


Figure 9. Mechanism of stress transfer along the small segment

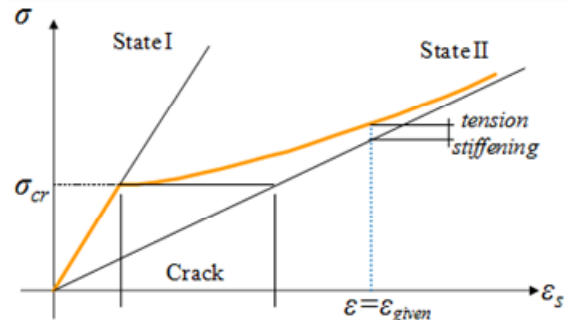


Figure 10. Tension-stiffening effect on steel stress

Satisfying the equilibrium conditions on a small segment along the reinforcing bar, the following equilibrium equation is derived:

$$\frac{d\sigma_s}{dx} = \tau \frac{U_s}{A_s} \quad (20)$$

where $\frac{d\sigma_s}{dx}$ is the gradient of steel stress along the bar, U_s and A_s are the bar perimeter and the bar area, respectively; τ is the average bond stress along the segment.

The relative slip between concrete and steel is originated by their different strain:

$$\frac{ds}{dx} = d\epsilon_s \quad (21)$$

Linear elastic behavior is assumed for steel under service conditions (an appropriate elastic–plastic behavior would be needed for an ultimate limit state analysis):

$$\sigma_s = E_s \epsilon_s$$

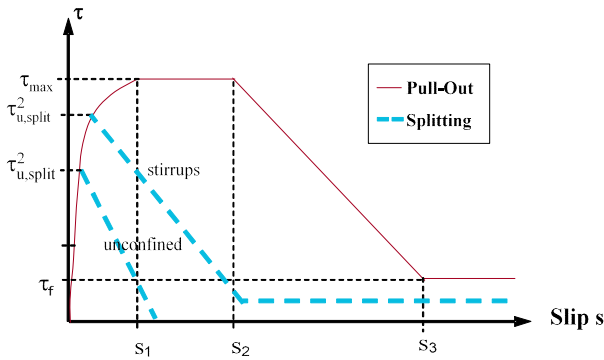
At the crack it is adopted that the external load is only carried by the reinforcement. The bond stress and the slip at the midway between two adjacent cracks are zero, which are the boundary conditions for the first finite segment. Assuming strain value at the middle of two cracks, the stress and strain

profiles are computed by solving the equilibrium and slip compatibility equations, segment by segment along the re-bar.

To complete the problem formulation, the bond-slip behavior is needed. The nonlinearity is only introduced by the nonlinear bond behavior: the chosen static formulation is that provided by the Model Code 2010.

$$\begin{aligned} \tau_0 &= \tau_{\max} \left(\frac{s}{s_1} \right)^\alpha && \text{for } 0 \leq s \leq s_1 \\ \tau_0 &= \tau_{\max} && \text{for } s_1 < s \leq s_2 \\ \tau_0 &= \tau_{\max} - (\tau_{\max} - \tau_f) (s - s_2) / (s_3 - s_2) && \text{for } s_2 < s \leq s_3 \\ \tau_0 &= \tau_f && \text{for } s_3 < s \end{aligned}$$

Where the parameters are given in below table.



	1	2	3	4	5	6
	Pull-Out (PO)		Splitting (SP)			
	$\epsilon_s < \epsilon_{s,y}$		$\epsilon_s < \epsilon_{s,y}$			
	Good bond cond.	All other bond cond.	Good bond cond.		All other bond cond.	
			unconfined	stirrups	unconfined	stirrups
τ_u	$2.5\sqrt{f_{cm}}$	$1.25\sqrt{f_{cm}}$	$7.0 \cdot \left(\frac{f_{cm}}{25}\right)^{0.25}$	$8.0 \cdot \left(\frac{f_{cm}}{25}\right)^{0.25}$	$5.0 \cdot \left(\frac{f_{cm}}{25}\right)^{0.25}$	$5.5 \cdot \left(\frac{f_{cm}}{25}\right)^{0.25}$
s_1	1.0 mm	1.8 mm	$s(\tau_u)$	$s(\tau_u)$	$s(\tau_u)$	$s(\tau_u)$
s_2	2.0 mm	3.6 mm	s_1	s_1	s_1	s_1
s_3	$c_{clear}^{1)}$	$c_{clear}^{1)}$	$1.2s_1$	$0.5c_{clear}^{1)}$	$1.2s_1$	$0.5c_{clear}^{1)}$
α	0.4	0.4	0.4	0.4	0.4	0.4
τ_f	$0.40\tau_u$	$0.40\tau_u$	0	$0.4\tau_u$	0	$0.4\tau_u$

Figure 11. Analytical bond-slip relationship for monotonic loads

3.1.7. PARC CL 2.0

The concrete and steel behaviors as well as their interaction effects are modeled with constitutive relationships for loading-unloading-reloading conditions, as shown above.

The total stresses in the x,y -system are obtained by assuming that concrete and reinforcement behave like two springs placed in parallel:

$$\{\sigma_{x,y}\} = \{\sigma_{x,y}\}_c + \sum_{i=1}^n \rho_i \{\sigma_{x,y}\}_{s,i} \quad (22)$$

where n is the total number of the order of the bar, $\{\sigma_{x,y}\}_c$ are the stresses of the concrete in the x,y -system obtained by Eq. (23) and $\{\sigma_{x,y}\}_{s,i}$ are the stresses of the steel bars obtained by Eq.(24):

$$\{\sigma_{x,y}\}_c = [T_\sigma(\psi)]^t \{\sigma_{1,2}\} \quad (23)$$

$$\{\sigma_{x,y}\}_{s,i} = [T_\sigma(\theta_i)]^t \{\sigma_i\} \quad (24)$$

The proposed PARC_CL model is based on a tangent approach, in which the jacobian matrix in the local coordinate system for each material is composed by derivatives as shown in Eq.(25):

$$[D_{1,2}]_c = \begin{bmatrix} \frac{\partial \sigma_1}{\partial \varepsilon_1} \frac{1}{(1-\nu^2)} & \frac{\partial \sigma_1}{\partial \varepsilon_2} \frac{\nu}{(1-\nu^2)} & 0 \\ \frac{\partial \sigma_2}{\partial \varepsilon_1} \frac{\nu}{(1-\nu^2)} & \frac{\partial \sigma_2}{\partial \varepsilon_2} \frac{1}{(1-\nu^2)} & 0 \\ 0 & 0 & \frac{\partial \tau_{12}}{\partial \gamma_{12}} \end{bmatrix} \quad [D_i]_s = \begin{bmatrix} \frac{\partial \sigma_i}{\partial \varepsilon_i} & 0 & 0 \\ 0 & 0 & 0 \\ 0 & 0 & 0 \end{bmatrix} \quad (25)$$

When, after the first crack the Poisson's ratio is assumed to be zero, the terms out of the diagonal become zero. The global stiffness matrix is obtained by:

$$[D_{x,y}] = [T_\psi] [D_{1,2}]_c [T_\psi] + \sum_{i=1}^n \rho_i [T_{\theta_i}] [D_i]_s [T_{\theta_i}] \quad (26)$$

4. CASE STUDY MODEL

In this work, a prestressed T-shaped girder with flange 1.5 m wide and 0.07 m thick has been studied (see Figure 12.a); the web is 0.14 m wide and 0.23 m high. The total length of the girder is 5 m. The girder has four different pre-stressed reinforcement layouts, each one characterized by 2 tendons St 1570/1770, pre-stressed with 451 MPa. The reinforcement layouts are placed at 7 cm, 11 cm, 15 cm and 19 cm respectively from the bottom of the girder. Even though basically no stirrups reinforcement was planned, in order to provide a shear failure mechanism, 10 stirrups with a diameter of 6 mm and a spacing of 500 mm are allocated in the girder, to allow the attachment of electrical strain gauge sensors (ESGs), useful for the monitoring system which was one of the fundamental aspect of this project research. As shown in Figure 12.b the tested girder was subjected to three different loads: the self-weight (g_{lk}), the prestressing force ($P+M$) and a concentrated force (F) located at 110 cm from the left support and at 390 cm from the right support.

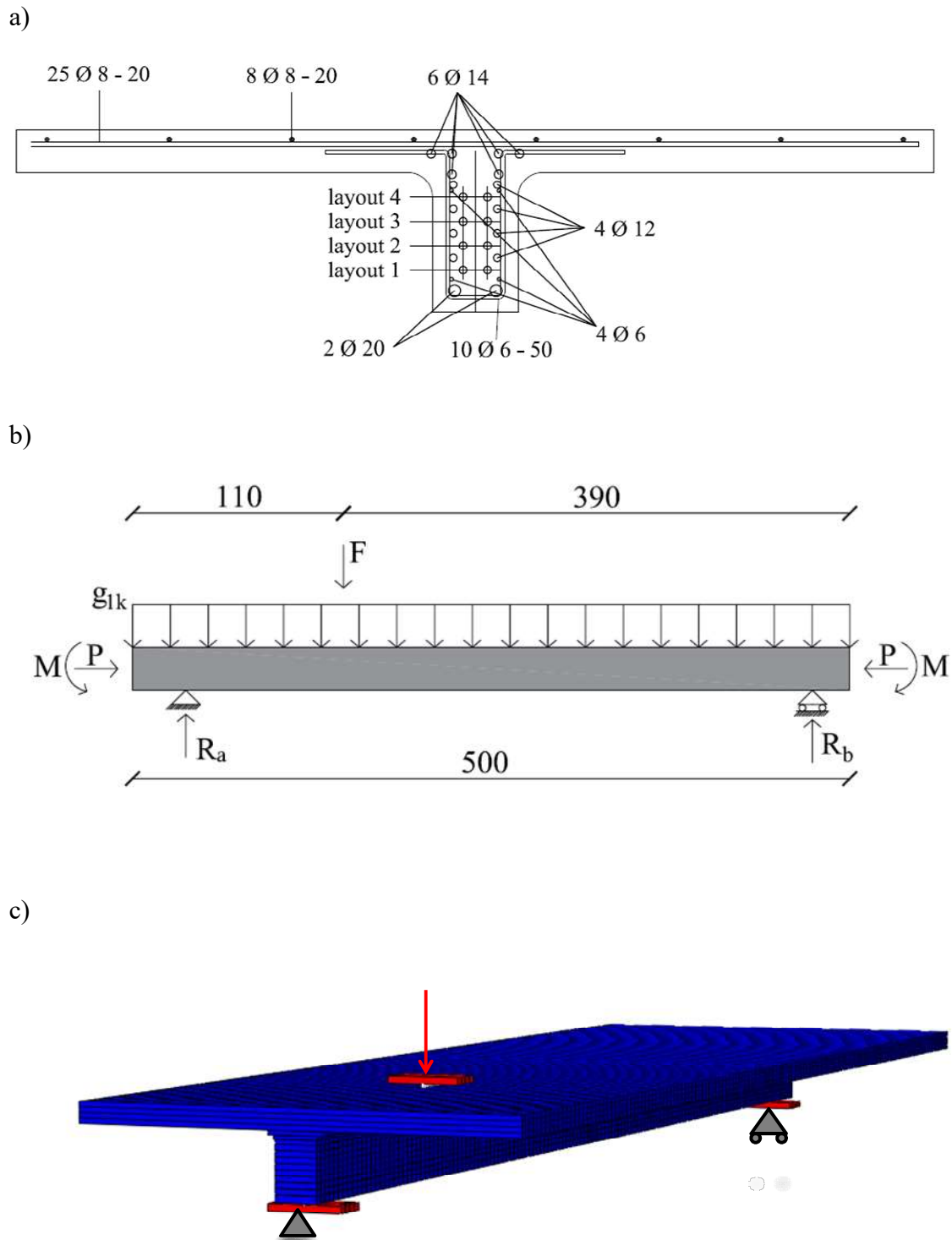


Figure 12. Illustration of the T-shaped analyzed girder; a) main geometry, reinforcement bars and tendons position; b) scheme of the applied loads; c) mesh

The load position was a fundamental aspect in order to provide a shear failure mechanism.

The mesh of the girder was created by using Membrane Elements M3D8R (8 nodes membrane elements with reduced integration) with an average size of 25 mm x 35 mm. The developed mesh is reported in Figure 12.c. The tested T-shaped girder was simply supported, therefore the two steel plates, adopted in the experimental setup, have been modeled and connected to the intrados of the girder using spring elements with no tension behavior. In the Abaqus Software the loads are applied in two different steps: firstly, the self-weight and the prestressing force; secondly the concentrated force is applied in displacement control. Prestressing was inserted into the FE model using "rebar layer" embedded into "host" RC elements. For prestressing strands, an elastic-hardening stress-strain relationship provided by FE Code library was used. Prestressing, assigned to each rebar layer as an initial condition at the beginning of the FE analysis, enables the evaluation of the actual state of coaction before the application of external loads, therefore the losses due to elastic deformation of concrete are explicitly evaluated. According to Model Code 2010 (fib, 2013) formulations, immediate and time-dependent losses are calculated and considered in the model. The immediate losses were detracted from the cable tension (451MPa) and the resulting value was applied in Abaqus as a stress rebar. Time-dependent losses (the creep of the concrete and the long term relaxation of the prestressing) were calculated and applied in NLFEA as a temperature variation. Shrinkage of the concrete are explicitly evaluated in PARC_CL 2.0 crack model by the application of a constant value of strain.

4.1. Experimental test and check of the model prediction

In order to check the accuracy of the NLFEA model, the presented girder was casted and tested in the laboratory. Once developed the NLFEA model, a non-linear analysis by using mean mechanical parameters reported in Table 1 was led. The result of this analysis and a comparison with the L-D curve obtained *via* experimental test is shown in Figure 13.



Figure 13. Test of T-shaped prestressed concrete girder

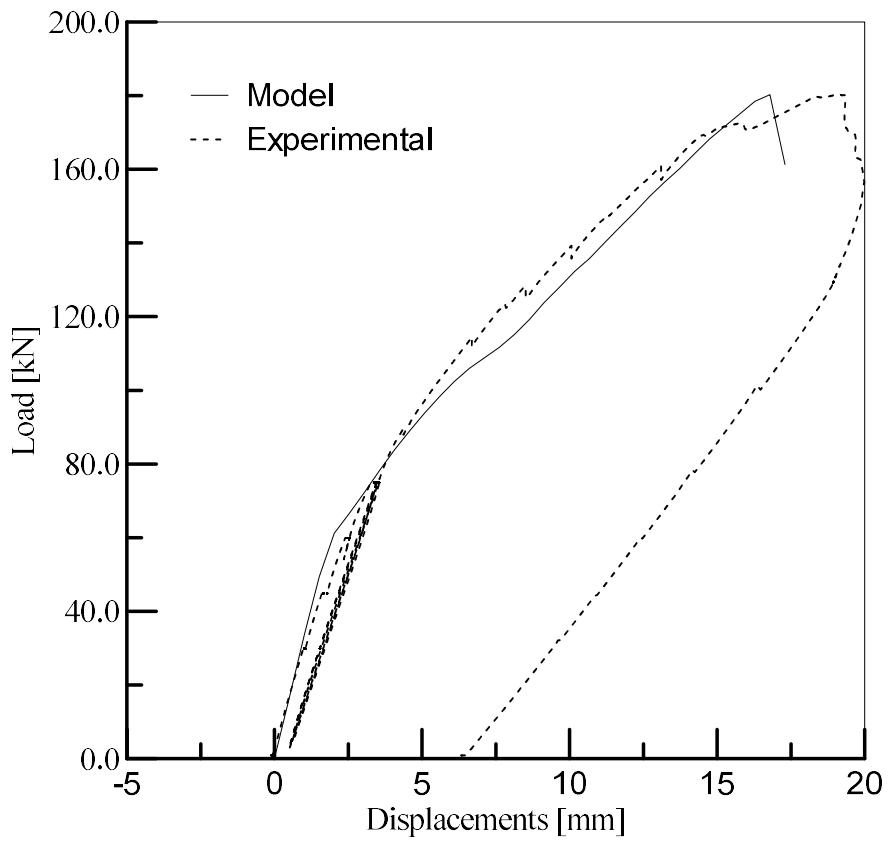


Figure 14. L-D curve: experimental VS model

5. FULLY PROBABILISTIC APPROACH

The presence of uncertainty in the analysis and design of engineering systems has always been recognized. Uncertainties are involved in every part of the system: structure – load – environment. Traditional approaches simplified the problem by considering the uncertain parameters to be deterministic, and accounted for the uncertainties through the use of partial safety factors in the context of limit states. Such approaches do not absolutely guarantee the required reliability and they do not provide information on the reliability achieved and/or on the influence of individual parameters on reliability. Therefore, attention is being given today to fully probabilistic approaches and software tools which can be used for such purposes. Important topics can thus be treated in an advanced manner, e.g. the probabilistic vulnerability assessment of civil infrastructure systems followed by efficient decision-making processes. The standard definition of an engineering problem featuring uncertainty or randomness which is to be analyzed using computers is as follows. A random response of the studied engineering system (e.g. a structure) is represented by random variable Z . In statistical analyses, Z may represent a random response of a system (e.g. deflection, stress, ultimate capacity, etc.) or, during reliability determination, Z is called a safety margin. Random variable Z is a function of basic random variables $X = X_1, X_2 \dots X_{N_{\text{var}}}$ where N_{var} represents the number of random variables which influence the behavior of the structural system:

$$Z = g(X) \tag{27}$$

where $g(X)$ is a function of a random vector X (and also of other, deterministic quantities). Random vector X follows a joint *probability distribution function* (PDF) $f_X(X)$ and, in general, its marginal variables can be statistically correlated.

In this work, the information about $f_x(X)$ is limited to the knowledge of univariate marginal distributions $f_1(x) \dots f_{N_{\text{var}}}(x)$ and a correlation matrix, T (a symmetric square matrix of order N_{var}).

The output variable (or generally a vector) Z represents a transformed variable and the task is to perform statistical, sensitivity and possibly reliability analyses upon it. It is assumed that the analytical analysis of the transformation of input variables to Z is not possible.

The fully probabilistic approach is focused on the estimate of statistical moments of response quantities, such as means or variances, so it represents commonly a statistical analysis. Statistical analysis can be viewed as an estimation of probabilistic integral of (27) . For example, the estimate of the mean value of Z is an approximation to the following integral:

$$u_g = \int g(x) \cdot f_x(X) \cdot dX \quad (28)$$

The aim of a reliability analysis is therefore to estimate a quantity that the designer think is important for the design of the analyzed structural element and also the probability of failure of that quantity. From deterministic method (see Partial Safety Factor Method) there is not a way to estimate the probability of failure; from that method can be conclude that the structure is safe but how the structure is safe is not known.

The failure probability is calculated as a probabilistic integral:

$$p_f = \int I[g(x)] \cdot f_x(X) \cdot dX = \int_{D_f} f_x(X) \cdot dX \quad (29)$$

The function $I[g(x)]$ is an indicator function which equals one for failure event ($g \leq 0$) and zero otherwise. In this way, the domain of integration of the joint PDF above is limited to the failure domain D_f where $g \leq 0$. The explicit calculation of the integral in Eq.(28) or the failure probability integral in Eq.(29) is generally impossible. A large number of efficient stochastic analysis methods were therefore developed during the least seven decades.

A straightforward solution for these tasks is numerical simulation. The interest in simulation methods started in the early 1940s with the purpose of developing inexpensive techniques for testing engineering systems by imitating their real behavior. These methods are commonly called Monte Carlo simulation techniques.

As it will be shown, the computational effort of these methods is very high. For this reason, aiming of this work is to propose a more efficient probabilistic method such as to reduce the computational effort but maintaining the same correct solution.

5.1. Basic Probabilistic Concepts and main Probability Distribution Functions

As shown in §5, to take into account uncertainties of a variable describing the engineering problem, *probability distribution function* are used. In the context of continuous distributions (opposite to discrete distribution, not used in this work), *probability distribution function* satisfies the following properties:

- p is the probability to find x between an interval [a,b]:

$$p[a \leq x \leq b] = \int_a^b f(x)dx \quad (30)$$

where $f(x)$ is the *probability density function* (PDF).

- p is non-negative for all real x values;
- the integral of the probability density function is equal to one:

$$\int_{-\infty}^{+\infty} f(x)dx = 1 \quad (31)$$

The probability distribution function could be described by using two different expressions, the *probability density function*, $f(x)$, as seen in the previous expressions and the *cumulative density function* (CDF), $F(x)$. The last one is related to the “fractile” concept. As it will be shown in the following pages of this work, fractile (or fractiles, in plural version) will be a fundamental concept to know. In this way, a fractile represents the probability to find a value of x less than a specific value X given:

$$F(x) = p[x \leq X] \quad (32)$$

Table 2. Fractiles used in the context of FBSP

Fractile	$F(x)$
5 th	0.05
15 th	0.15
30 th	0.30
50 th	0.50
70 th	0.70
85 th	0.85
95 th	0.95

In this way, for example, the 30th fractile means that the probability to find a value x less than a specific value X is equal to 30% and correspondingly, the probability to find a value x greater than the same specific value X will be equal to 70%. The relationship between these two quantities is such that:

$$\frac{d}{dx}F(x) = f(x) \tag{33}$$

In the following paragraphs will be shown the main PDFs used in this work.

5.1.1. Normal Distribution

Perhaps the most well known and important continuous probability distribution is the Normal distribution (sometimes called Gaussian distribution). The normal PDF has the symmetric bell-shaped curve called the normal curve. In 1733, De Moivre developed the mathematical representation of the normal PDF, as follows:

$$f(x) = \frac{1}{\sigma\sqrt{2\pi}} \exp\left[-\frac{(x-\mu)^2}{2\sigma^2}\right] \tag{34}$$

where μ is the mean value of x , evaluated with:

$$\mu = \frac{1}{N} \sum_{i=1}^N x_i \tag{35}$$

and σ is the standard deviation of x evaluated with:

$$\sigma = \sqrt{\frac{\sum_{i=1}^N (x_i - \mu)^2}{N}} \quad (36)$$

in which N is the size of the sample. It is important to notice that μ and σ , described here in the context of Normal Distribution, are actually used in all the probabilistic distributions, i.e. they are general statistical quantities, which are used in many applications.

5.1.2. Log-Normal Distribution

A positively defined random variable is said to be log-normally distributed if its logarithm is normally distributed. The lognormal distribution has considerable applications in engineering. One major application of this distribution is to represent a random variable that is the result of multiplication of many independent random variables. If x is a normally distributed random variable., the transformation $y = \exp(x)$ transforms the normal PDF representing x with mean μ , and standard deviation σ , to a log-normal PDF $f(y)$ which is given by:

$$f(y) = \frac{1}{\sigma \cdot y \sqrt{2\pi}} \exp\left[-\frac{(\ln y - \mu)^2}{2\sigma^2}\right] \quad (37)$$

It is important underline that in the Eq.(37), μ and σ are respectively the mean value and the standard deviation of x normal-distributed (and not of the log-normal). Therefore, these two parameters have to be calculated before to apply the transformation.

5.1.3. Gumbel Distribution

The Gumbel distribution has two possible form. One is based on the smallest extreme (GMB MIN EVI) see Eq.(38) and the other one is based on the largest extreme (GMB MAX EVI) see Eq.(39).

$$f(x) = \frac{1}{\alpha} \exp \left[\frac{x - \beta}{\alpha} - \exp \left(\frac{x - \beta}{\alpha} \right) \right] \quad (38)$$

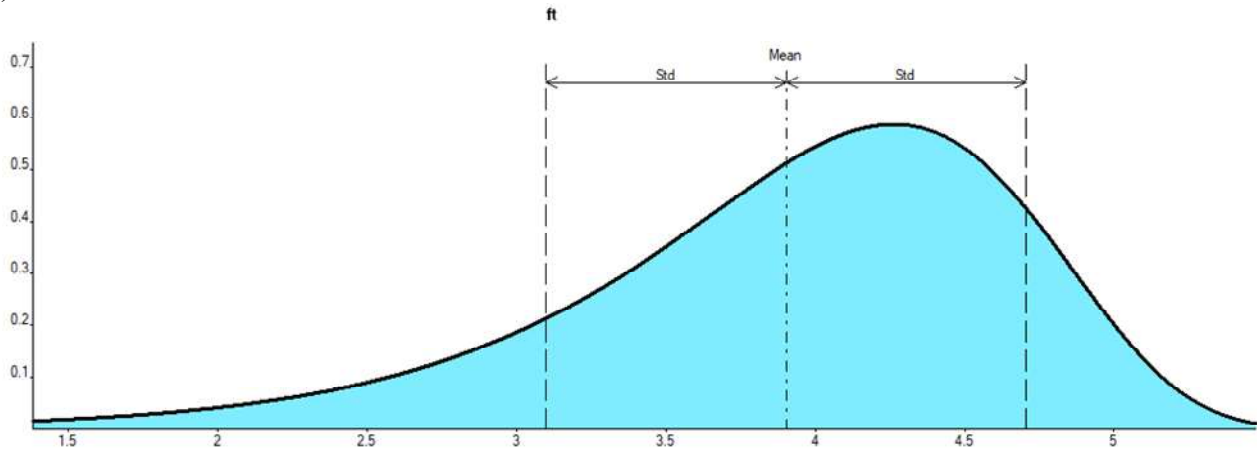
$$f(x) = \frac{1}{\alpha} \exp \left[-\frac{x - \beta}{\alpha} - \exp \left(-\frac{x - \beta}{\alpha} \right) \right] \quad (39)$$

Both distributions requiring to evaluate α and β which are the two Gumbel Distribution Probabilistic parameters. These parameters could be evaluated by using Eq. (40)-(41).

$$\alpha = \frac{\sqrt{6} \cdot \sigma}{\pi} \quad (40)$$

$$\beta = \mu - 0.5772 \cdot \alpha \quad (41)$$

a)



b)

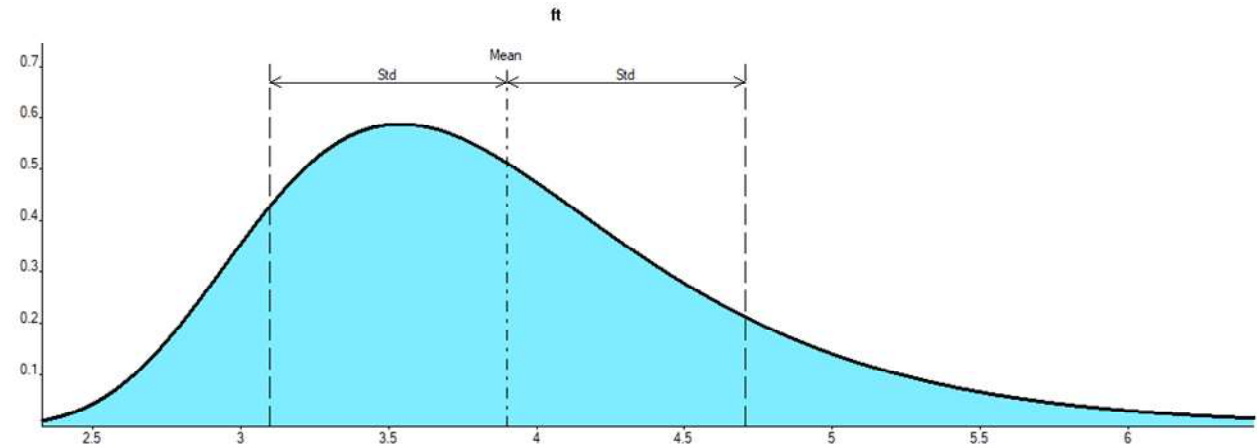


Figure 15. Different Gumbel PDFs for the same mechanical parameter; a) GMB MIN EVI and b)GMB MAX EVI

The choice of one of these illustrated probability distribution function (or others not included in this work) depends by the distribution values of the analyzed variable. Therefore, from the N values that a variable has assumed (for example in a experimental test), it could be chose a probability distribution function by using a *fitting procedure*; to check the applicability of a chosen distribution a statistical test should be led. If the result of the statistical test is positive, that probability distribution function can be used to describe the variable; otherwise, a change of the probability density function is requested and another statistical test will be led. Usually, from the experience, know the frequency values of a variable, by observing the distribution in histogram form, the appropriate distribution could be easily evaluated (see Figure 16).

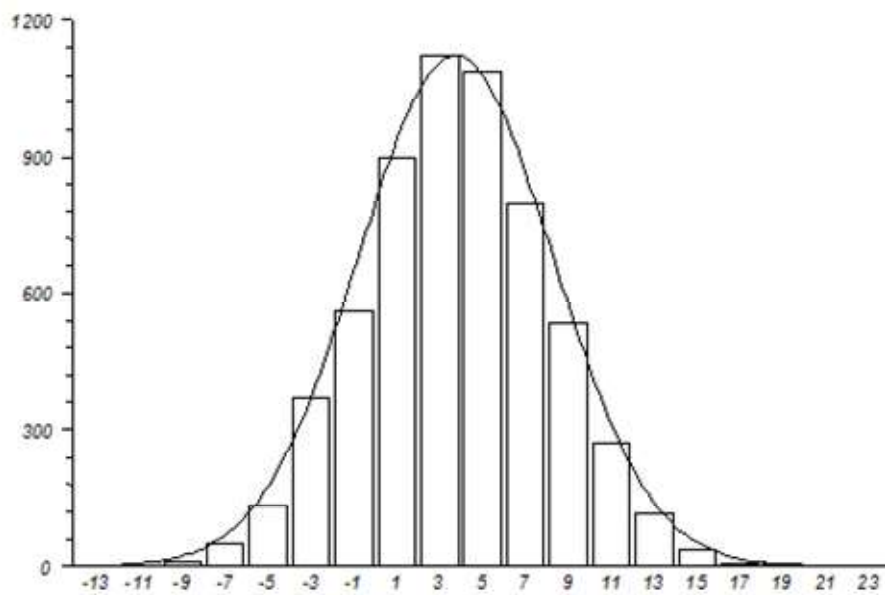


Figure 16. Choice of the probability distribution function, known the frequency that a variable assumes. The vertical column indicates how many times the variable assumes that specific value (to read on the x-axis). An appropriate probability distribution function should fit correctly vertical columns.

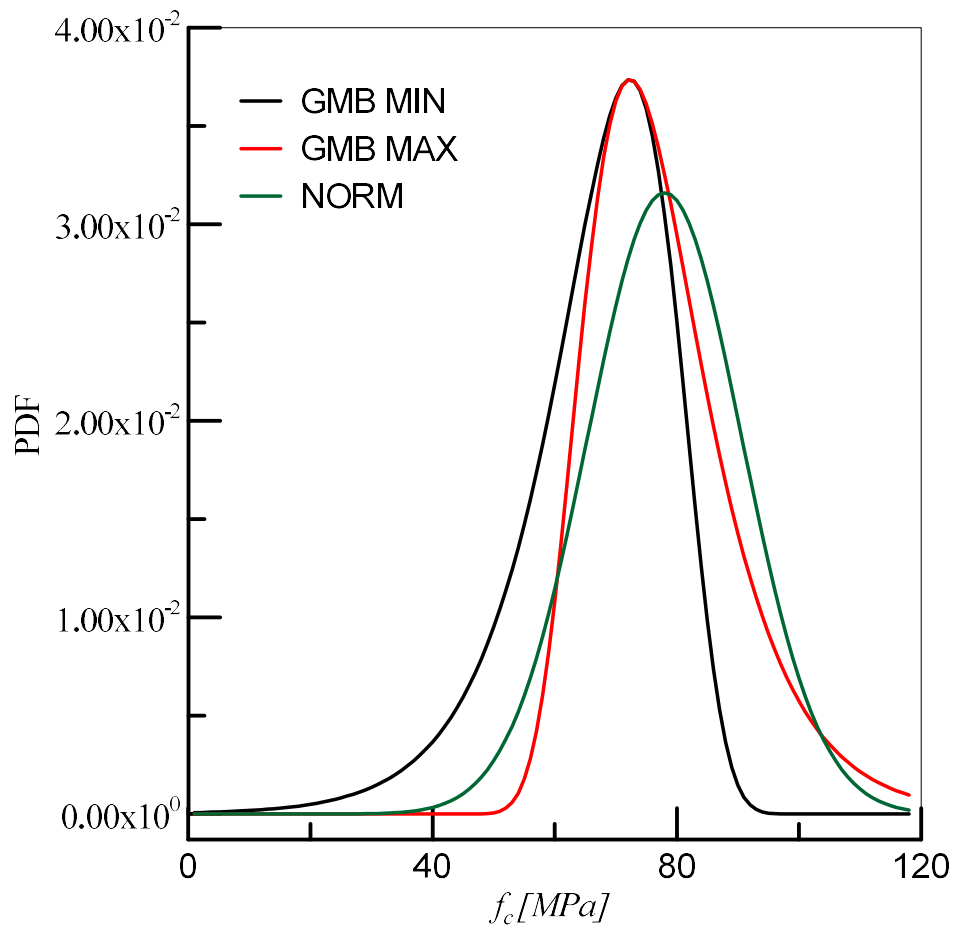


Figure 17. Different PDFs for the same mechanical parameter (compressive strength, experimental values)

5.2. Monte Carlo type simulation

The Monte Carlo method ([9], [27]) is a statistical sampling technique that over the years has been applied successfully to a vast number of scientific problems. The invention of the first electronic computer (ENIAC, 1946) was triggered the spark that led to the Monte Carlo Method. The origin of the method is mainly attributed to John von Neumann (1903-1957) and Stanislaw Ulam (1909-1984); the latter had the intuition thinking about the possible cards combination in the Poker game and he gave the name at the method, which recalled the known casinò (Casino de Monte-Carlo). The firstly application of the method was of Enrico Fermi (FERMIAC device). The FERMIAC developed neutron genealogies in two dimensions, by generating the site of the next collision. Each generation was based on a choice of parameters that characterized the particular material being traversed.

The principle behind the method is to develop an analytical model – a computer based response or limit state function that predicts the behavior of the studied system and repeats it many times under many possible conditions. On the other hand, the response of the system is calculate for each of the many possible conditions and then the global response is numerically estimate. For example:

$$u_g ; \frac{1}{N_{sim}} \sum_{i=1}^{N_{sim}} g(X_i) \quad (42)$$

The N_{sim} samples X_i (realizations, integration points) of the basic random vector X are selected to have an identical probability $1/N_{sim}$. Similarly, the failure probability can be estimated as the ratio of the number of samples that yield failure to the total number of samples N_{sim} .

Crude Monte Carlo method cannot be applied to time-consuming problems, as it requires a large number (thousands or tens of thousands) of simulations (the repeated calculation of structural response) to deliver statistically significant estimates of the outputs. In the context of reliability analyses, this obstacle was historically successfully solved for by the approximation techniques FORM and SORM, e.g. ([17], [24]). In spite of some problems concerning accuracy, these techniques are widely accepted today and have become in some cases standard tools in code calibration.

Once this was achieved, research then focused on the development of advanced simulation techniques which concentrate simulations in the failure region. Among the many efficient methods developed during the last decades, Latin Hypercube Sampling and response surface methodologies are often used e.g. for computationally demanding continuum mechanics problems.

5.3. Latin Hyperbolic Sampling

For time-intensive calculations, “small-sample” simulation techniques based on stratified sampling of the Monte Carlo type represent a rational compromise between feasibility and accuracy. Therefore, Latin Hypercube Sampling (LHS), which is well known today, has been selected as a key fundamental technique. LHS belongs to the category of advanced stratified sampling techniques which result in the very good estimate of statistical moments of response using “small-sample” simulation. More accurately, LHS lead to lower variance in statistical moment estimates compared to crude Monte Carlo sampling at the same sample size. This is the reason the technique became very attractive for dealing with computationally intensive problems like e.g. complex finite element simulations.

The basic feature of LHS is that the range of univariate random variables ($X_1, X_2..$) is divided into N_{sim} intervals (N_{sim} is a number of simulations). The selection of the intervals is performed in such a way that the range of the probability distribution function of each random variable is divided into intervals of equal probability, $1/N_{sim}$. The samples are chosen directly from the distribution function based on an inverse transformation of the univariate distribution function. The representative parameters of variables are selected randomly, being based on random permutations of integers $k = 1, 2, \dots, N_{sim}$. It has been shown that a preferable LHS strategy is the approach suggested in ([20], [23]) where the representative value of each interval is the mean value:

$$x_{i,k} = N_{sim} \cdot \int_{y_{i,k-1}}^{y_{i,k}} x \cdot f_i(x) \cdot dx \quad (43)$$

In the Eq.(43) f_i is the PDF of variable X_i and the integration limits are evaluated as reported in Eq.(44) in which $k=1, \dots, N_{sim}$.

$$y_{i,k} = F_i^{-1} \left(\frac{k}{N_{sim}} \right) \quad (44)$$

*This figure is not available.
Please contact the Author.*

Figure 18. Samples as the probabilistic means of the intervals

On the other hand, once the PDF of each random variables were subdivided into N_{sim} intervals, to create a set of mechanical parameters one random value for each mechanical parameters is selected by the N_{sim} available. Every interval of each variable must be used only once during the simulation. In the Table 3 is reported an example of the procedure, by assuming both to have only two random variable and to lead 6 simulations. The PDF of X_2 (f_{x_2}) was subdivided into 6 intervals and the corresponding value of the random variable were random selected and assigned to one of the six simulations.

Table 3. Sampling plan for two random variables

var. /sim.:	1	2	3	4	5	6
X_1	$x_{1,1}$	$x_{1,2}$	$x_{1,3}$	$x_{1,4}$	$x_{1,5}$	$x_{1,6}$
X_2	$x_{2,6}$	$x_{2,2}$	$x_{2,4}$	$x_{2,1}$	$x_{2,3}$	$x_{2,4}$

In this way there is no physical correlation between the parameters and this is not right in a structural problem (e.g. there is a correlation between the concrete mechanical parameters).

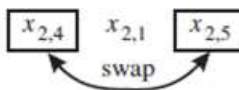
Once N_{sim} samples of each marginal variable are generated separately, the correlation structure prescribed by the target correlation matrix must be taken into account. There are generally two problems related to the statistical correlation: First, during sampling an undesired correlation can occur between the random variables. For example, instead of a correlation coefficient of zero for the uncorrelated random variables an undesired correlation of e.g. 0.4 can be generated.

This can happen especially in the case that only a very small number of simulations (in the order of tens) are carried out, where the number of interval combinations is rather limited. The second task is to introduce the prescribed statistical correlation between the random variables defined by the correlation matrix. This can be achieved by rearranging the order of samples of each variable in the LHS simulation plan in such a way that either they decrease the undesired random correlation when unit matrix \mathbf{T} is required or they introduce a target correlation structure. Such a rearrangement of the sample ordering can be achieved via several different techniques published in the literature on LHS (e.g. [21],[36]); however, some serious limitations have been found by the authors while using them. A robust technique to impose statistical correlation based on the stochastic method of optimization called “Simulated Annealing” has been proposed by Vorechovsky and Novak [41]. The imposition of the prescribed correlation matrix on the sampling scheme can be understood as a combinatorial optimization problem: the difference between the prescribed target matrix (\mathbf{T}) and the generated actual matrix \mathbf{A} , should be as small as possible. The difference between \mathbf{T} and \mathbf{A} represents the error-matrix (denoting here as \mathbf{E}):

$$\mathbf{E} = \mathbf{T} - \mathbf{A} \tag{45}$$

To obtain a scalar measure of the error a suitable norm of the matrix \mathbf{E} is introduced. Two different norms have been defined in [41], denoted as ρ_{\max} and ρ_{rms} . These norms have to be minimized. The objective function is the error norm and the design variables are related to the ordering in the sampling scheme; on the other hand, in order to introduce the correlation, random variables were swapped until to minimize the norm of \mathbf{E} (see Figure 19).

var \ sim.:	1	2	3	4	5	6
X_1	$x_{1,1}$	$x_{1,2}$	$x_{1,3}$	$x_{1,4}$	$x_{1,5}$	$x_{1,6}$
X_2	$x_{2,2}$	$x_{2,6}$	$x_{2,4}$	$x_{2,1}$	$x_{2,5}$	$x_{2,3}$



The diagram shows a curved arrow labeled "swap" pointing from the cell containing $x_{2,4}$ to the cell containing $x_{2,5}$ in the second row of the table.

Figure 19. Sampling plan for two random variables/including correlation

In each step of the combinatorial optimization algorithm (Simulated Annealing), mutation is performed by a transition called a swap from the parent configuration to the offspring configuration. A swap (or a trial) is a small change to the arrangement of the sampling table in Figure 19

. It is done by randomly interchanging a pair of values, X_{ij} and X_{ik} . In other words, one needs to select the variable i , and a pair, j, k , (select the pair of realizations to interchange). One swap may or

may not lead to a decrease (improvement) in the error norm. Immediately, one configuration between the parent and offspring is selected to survive. The Simulated Annealing algorithm is employed for the selection step. The advantage of this compared to some simple evolution strategies is that there is a nonzero probability of accepting an offspring configuration with a higher error than its parent (hill climbing). The acceptance rule with decaying probability of hill climbing provides a mechanism for accepting increases in a controlled fashion (cooling schedule). It is possible that accepting an increase in the error norm will reveal a new configuration that will avoid a local minimum or at least a bad local minimum in future. Extensive studies on the performance of the algorithm show that it performs considerably better than other widely used algorithms for correlation control, namely both Iman and Conovers (1982) Cholesky decomposition [21] and Owen's (1994) Gram-Schmidt orthogonalization [22].

When Monte Carlo type simulation is adopted the adequacy of a given sample (the size) for the purpose of giving acceptable estimates of desired statistical quantities cannot be determined a priori, and thus the ability to extend or refine an experimental design may be important. Otherwise, in the context of Latin Hyperbolic Sampling application, it is necessary to specify the number of simulations in advance. If too small a sample set is used (i.e. a set that does not give acceptable statistical results), the analyst normally has to abandon the results and run new analyses with a larger sample set (and the previous analyses will have been canceled). It is thus desirable to start with a small sample and then extend (or refine) the design if deemed necessary. The extension would permit the use of a larger sample set without the loss of any of the already performed, and possibly quite expensive, calculations (experiments).

*This figure is not available.
Please contact the Author.*

Figure 20. Hierarchical Latin Hypercube Sample design with one sample in the initial design

This problem has been overcome by the method called Hierarchical Latin Hypercube Sampling, which was proposed recently in [42]. The method combines the addition of simulations to the current sample set (hierarchical refinement of sampling probabilities) while maintaining the desired correlation structure by employing an advanced correlation control algorithm [41] for the extended part of the sample. The initial LH-sample can have an arbitrary number of simulations and the added sample must have an even integer times more sampling points than the current sample size.

The concepts described in this paragraph were implemented in a software described in §5.3.1.

5.3.1. FReET Software

FReET is a multipurpose probabilistic software for the statistical, sensitivity and reliability analysis of engineering problems (Novak, Vorechovsky and Rusina ([33],[34])). This software is able to randomizing and correlating all the variables describing the structural system, with the aim to generate samples of mechanical parameters which will be the inputs of NLFEA. Here is reported a briefly flow-chart of the software:

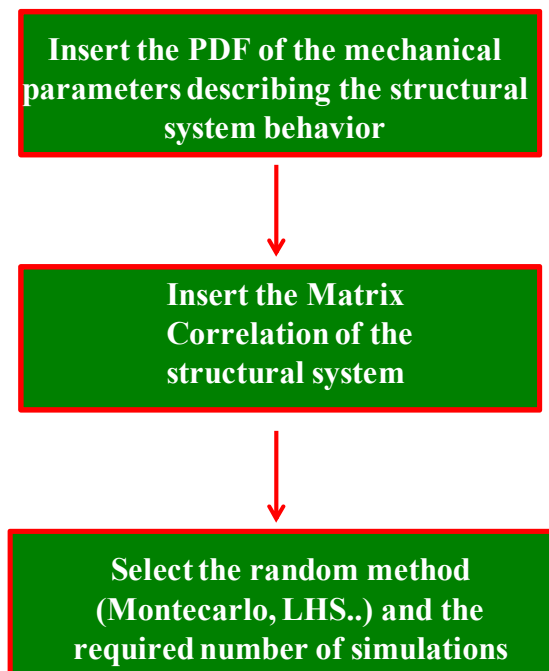


Figure 21. Flow-Chart FReET software

FReET has a user-friendly graphical. The insertion of the PDF mechanical parameters (see firstly box of the flow-chart in Figure 21) was made by the first window of the software (Random Variables window, see Figure 22).

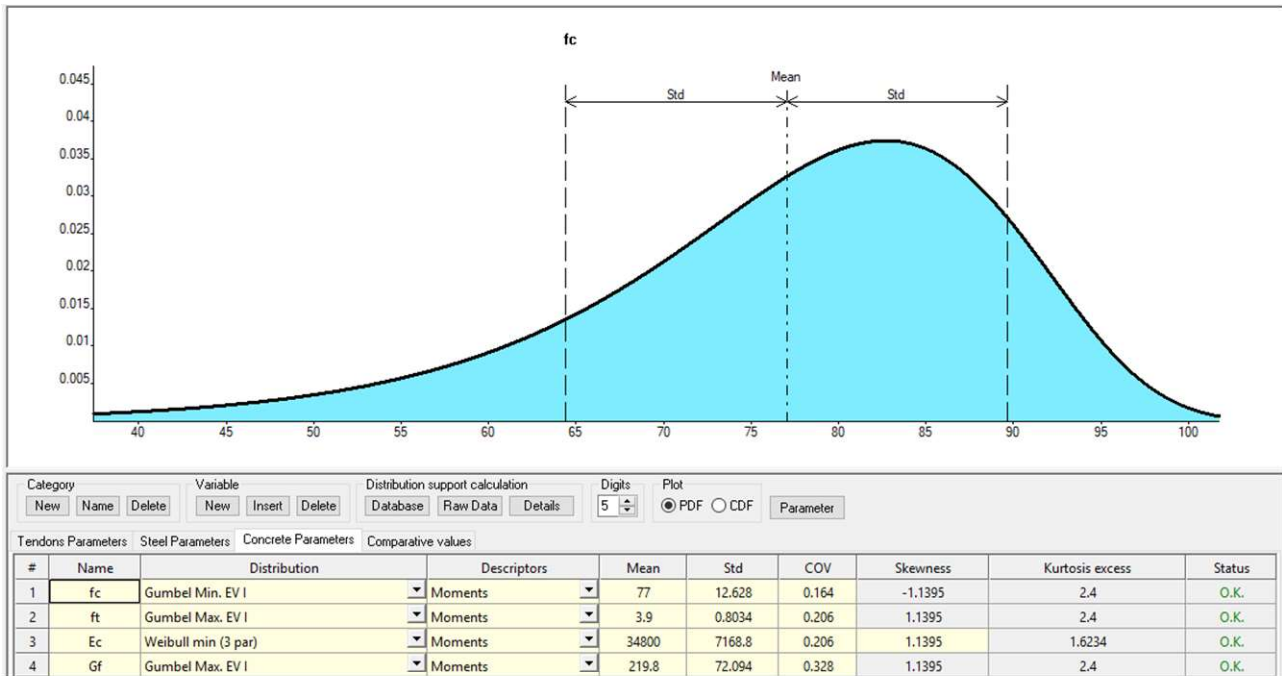


Figure 22. FReET Software, Random variables window

Secondly, by using the “Statistical Correlation” window, was inserted the structural target correlation matrix (\mathbf{T}).

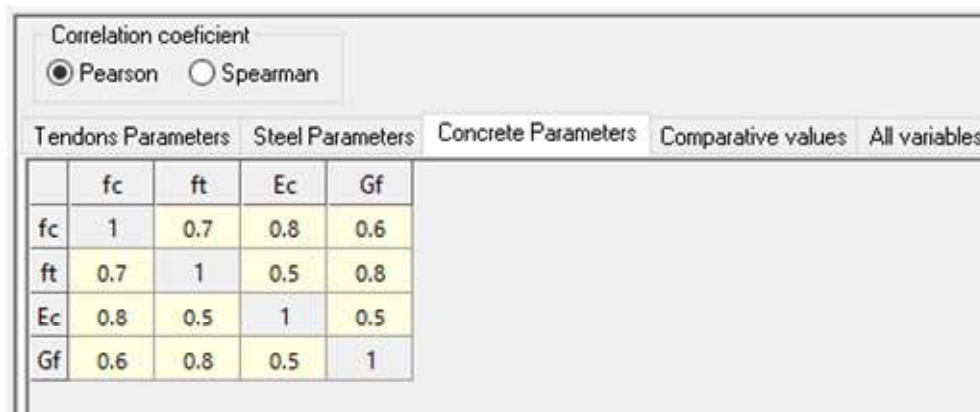


Figure 23. Target correlation matrix for concrete mechanical parameters

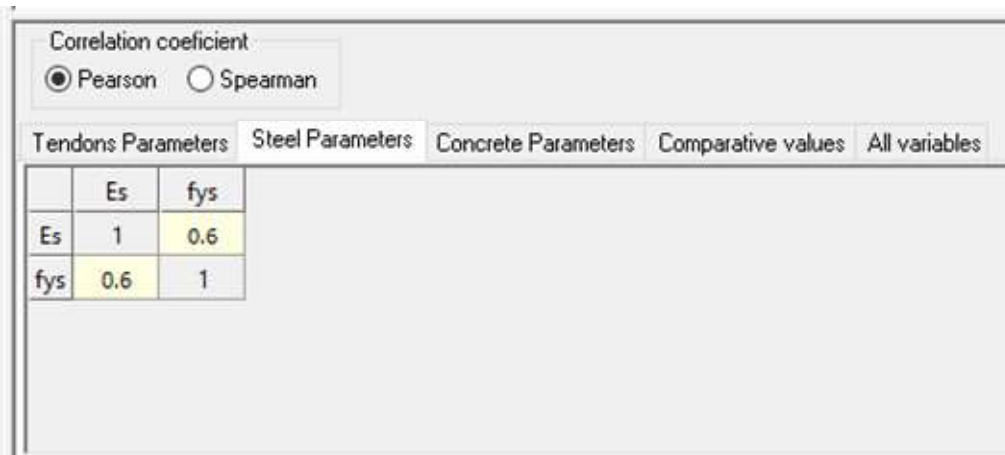
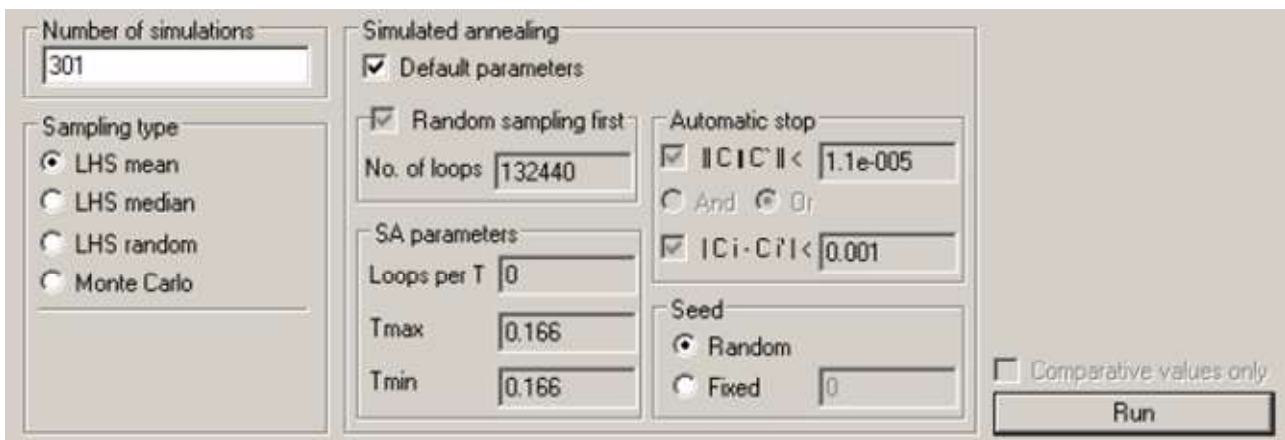


Figure 24. Target correlation matrix for steel mechanical parameters

Thirdly, a user defined numbers of random input parameters were generated according to their PDF by using the selected method (in this work, LHS sampling). As shown in §5.3.1 samples are reordered by using Simulated Annealing algorithm in order to match the required correlation matrix as closely as possible.



With these information, by click on “Run”, software FReET develops the 301 set of mechanical parameters.

	fc	ft	E	Gf
1	79.157	5.1478	38.288	245.78
2	72.706	3.5126	33.691	190.76
3	79.924	3.8994	33.522	226.36
4	75.112	3.6695	33.891	230.58
5	81.574	4.4348	35.791	207.29
6	73.616	3.3635	34.12	186.96
7	80.878	4.4699	40.052	232.11
8	74.204	3.5582	32.554	200.65
9	74.952	3.5907	30.36	212.08
10	76.387	4.1243	33.824	223.79
11	81.074	4.1781	37.098	246.29
12	74.265	3.6032	33.385	192.92
13	79.261	3.9925	35.758	210.47
14	84.237	4.5527	42.935	241.17
15	70.49	3.4691	30.539	176.71
16	81.444	4.1094	35.693	247.34
17	80.245	3.9061	34.637	219.31
18	79.33	4.2266	33.956	255.45
19	75.804	3.6636	36.772	234.72
20	79.434	3.8927	41.567	235.07
21	77.846	4.1294	33.623	222.57
22	77.243	3.8445	35.179	220.91
23	77.435	3.8699	33.281	211.88
24	82.752	4.6029	36.631	299.17
25	83.571	5.0663	39.29	273.13
26	70.206	3.5481	32.998	187.66
27	80.763	4.2818	36.153	222.81
28	68.83	3.209	30.04	177.65
274	75.318	3.7249	31.421	210.67
275	73.331	3.5811	30.819	202.5
276	69.902	3.3409	30.597	183.29
277	76.43	3.6547	32.36	174.37
278	74.079	3.8667	30.978	201.27
279	72.789	3.6125	31.13	191.87
280	77.81	4.2533	32.816	227.99
281	80.137	4.0809	42.117	280.36
282	83.235	3.687	40.79	208.48
283	67.377	3.4122	32.515	188.97
284	85.238	4.2077	45.062	248.43
285	79.713	3.8016	38.626	224.8
286	81.487	3.7133	36.915	217.97
287	85.627	5.001	42.613	278.33
288	76.641	4.1504	31.08	219.53
289	69.219	3.6517	25.084	200.24
290	74.142	3.5307	36.701	209.47
291	77.007	3.597	35.371	187.32
292	79.087	4.0285	31.326	220.68
293	78.137	3.7512	33.419	214.34
294	82.188	4.76	38.429	271.63
295	79.748	3.8167	35.564	211.07
296	74.844	3.8796	31.514	217.75
297	76.967	3.304	35.596	179.24
298	83.159	4.5686	36.458	252.02
299	79.469	3.8352	37.559	207.49
300	76.034	4.0411	31.029	212.9
301	82.947	5.7767	38.834	312.14

Figure 25. Mechanical parameters set generated by FReET

Finally, for each of the 301 samples generated by FReET a NLFEA was performed, by using software Abaqus.

5.3.2. Design Resistances Evaluation

For each set of mechanical parameters generated by FReET, NLFEA was conducted. The 301 peak loads obtained by the NLFEA were used subsequently to calculate the design resistance according to Model Code 2010 (*fib*, 2013), Eq.(46).

$$R_d = e^{R_m(1-\alpha\cdot\beta\cdot V)} \quad (46)$$

where R_m is the mean value of the 301 logarithmic peak loads. The variation coefficient V was calculated by adopting:

$$V = \frac{\sigma}{R_m} \quad (47)$$

in which σ is the standard deviation of the 301 logarithmic peak loads; according to the Model Code 2010 (*fib*, 2013), coefficient β is equal to 3.8 (see **Errore. L'origine riferimento non è stata trovata.**) while α which is a sensitivity factor was assumed equal to 0.8.

As shown until now, the design resistance was evaluated by the knowledge of the peak loads of each simulation. Specifically, in this work, the design resistances was evaluated in three different ways:

- Design Resistance at peak load (see §5.3.2.1);
- Design Resistance at various displacements fixed (see §5.3.2.2);
- Design Resistance at 2.5% deformation stirrups reached (see §5.3.2.3);

Indeed, as shown in the Eq. (46) Design Resistance is dependent from the standard deviation. The latter, as shown in the load-displacement graph of 301 NLFEA (see Figure 26), is not a constant value. Specifically, because of convergence error in NLFEA when the load is closer to the peak load, the standard deviation is higher. In other words, in a probabilistic approach, the closer you get to the peak load more lower will be the design resistance.

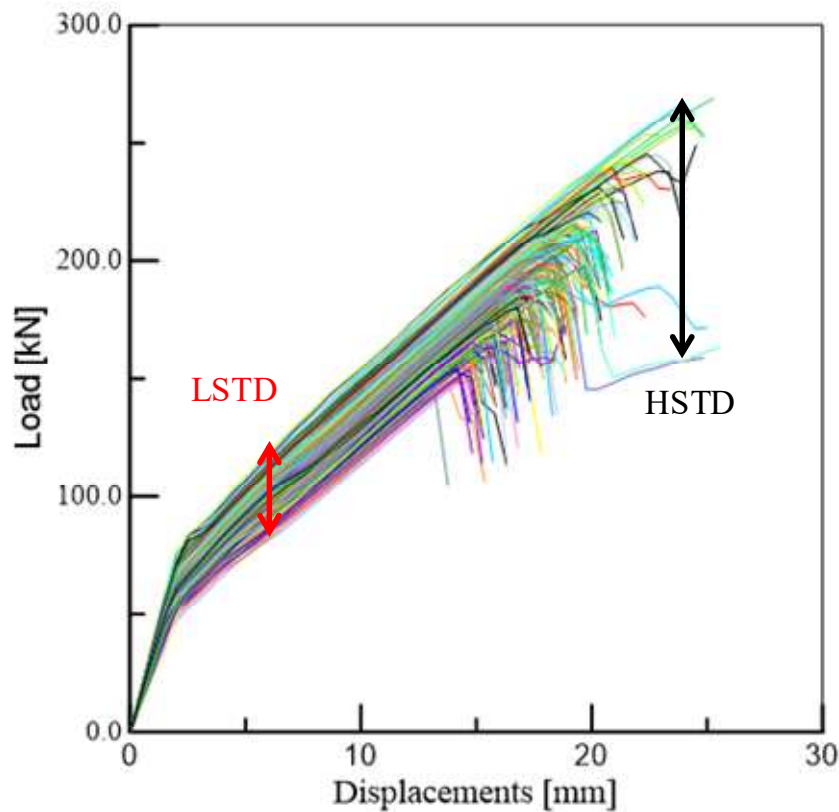


Figure 26. Load-Displacement curve obtained by 301 NLFEA

One can see from the Figure 26 and as explained in the above paragraph, far from the peak load the standard deviation is lower (LSTD) rather than the standard deviation closer to the peak load (HSTD).

5.3.2.1. Log-Normal design resistance at Peak Load

The estimation of the design resistance at peak load was made as shown in §5.3.2; known the peak load for each NLFEA, which was evaluated as the maximum load of the load-displacement curve generated by using software Abaqus, the logarithmic mean value and the standard deviation were evaluated.

Table 4. Probabilistic parameters and design resistance at peak load

Mein value [kN]	Logarithmic mean value [-]	Standard Deviation [kN]	Cov [%]	R _d [kN]
192.02	5.25	0.112	2.23	133.39

5.3.2.2. Log-Normal design resistance at various fixed displacement

Since NLFEA at displacement control were led, interestingly is the estimation of design resistance at various fixed displacement. Design resistance was calculated as shown in §5.3.2 but in which R_m is the mean value of the 301 loads for each displacement fixed (and not the mean value of the peak loads as shown previously). In the same way, the standard deviation was evaluated.

Table 5. Design resistance at various fixed displacements

Displacement [mm]	Mean Value [kN]	Logarithmic mean value [-]	Standard Deviation [kN]	Cov [%]	R _d [kN]
7.62	129.35	4.86	0.063	1.293	89.71
8.13	133.64	4.90	0.061	1.242	93.95
8.64	137.97	4.93	0.059	1.195	98.20
9.15	142.33	4.96	0.057	1.149	102.55
9.66	146.71	4.99	0.055	1.103	106.96
10.17	151.14	5.02	0.053	1.065	111.32
10.67	155.58	5.05	0.052	1.031	115.67
11.18	160.03	5.08	0.051	0.999	120.01
11.69	164.46	5.10	0.050	0.974	124.26
12.20	168.88	5.13	0.049	0.953	128.40
12.71	173.24	5.15	0.049	0.942	132.31
13.22	177.55	5.18	0.048	0.936	136.08
13.73	181.69	5.20	0.053	1.018	137.54
14.24	185.99	5.23	0.050	0.950	142.79
14.75	189.44	5.24	0.059	1.130	141.07
15.26	192.08	5.26	0.076	1.447	135.27

The design resistance is highest when the combination between mean value and standard deviation is favorable (i.e. when the Cov index assumes the lowest value). This happen when the displacement is equal to 14.24 mm.

Table 6. Comparison between different design resistances

	Mean Value [kN]	Logarithmic mean value [-]	Standard Deviation [kN]	Cov [%]	R _d [kN]
At Peak Load	192.02	5.25	0.112	2.23	133.39
At d=14.24 mm	185.99	5.23	0.050	0.950	142.79

In the comparison shown in Table 6, at a displacement fixed equal to 14.24 even if the mean value is lower than the mean value at peak load, the design resistance is higher because the covariance index is lower. However, the estimation of the design resistance at this fixed displacement is something not objective for a designer rather than the evaluation of the design resistance at peak load.

Looking at the results obtained from this paragraph, an objective criterion will be proposed in §5.3.2.3.

5.3.2.3. Log-Normal design resistance at 2.5% stirrups deformation reached

Both analytical calculation and NLFEA predictions show that the analyzed girder presents a shear diagonal tension failure mechanism. This means that the failure of the girder occurs when stirrups' yielding was reached. According to this evidence and by assuming that stirrups fall when their yielding deformation is 2.5% a new design resistance was evaluated.

This work was very expensive because of 301 NLFEA have been performed. For each of NLFEA with the aim to evaluate at what load the yielding of stirrups was reached, the following procedure has been adopted:

- I. Definition of the more stressed shear zone (immediately known for a three point bending as in this work), and FE selection in this zone:



Figure 27. Shear influence area

- II. Evaluation of the stirrups deformation (SDV_{10} , $Parc_{CL_2.0}$) for each of Gauss Points of the elements in the selected region, at each step:

Displacement [mm]	SDV_{10} El_1_1	SDV_{10} El_1_2	SDV_{10} El_1_3	SDV_{10} El_1_4	SDV_{10} El_2_1	SDV_{10} El_2_2
0	0	0	0	0	0	0
0.5	2.45E-4	2.45E-4	2.45E-4	2.45E-4	2.47E-4	2.48E-4
1	2.46E-4	2.48E-4	2.47E-4	2.46E-4	2.48E-4	2.49E-4

- III. Maximum stirrups deformation evaluation, at each displacement fixed:

$$eps_max_d = \max[SDV_{10}_{i,j}]$$

where d was the fixed displacement, $i=1,2,\dots,N$ with N is the number of finite elements in the selected region and $j=1,2,3,4$ (gauss points for each finite elements):

Displacement [mm]	eps_max
0	0
0.5	2.48E-4
1	2.49E-4
....

- IV. Find the displacement in which the stirrups deformation reaches for the first time a value greater or equal to 2.5% in at least one gauss point:

Displacement [mm]	eps_max
0	0
0.5	2.48E-4
1	2.49E-4
1.5	
2	
2.5	
3	
3.5	
....	...
....	0.0236
15	0.0273
....	0.0413
18	

- V. Assume the load in correspondence of the displacement found above as the limit load of that analysis;
- VI. Evaluate the design resistance with Eq.(46) in which mean logarithmic and standard deviation are evaluated by using the limit loads obtained in VI;

Table 7. Design resistance at yielding of stirrups reached

	Mean Value [kN]	Logarithmic mean value [-]	Standard Deviation [kN]	Cov [%]	R _d [kN]
At Peak Load	179.85	5.19	0.088	1.7	139.10

6. FRACTILES BASED SAMPLING PROCEDURE

The Fractile Based Sampling Procedure is primarily based on the LHS sampling (see §5.3) and the Simulating Annealing procedure for setting up the correlation between the inputs for the non-linear numerical models. The basis of FBSP is the realizations shown in Table 8 in the “Variable vs. Simulation (var/sim.)” matrix.

Table 8. Sampling plan for two random variables including correlation

var. /sim.:	1	2	3	4	5	6
X_1	$x_{1,1}$	$x_{1,2}$	$x_{1,3}$	$x_{1,4}$	$x_{1,5}$	$x_{1,6}$
X_2	$x_{2,6}$	$x_{2,2}$	$x_{2,4}$	$x_{2,1}$	$x_{2,3}$	$x_{2,4}$

In the Table 8 the generic variable X_i represents a generic mechanical properties used in the NLFEA (compressive strength, tensile strength...). For a selected leading variable X_i (Row i) those simulation sets k (Column vectors, k , see Table 8) are chosen, for which the realization values x_{ik} are closest to the predefined fractile values $x_{i,p\%}$.

Table 9. Values of leading parameter for different fractiles

Fractiles	$x_{i,p\%}$
1 th	$x_{i,5\%}$
2 th	$x_{i,15\%}$
3 th	$x_{i,30\%}$
4 th	$x_{i,50\%}$
5 th	$x_{i,70\%}$
6 th	$x_{i,85\%}$
7 th	$x_{i,95\%}$

On the other hand, known the leading parameter that most influence the behavior of the structural element (see §6.1), the probability density function of the FP method will be approximated by leading only seven NLFEA with the seven samples of the mechanical parameters chosen as shown above; the design resistance was calculated as shown in §5.3.2.1.

By using this method, the correlation between the mechanical parameters is ensured by means of a correlation matrix (based on experimental test, experience and literature), while in the context of ECOV application is not clearly specified what is the correlation between the mechanical parameters, and how should be evaluated the mean and characteristic mechanical parameters which are necessary for the design resistance evaluation. On the other hand, the computational effort required by the new proposed method is comparable with ECOV.

6.1. Validation of the Leading Parameter

As learned from the previous topics, the choice of the leading parameter plays an important role in the context of FBSP applications. Leading parameter validation is a difficult topic because there are different ways to reach this result and because this parameter seems to depend by the failure mechanism of the analyzed structural element. From the results shown in the previous paragraphs and from other considerations that will be lead in this paragraph, a justified choice for the analyzed T-shaped girder will be achieved. Specifically, to correctly choose the leading parameter, three approaches will be discussed in this paragraph:

- Validation based on Input-Output comparison (§6.1.1);
- Validation based on sensitivity analyses (§6.1.2);
- Validation based on Target Correlation Matrix (§6.1.3);
- Validation based on FBSP (§6.1.4);

It will be shown that each one of this method leads to a unique leading parameter choice.

6.1.1. Validation based on Input-Output Comparison

In order to conduct a lower number of NLFEA, aim of this study is to understand which mechanical parameter influences the failure mechanism more than the other ones; this parameter could be the best leading parameter to use in FBSP application. Known the probabilistic distribution of a generic mechanical parameter, its value was calculated in correspondence of seven fractiles (5th, 15th, 25th, 50th, 70th, 85th and 95th). The value that the parameter assumes in correspondence of the fractile was used to select the sample (from the 301 samples) with the parameter value closest to the fractile one. Known the log-normal distribution of the peak loads and the peak load assumed by the selected sample, the output fractile is determined (see Table 10). This table shows the results of the

previous described procedure for the specific case of compressive strength parameter. For example, at the 15% fractile, the value of compressive strength (using GMB MIN EVI distribution) is 64.79MPa; the 117th set of 301 is the set in which the compressive strength is closest to 64.79MPa; the NLFEA peak load associated to this set is equal to 178.38kN that corresponds to 28.3% fractile (calculated on the base of log-normal distribution of all the N_{set} peak loads).

Table 10. Correspondence between input and output starting from compressive strength.

Fractiles Input	f_c [MPa]	Set	Peak Load [kN]	Fractiles Output [%]
5%	53.44	212	153.83	3.3
15%	64.79	117	178.38	28.3
30%	72.53	13	186.19	41.8
50%	79.08	99	194.71	56.8
70%	84.51	87	217.51	86.7
85%	88.98	174	210.85	80.2
95%	93.49	46	213.00	82.5

By repeating this procedure changing the leading parameter, Table 11 was built. To individuate the mechanical parameter that most influences the girder failure mechanism, is sufficient to identify the fractile output closest to the fractile input. Looking at Table 11 in vertical row, the best matches seem to be the tensile strength and the compressive strength.

Table 11. Fractile outputs (in terms of peak load) for different mechanical parameters.

Input	Output [%]					
	f_c	f_t	G_f	f_{ys}	P	f_{yt}
5%	3.3	8.59	11.90	84.77	23.72	46.78
15%	28.3	15.43	29.15	19.30	33.21	39.41
30%	41.8	25.23	83.02	49.65	71.07	68.70
50%	56.8	62.97	75.07	31.35	11.90	44.64
70%	86.7	63.36	84.67	97.41	80.38	70.42
85%	80.2	89.86	66.92	78.21	35.86	46.39
95%	82.5	95.53	85.09	73.02	68.72	49.65

To better explain this concept in Figure 28 and Figure 29 are reported the results of Table 11 for tensile strength and precompression force.

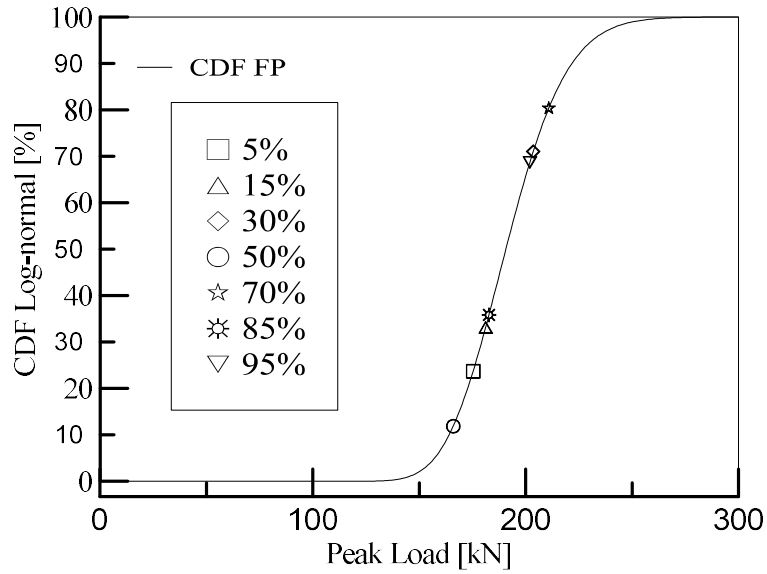


Figure 28. Input-Output correspondence with precompression force leading parameter

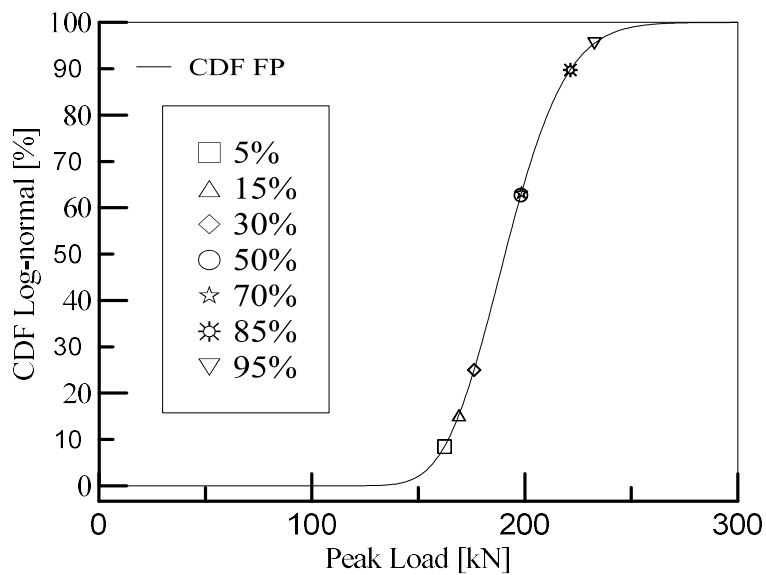


Figure 29. Input-Output correspondence with tensile strength leading parameter

6.1.2. Validation based on sensitivity analyses

The sensitivity analysis is an important process into statistical analysis which allow to evaluate which is the response change occurs in an engineering system, provided by little changes in mechanical parameters values. Specifically, in this work, a simplified approach to the sensitivity analysis will be shown, indeed it is focus on the FBSP (limited number of samples) while an exact study would require a greater number of samples (FP approach). The results obtained by sensitivity analyses could be used for the stochastic optimization, which was one of the main topic of this work. As it is known, the behavior of a general structural element depends on many mechanical parameters. In particular, the structural element failure mechanism characterizes the type of mechanical parameters that are most important between all the parameters describing the engineering system. The T-shaped girder analyzed in this work, shows a shear diagonal failure mechanism; the most important mechanical parameters influencing this failure mechanism are compressive strength, fracture energy and tensile strength, therefore will be shown the comparison of a dominant mechanical parameter with the other parameters describing the system, at different load levels applied to the girder, to understand if there is a change of a dominant mechanical parameter corresponding at a change of the applied load to the structural element.

By using a generic leading parameter (x), seven samples on the base of x fractile values were selected from the N_{set} ; this procedure led to the “ x original matrix”, which is a matrix containing a mechanical parameter sample in each row, as shown in the §6 . From the “ x original matrix” other two matrices were obtained; the first matrix, called “ $x + 10\%$ matrix”, was obtained from " x original matrix" increasing the values of " x " by 10% and leaving the other mechanical parameters unchanged. In the same way, the last matrix, called “ $x - 10\%$ matrix”, was obtained from " x original matrix" decreasing the values of " x " by 10% without changing the other mechanical parameters. For each of the one matrix reported above, seven NLFEA were performed and the global structural response (in term of load and displacement) was assumed to be equal to the average of the values obtained from the seven NLFEA. In this sense, if “ x ” is a dominant mechanical parameter the change in term of mean load or mean displacement should be higher rather than the same change obtained by another mechanical parameter change.

Tables of mechanical parameters used in the sensitivity analyses are reported in the following pages.

FRACTILES BASED SAMPLING PROCEDURE

Table 12. Mechanical parameters input based on compressive strength sensitivity analyses

<i>Fractiles</i>	f_c [MPa]	<i>SET</i>	G_F [N/mm]	f_t [MPa]	E_c [MPa]	f_{ys} [MPa]	E_s [MPa]	f_{yt} [MPa]	E_t [MPa]	P [MN]
<i>“f_c original matrix”</i>										
5%	53.4	212	0.139	2.6	3.11E+04	579.81	1.98E+05	1381.1	1.91E+05	0.041
15%	64.8	117	0.220	4.0	3.13E+04	623.69	2.00E+05	1371.2	1.97E+05	0.043
30%	72.5	13	0.146	3.3	3.31E+04	607.15	1.96E+05	1390	1.97E+05	0.041
50%	79.1	99	0.261	4.3	3.91E+04	562.14	2.02E+05	1430	2.02E+05	0.039
70%	84.5	87	0.217	4.7	3.65E+04	645.17	2.09E+05	1410.2	2.01E+05	0.043
85%	89.0	174	0.288	4.6	3.45E+04	623.22	2.08E+05	1385.6	2.03E+05	0.043
95%	93.5	46	0.174	3.4	3.89E+04	656.54	2.06E+05	1352.5	1.89E+05	0.035
<i>“f_c + 10% matrix”</i>										
-	58.8	212	0.139	2.6	3.11E+04	579.81	1.98E+05	1381.1	1.91E+05	0.041
-	71.3	117	0.22	4.0	3.13E+04	623.69	2.00E+05	1371.2	1.97E+05	0.043
-	79.8	13	0.146	3.3	3.31E+04	607.15	1.96E+05	1390	1.97E+05	0.041
-	87.0	99	0.261	4.3	3.91E+04	562.14	2.02E+05	1430	2.02E+05	0.039
-	93.0	87	0.217	4.7	3.65E+04	645.17	2.09E+05	1410.2	2.01E+05	0.043
-	97.9	174	0.288	4.6	3.45E+04	623.22	2.08E+05	1385.6	2.03E+05	0.043
-	102.8	46	0.174	3.4	3.89E+04	656.54	2.06E+05	1352.5	1.89E+05	0.035
<i>“f_c - 10% matrix”</i>										
-	48.1	212	0.139	2.6	3.11E+04	579.81	1.98E+05	1381.1	1.91E+05	0.041
-	58.3	117	0.22	4.0	3.13E+04	623.69	2.00E+05	1371.2	1.97E+05	0.043
-	65.3	13	0.146	3.3	3.31E+04	607.15	1.96E+05	1390	1.97E+05	0.041
-	71.2	99	0.261	4.3	3.91E+04	562.14	2.02E+05	1430	2.02E+05	0.039
-	76.1	87	0.217	4.7	3.65E+04	645.17	2.09E+05	1410.2	2.01E+05	0.043
-	80.1	174	0.288	4.6	3.45E+04	623.22	2.08E+05	1385.6	2.03E+05	0.043
-	84.1	46	0.174	3.4	3.89E+04	656.54	2.06E+05	1352.5	1.89E+05	0.035

FRACTILES BASED SAMPLING PROCEDURE

Table 13. Mechanical parameters input based on fracture energy sensitivity analyses

Fractiles	G_F [N/mm]	SET	f_c [MPa]	f_t [MPa]	E_c [MPa]	f_{ys} [MPa]	E_s [MPa]	f_{yt} [MPa]	E_t [MPa]	P [MN]
“ G_F original matrix”										
5%	0.126	118	66.8	3.1	3.23E+04	606.94	2.04E+05	1405.7	1.97E+05	0.042
15%	0.152	135	75.0	3.2	3.40E+04	616.16	1.97E+05	1415.0	1.98E+05	0.044
30%	0.177	84	87.4	3.5	3.97E+04	615.53	2.00E+05	1372.3	1.98E+05	0.041
50%	0.208	31	80.3	3.5	3.69E+04	649.04	2.04E+05	1394.9	1.95E+05	0.045
70%	0.245	181	91.8	4.4	3.81E+04	615.95	1.98E+05	1391.6	1.96E+05	0.041
85%	0.289	244	80.6	4.8	3.57E+04	620.7	1.93E+05	1450.9	1.94E+05	0.038
95%	0.354	266	74.3	5.0	3.46E+04	627.43	2.08E+05	1393.9	1.96E+05	0.038
“ G_F + 10% matrix”										
-	0.139	118	66.8	3.1	3.23E+04	606.94	2.04E+05	1405.7	1.97E+05	0.042
-	0.167	135	75.0	3.2	3.40E+04	616.16	1.97E+05	1415	1.98E+05	0.044
-	0.195	84	87.4	3.5	3.97E+04	615.53	2.00E+05	1372.3	1.98E+05	0.041
-	0.229	31	80.3	3.5	3.69E+04	649.04	2.04E+05	1394.9	1.95E+05	0.045
-	0.270	181	91.8	4.4	3.81E+04	615.95	1.98E+05	1391.6	1.96E+05	0.041
-	0.318	244	80.6	4.8	3.57E+04	620.7	1.93E+05	1450.9	1.94E+05	0.038
-	0.389	266	74.3	5.0	3.46E+04	627.43	2.08E+05	1393.9	1.96E+05	0.038
“ G_F - 10% matrix”										
-	0.113	118	66.8	3.1	3.23E+04	606.94	2.04E+05	1405.7	1.97E+05	0.042
-	0.136	135	75.0	3.2	3.40E+04	616.16	1.97E+05	1415	1.98E+05	0.044
-	0.159	84	87.4	3.5	3.97E+04	615.53	2.00E+05	1372.3	1.98E+05	0.041
-	0.187	31	80.3	3.5	3.69E+04	649.04	2.04E+05	1394.9	1.95E+05	0.045
-	0.221	181	91.7	4.4	3.81E+04	615.95	1.98E+05	1391.6	1.96E+05	0.041
-	0.260	244	80.5	4.8	3.57E+04	620.7	1.93E+05	1450.9	1.94E+05	0.038
-	0.318	266	74.3	5.0	3.46E+04	627.43	2.08E+05	1393.9	1.96E+05	0.038

FRACTILES BASED SAMPLING PROCEDURE

Table 14. Mechanical parameters input based on tensile strength sensitivity analyses

Fractiles	f_t [MPa]	SET	G_F [N/mm]	f_c [MPa]	E_c [MPa]	f_{ys} [MPa]	E_s [MPa]	f_{yt} [MPa]	E_t [MPa]	P [MN]
“ f_t original matrix”										
5%	2.9	69	0.154	67.5	3.50E+04	618.28	2.00E+05	1392.8	1.96E+05	0.042
15%	3.1	7	0.144	67.1	3.29E+04	602.14	2.04E+05	1339.8	1.89E+05	0.040
30%	3.4	139	0.145	69.3	3.06E+04	599.08	2.00E+05	1360.8	1.85E+05	0.042
50%	3.8	176	0.201	74.7	3.53E+04	631.33	2.00E+05	1360.4	1.93E+05	0.041
70%	4.2	288	0.215	82.1	3.58E+04	598.17	1.97E+05	1365.3	1.92E+05	0.045
85%	4.7	249	0.456	88.4	3.96E+04	602.36	2.01E+05	1442.3	1.99E+05	0.044
95%	5.4	89	0.265	104.2	4.03E+04	636.59	2.01E+05	1398	1.91E+05	0.043
“ f_t + 10% matrix”										
-	3.2	69	0.154	67.5	3.50E+04	618.28	2.00E+05	1392.8	1.96E+05	0.042
-	3.5	7	0.144	67.1	3.29E+04	602.14	2.04E+05	1339.8	1.89E+05	0.040
-	3.8	139	0.145	69.3	3.06E+04	599.08	2.00E+05	1360.8	1.85E+05	0.042
-	4.2	176	0.201	74.7	3.53E+04	631.33	2.00E+05	1360.4	1.93E+05	0.041
-	4.6	288	0.215	82.1	3.58E+04	598.17	1.97E+05	1365.3	1.92E+05	0.045
-	5.1	249	0.456	88.4	3.96E+04	602.36	2.01E+05	1442.3	1.99E+05	0.044
-	5.9	89	0.265	104.2	4.03E+04	636.59	2.01E+05	1398	1.91E+05	0.043
“ f_t - 10% matrix”										
-	2.6	69	0.154	67.5	3.50E+04	618.28	2.00E+05	1392.8	1.96E+05	0.042
-	2.8	7	0.144	67.1	3.29E+04	602.14	2.04E+05	1339.8	1.89E+05	0.040
-	3.1	139	0.145	69.3	3.06E+04	599.08	2.00E+05	1360.8	1.85E+05	0.042
-	3.4	176	0.201	74.7	3.53E+04	631.33	2.00E+05	1360.4	1.93E+05	0.041
-	3.8	288	0.215	82.1	3.58E+04	598.17	1.97E+05	1365.3	1.92E+05	0.045
-	4.2	249	0.456	88.4	3.96E+04	602.36	2.01E+05	1442.3	1.99E+05	0.044
-	4.8	89	0.265	104.2	4.03E+04	636.59	2.01E+05	1398	1.91E+05	0.043

6.1.2.1. Load Levels definition

In general, sensitivity analyses should be performed at different load levels in order to determine the load dependency of the important parameters on the structural response.

For the predefined load levels of 30%, 60%, 90% of the peak loads the simplified sensitivity analyses by varying the model parameter “x original matrix” to “x + 10% matrix” and to “x - 10% matrix” have been performed using the seven FBSP analyses. The load levels for the sensitivity analyses have been characterized, since the peak loads of the seven FBSP differ, by the percentage of each of the seven peak load, see Figure 30 .

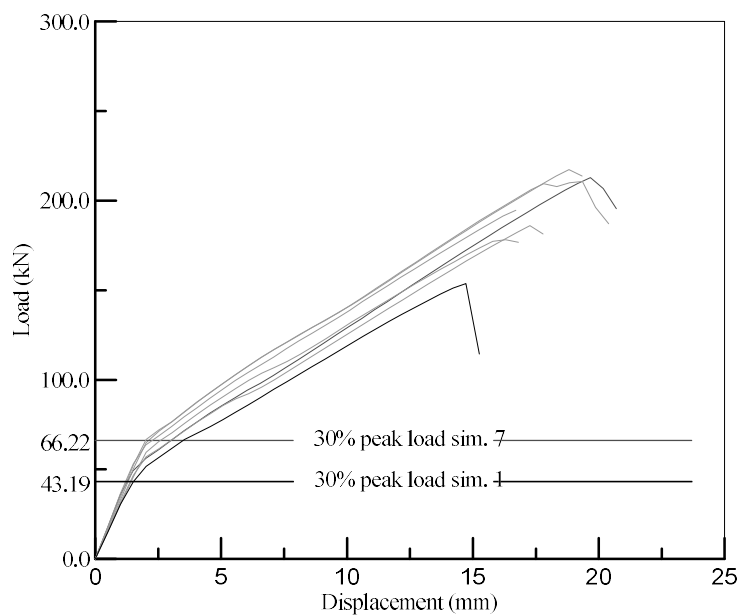


Figure 30. Load evaluation

The pre-defined load levels of 30%, 60%, and 90% are defined for the investigated shear failure mechanism based on the experimental & numerical identified and Model Code 2010 (*fib*, 2013) pre-defined characteristics. For instance, the first crack formation occurred at 30% of the peak load, the yielding of the stirrups of 1.97 % lengthening occurred at 60% of the peak load, and the maximum lengthening of the stirrups of 25.00 % occurred at 90% of the peak load. The levels have been verified by analyzing the crack pattern and the stirrups deformation obtained by the NLFEA studies.

➤ First crack formation

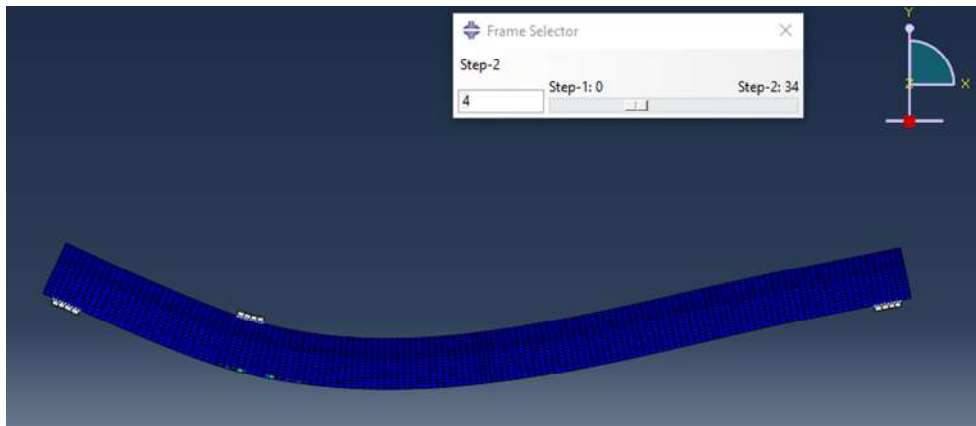


Figure 31. First crack formation – step individuation

➤ Yielding of the stirrups

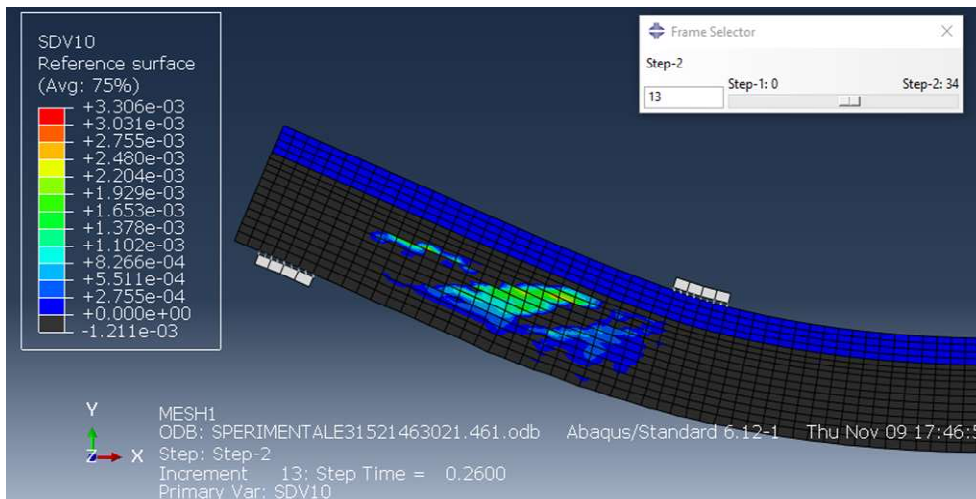


Figure 32. Yielding of the stirrups – step individuation

➤ Maximum lengthening of the stirrups

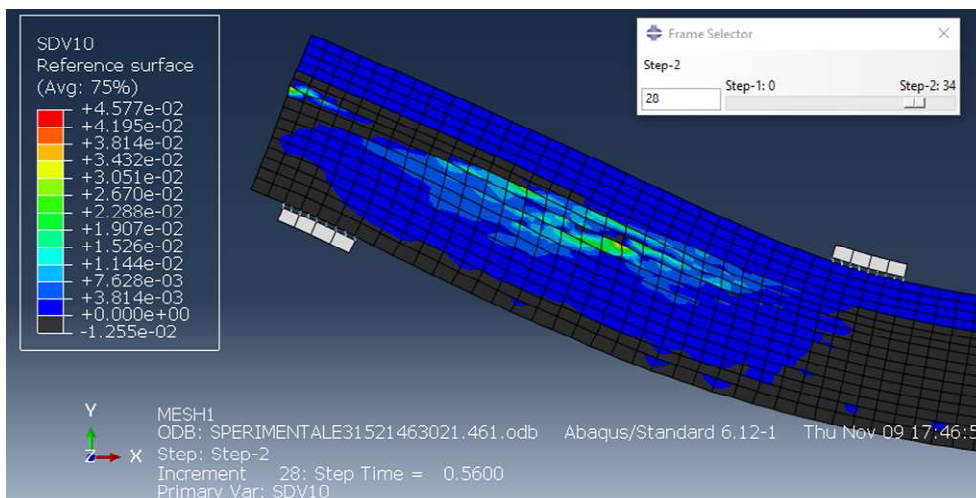


Figure 33. Maximum lengthening of the stirrups – step individuation

Table 15. NLFEA experimental simulation result

Step	u (mm)	P (kN)	$\frac{P}{P_u} \cdot 100$	Limit State
1	0.00	0.00	0.00	
1.02	0.50	16.75	9.29	
1.04	1.01	33.50	18.59	
1.06	1.51	49.41	27.42	
1.08	2.02	61.18	33.95	First crack formation
1.1	2.53	66.62	36.97	
1.12	3.04	72.18	40.05	
1.14	3.54	78.04	43.31	
1.16	4.05	83.75	46.47	
1.18	4.56	88.83	49.29	
1.2	5.07	93.67	51.98	
1.22	5.58	98.24	54.52	
1.24	6.09	102.38	56.81	
1.26	6.60	105.92	58.77	Yielding of the stirrups
1.28	7.11	108.82	60.38	
1.3	7.62	111.71	61.99	
1.32	8.13	115.18	63.91	
1.34	8.63	119.29	66.19	
1.36	9.14	123.89	68.74	
1.38	9.65	127.97	71.01	
1.4	10.16	132.19	73.35	
1.42	10.67	135.74	75.32	
1.44	11.18	140.03	77.70	
1.46	11.69	144.16	79.99	
1.48	12.20	148.25	82.27	
1.5	12.71	152.63	84.69	
1.52	13.22	156.51	86.84	
1.54	13.73	160.19	88.89	
1.56	14.23	164.29	91.16	Maximum lengthening of the stirrups
1.58	14.74	168.24	93.36	
1.6	15.25	171.68	95.26	
1.62	15.76	175.05	97.14	
1.64	16.27	178.44	99.02	
1.66	16.78	180.21	100.00	Peak Load
1.68	17.30	161.27	89.49	

The result obtained by experimental NLFEA are shown in Table 15; from this table, it could be concluded that the first crack formation occurs when the ratio between current load and peak load is roughly equal to 30%; the yielding stirrups was reached at the 60% while at 90% the limit stirrups deformation was reached. These 3 percentage levels and the peak load was used for the sensitivity analyses.

6.1.2.2. Sensitivity studies in deformation and load capacities

The results of the sensitivity studies for load levels of 30%, 60%, 90% and the peak load are shown for the variation in " f_c " in particular " $f_c + 10\%$ " and " $f_c - 10\%$ " in Table 16 and in Figure 34-Figure 35. The results for the load levels of 30%, 60% and 90% are significantly nonlinear in the forces (see Figure 34) and displacements (see Figure 35) for the investigated shear fracture process associated with the variations in f_c . This significant nonlinearity might be caused by a change in the shear fracture process. The results for the variation in " G_f " and " f_t " (sensitivity of the shear fracture process with respect to a variation in " G_f " or " f_t ") are shown in Table 17 and Table 18 respectively and in Figure 34-Figure 35. In these representations, significant nonlinear effects in the system response but also linear or no effects are again evident. In particular there are the following observations:

(a) sensitivity analyses at 30% of peak load (Figure 34.a): the changes are symmetric or linear except the f_c related ones. The f_c seems to be the most important parameter at this load level because of it provides a total jump between the columns higher than the total jump provided by the other mechanical parameters. With respect to the displacement (Figure 35.a), the change in f_t do not have an effect, the change in G_f shows a linear behavior and the change in f_c shows a non linear behavior. All the parameters except f_t seem to be significant for the displacement performance on this load level.

(b) sensitivity analyses at 60% of peak load (Figure 34.b): the changes are characterized by a nonlinear behavior for all the three mechanical parameters. Both f_c and f_t seem to be the most important parameters at this load level because the total jump between the columns provided by these parameters is higher than jump provided by G_f , and between these two there is almost no difference. With respect to the displacement (Figure 35.b), the change in f_t has a small effect, the change in G_f shows a non-linear and not-symmetric behavior while the change in f_c shows a non linear but symmetric behavior. In contrast to the load performance, only f_c seems to be the most significant parameter for the displacement performance on this load level.

(c) sensitivity analyses at 90% of peak load (Figure 34.c): the changes are non-linear except for f_t . The f_c seems to be the most important parameter at this load level because the total jump between the columns provided by this parameter is higher than jumps provided by the others mechanical paramaters. With respect to the displacement (Figure 35.c), the changes are also non-linear except for f_t ; the change in G_f shows a decrease in the displacement provided by a decrease in G_f while

almost no effects are derived by an increase in G_f . The f_c seems to be the most significant parameter also for the displacement performance on this load level.

(d) sensitivity analyses at peak load (Figure 34.d): substantially, this case is similar to the case (c); the changes are non-linear except for f_t and the f_c seems to be the most important parameter. With respect to the displacement, some differences occur; the changes are non-linear except for G_f which provides small effects. The f_c seems to be the most significant parameter also for the displacement performance on this load level.

Table 16. NLFEA results based on compressive strength sensitivity analyses

Sim.	Load Levels							
	30% Peak Load		60% Peak Load		90% Peak Load		Peak Load	
	Load (kN)	Displacement (mm)	Load (kN)	Displacement (mm)	Load (kN)	Displacement (mm)	Load (kN)	Displacement (mm)
From “ f_c original matrix”								
1	43.19	1.5	90.3	6.6	136.64	12.2	153.71	14.7
2	59.53	2.0	106.84	7.1	161.95	13.7	178.26	16.3
3	56.99	2.0	113.34	8.6	166.23	14.7	186.07	17.3
4	63.66	2.0	117.32	7.6	174.72	14.2	194.59	16.7
5	66.79	2.0	129.38	8.6	196.82	16.3	217.39	18.8
6	64.98	2.0	125.42	8.1	188.86	15.3	210.74	19.4
7	66.22	3.0	129.81	10.1	193.42	17.1	212.88	19.7
Mean Value	60.19	2.1	116.06	8.1	174.09	14.8	193.38	17.5
From “ $f_c + 10\%$ matrix”								
1	43.64	1.5	95.12	7.1	141.75	12.7	156.63	14.7
2	59.79	2.0	118.77	8.6	179.47	15.8	200.80	18.9
3	57.36	2.0	109.21	8.1	166.66	14.7	185.57	17.3
4	63.92	2.0	122.15	8.1	184.85	15	207.25	19.2
5	66.9	2.0	125.37	8.1	183.38	14.8	205.62	18.8
6	65.12	2.0	121.73	7.6	183.6	14.8	204.78	17.3
7	66.55	3.0	130.32	10.1	194.96	17.1	218.52	20.2
Mean Value	60.47	2.1	117.52	8.2	176.38	15.0	197.02	18.1
From “ $f_c - 10\%$ matrix”								
1	43.29	1.5	81.36	5.6	123.15	10.6	137.88	12.7
2	46.62	1.5	99.33	6.1	151.87	12.7	168.07	15.3
3	56.89	2.0	108.44	8.1	163.92	14.7	180.48	17.3
4	53.45	1.5	112.68	7.1	168.56	13.7	187.57	16.2
5	66.7	2.0	125.36	8.1	186.52	15.2	206.59	17.8
6	50.7	1.5	112.41	6.6	168.48	13.2	188.97	16.8
7	66.24	3.0	129.14	10.1	188.53	16.6	211.28	19.7
Mean Value	54.84	1.9	109.82	7.4	164.43	13.8	182.98	16.5

FRACTILES BASED SAMPLING PROCEDURE

Table 17. NLFEA results based on fracture energy sensitivity analyses

Sim.	Load Levels							
	30% Peak Load		60% Peak Load		90% Peak Load		Peak Load	
	Load (kN)	Displacement (mm)	Load (kN)	Displacement (mm)	Load (kN)	Displacement (mm)	Load (kN)	Displacement (mm)
From " G_f original matrix"								
1	46.15	1.5	99.95	7.1	149.33	12.7	165.87	14.7
2	59.8	2.0	109.04	7.6	162.35	13.8	178.65	15.8
3	61.77	2.0	125.98	9.2	193.79	16.7	213.22	19.3
4	63.71	2.0	124.96	8.7	187.59	15.8	206.36	18.4
5	65.3	2.0	130.5	9.2	192.4	16.3	214.92	19.3
6	63.53	2.0	120.03	8.1	178.6	15.2	200.64	18.2
7	63.5	2.0	127.52	8.6	192.98	16.2	215.37	19.2
Mean Value	60.54	1.9	119.71	8.4	179.58	15.2	199.29	17.8
From " $G_f + 10\%$ matrix"								
1	56.59	2.0	105.06	7.6	158.08	13.7	173.32	15.8
2	60.01	2.0	109.67	7.6	162.6	13.8	182.52	16.3
3	61.93	2.0	126.46	9.1	194.95	16.7	213.75	19.3
4	63.93	2.0	120.82	8.2	179.6	14.8	198.87	17.3
5	65.34	2.0	127.67	8.7	193.39	16.2	213.49	19.3
6	63.36	2.0	120.61	8.2	179.2	15.2	199.69	18.2
7	63.05	2.0	127.81	8.7	192.73	16.2	214.95	19.2
Mean Value	62.03	2.0	119.73	8.3	180.08	15.2	199.51	17.9
From " $G_f - 10\%$ matrix"								
1	46.5	1.5	99.57	7.1	148.63	12.7	167.29	15.2
2	48.81	1.5	112.78	8.2	166.24	14.3	184.18	16.8
3	61.81	2.0	120.32	8.7	180.00	15.2	198.47	17.8
4	63.92	2.0	119.62	8.2	174.56	14.3	195.75	17.4
5	65.27	2.0	121.68	8.2	182.94	15.2	203.11	19.3
6	63.29	2.0	119.3	8.1	181.84	15.7	201.11	18.7
7	63.00	2.0	117.88	7.6	177.57	14.7	197.15	18.7
Mean Value	58.94	1.9	115.88	8.0	173.11	14.6	192.44	17.7

FRACTILES BASED SAMPLING PROCEDURE

Table 18. NLFEA results based on tensile strength sensitivity analyses

Sim.	Load Levels							
	30% Peak Load		60% Peak Load		90% Peak Load		Peak Load	
	Load (kN)	Displacement (mm)	Load (kN)	Displacement (mm)	Load (kN)	Displacement (mm)	Load (kN)	Displacement (mm)
	From " f_t original matrix"							
1	47.72	1.5	97.06	6.6	146.19	12.2	162.27	14.2
2	55.8	2.0	99.6	7.1	152.76	13.2	169.06	15.2
3	56.76	2.0	104.39	7.6	160.33	14.3	176.18	16.3
4	60.67	2.0	119	8.6	177.01	15.2	198.14	18.3
5	65.44	2.0	118.51	7.7	177.8	14.8	198.38	18.4
6	69.55	2.0	133.11	8.1	199.8	15.8	221.37	18.8
7	72.29	2.0	139.91	9.2	210.81	17.3	232.72	20.7
Mean Value	61.18	1.9	115.94	7.8	174.96	14.7	194.02	17.4
	From " $f_t + 10\%$ matrix"							
1	48.76	1.5	103.04	7.1	156.12	13.2	172.10	15.2
2	57.31	2.0	109.27	8.1	166.21	14.7	185.21	17.8
3	58.2	2.0	109.49	8.1	161.28	14.3	179.64	16.8
4	62.29	2.0	133.47	7.6	169.28	14.2	190.29	17.8
5	66.78	2.0	121.03	7.6	183.41	15.3	202.79	17.9
6	71.19	2.0	130.16	7.6	191.9	14.7	215.38	18.8
7	73.9	2.0	142.16	9.2	211.97	17.3	235.52	20.4
Mean Value	62.63	1.9	121.23	7.9	177.17	14.8	197.28	17.8
	From " $f_t - 10\%$ matrix"							
1	47.15	1.5	96.34	6.6	145.13	12.2	161.00	14.2
2	54.57	2.0	103.12	7.6	156.02	13.7	175.27	16.2
3	55.72	2.0	103.69	7.6	150.98	13.2	169.95	15.8
4	59.15	2.0	117.63	8.6	179.21	15.7	197.22	18.3
5	64.37	2.0	115.39	7.6	173.39	14.3	193.86	16.9
6	67.74	2.0	134.63	8.6	205.43	16.8	226.69	19.9
7	70.5	2.0	129.51	8.1	190.89	15.3	213.96	19.3
Mean Value	59.89	1.93	114.33	7.81	171.58	14.5	191.14	17.2

6.1.2.3. Sensitivity studies in crack pattern developments

To justify the different behavior which occurs in the load variations (linear and non linear trend of variation) an interestingly study on the crack pattern development in the shear failure region area was led. The aim of this topic was therefore evaluate the difference in term of shape, size and orientation of the crack, provided by mechanical parameters changes. Preliminary observation could be made by observing:

- Figure 36, crack pattern development with crack width $w_c = 0.5$ to 1.0 mm at different load levels;
- Figure 37, Crack pattern development at 90% of peak load associated with different crack width limits;

Since at 30% of peak load no crack occur in the selected area and at 90% of peak load the crack development was just stabilized and perhaps affected by uncertainties provided by numerical errors occurring near the peak load, the crack pattern at 60% of peak load was chosen to pursue this discussion (Figure 38). It is important to highlight that only a simplified visual study is proposed, while a more precise study based for instance on the Digital Image Correlation (DIC), that it should be recommended, will be shown in a next step of this research program. In particular, for each of the three mechanical parameters investigated, the following observations are possible:

(f_c) crack development (Figure 38): two branches are visible in the reference state (crack pattern obtained by the original compressive strength) and the crack width in the main branch reach a value greater than 1 mm; an increase by 10% of compressive strength leads to a crack pattern made of only one branch with a crack width standing around 0.5 mm while a decrease in the same value provides almost no crack in the region.

(G_f) crack development (Figure 38): three branches could be seen from the reference state and the crack width of the great size one has a value around 0.5 mm / 0.7 mm; an increase by 10% of G_f provides almost no effect in the crack pattern development (indeed from the histogram reported in Figure 34.b there are no change in term of load). Otherwise, one more branch is drawn in the crack pattern corresponding at a 10% decrease of G_f , with respect to the reference state. This one, provides a decrease in term of load (see fourth and fifth column reported in Figure 34.b).

(f_t) crack development (Figure 38): also in this case, roughly three branches are drawn in the reference state; an increase by 10% of f_t provides evident difference from the reference state, indeed only one crack is drawn. This fact, provides an high load variation. On the other hand, a decrease by 10% of f_t leads to the same truss system developed in the reference state but with one more branch which as seen in the case of G_f , afford a small load decrease. For this reason, one can see from the last three columns of Figure 34.b there is overall a non-linear variation.

FRACTILES BASED SAMPLING PROCEDURE

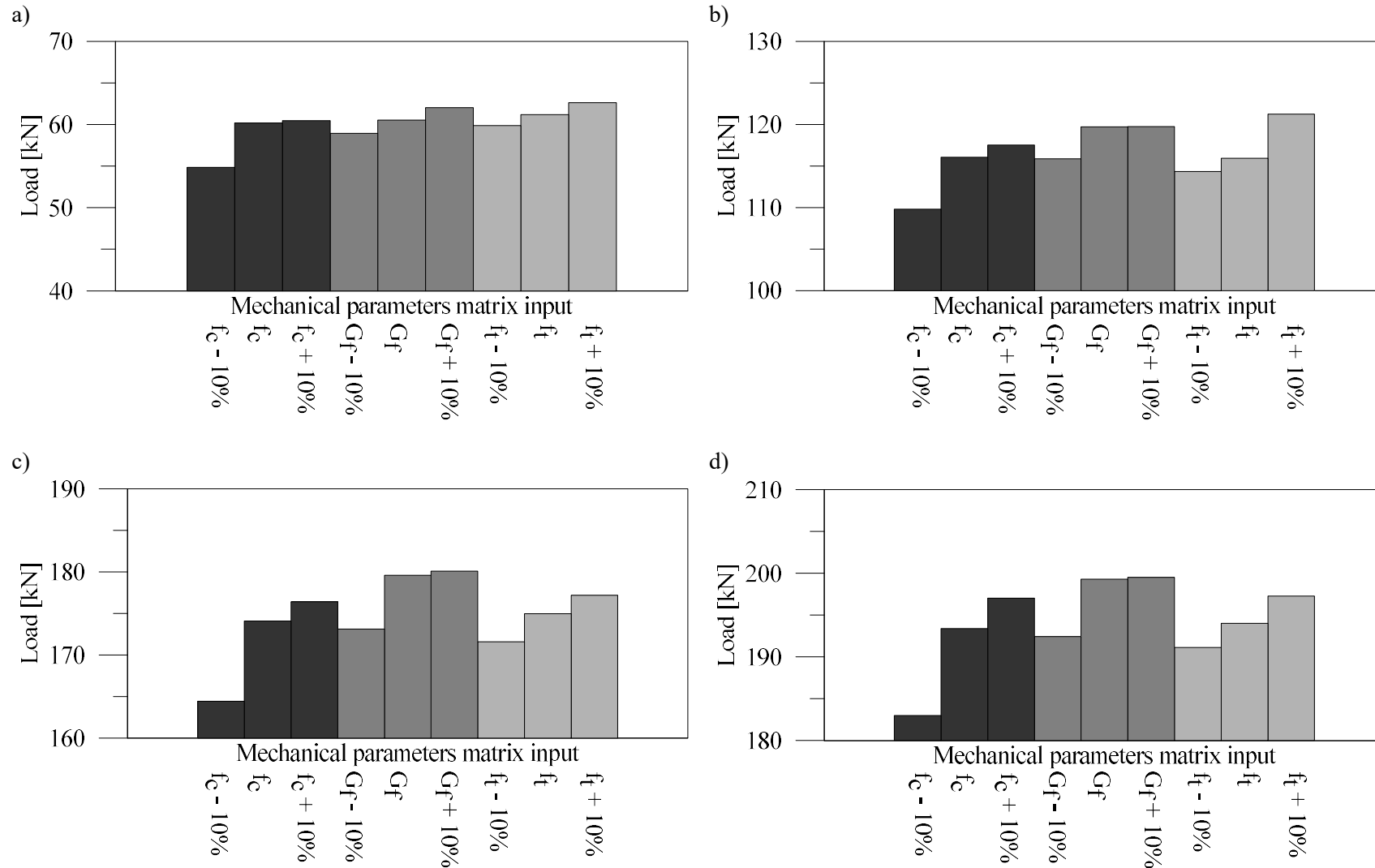


Figure 34. Sensitivity Analyses results: the figure shows the change in term of *load* at (a) 30% of peak load, (b) 60% of peak load, (c) 90% of peak load, (d) peak load. Going from lower load to the peak load, the influence of compressive strength is most important rather than the other mechanical parameters.

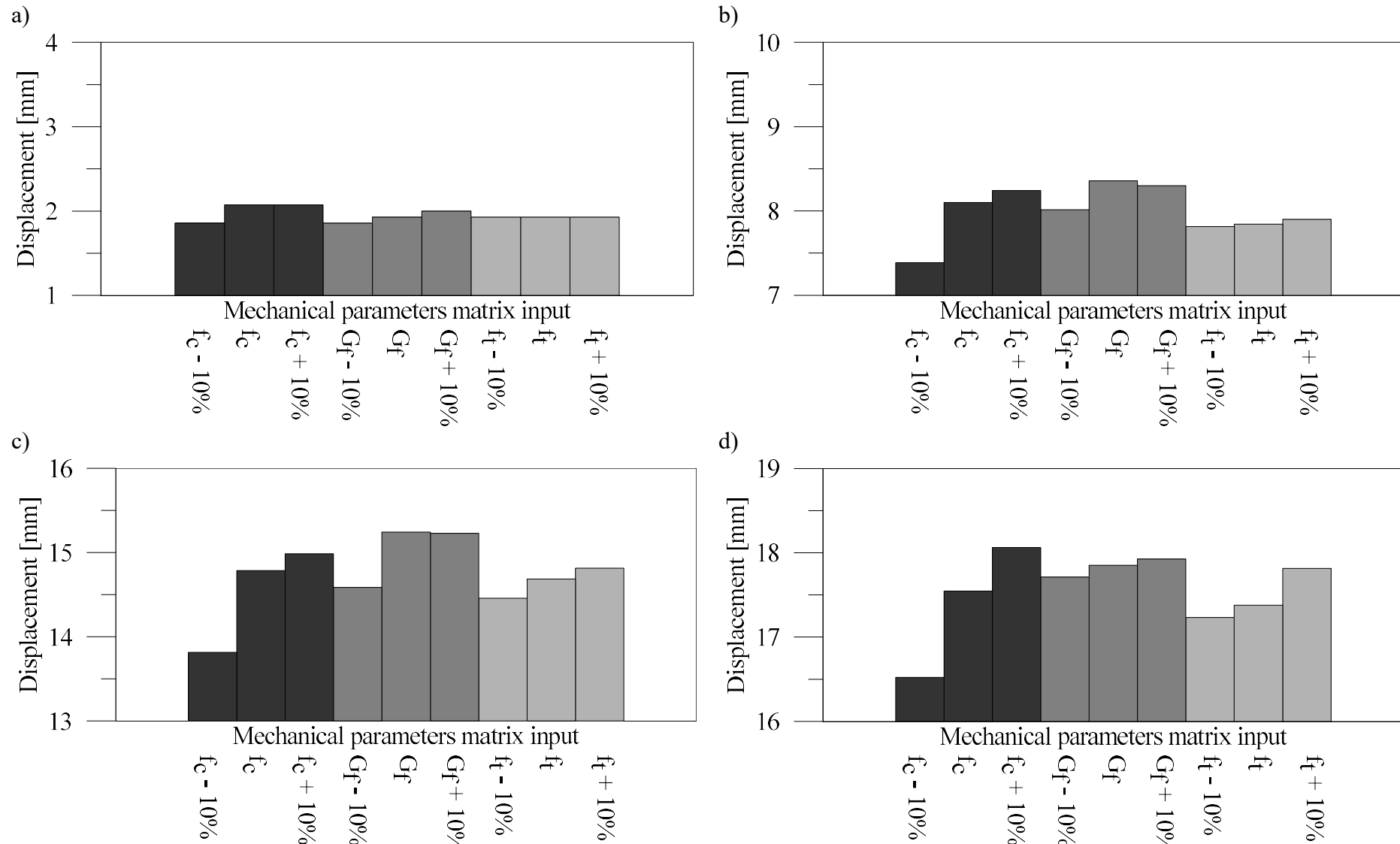


Figure 35. Sensitivity Analyses results: the figure shows the change in term of *displacement* at (a) 30% of peak load, (b) 60% of peak load, (c) 90% of peak load, (d) peak load. Also in this case, going from lower load to the peak load, the influence of compressive strength is most important rather than the other mechanical parameters.

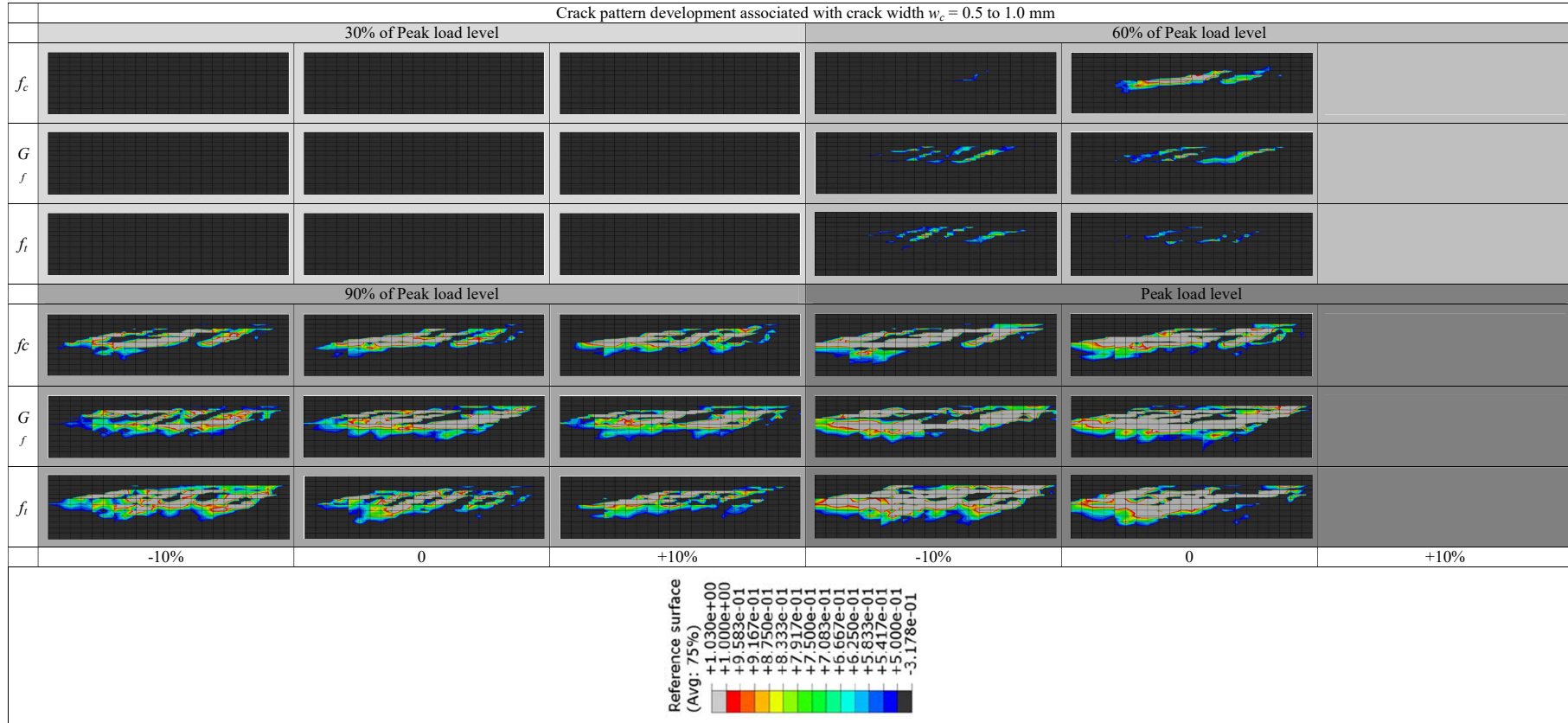


Figure 36. Crack pattern development associated with crack width $w_c = 0.5$ to 1.0 mm at different load levels;

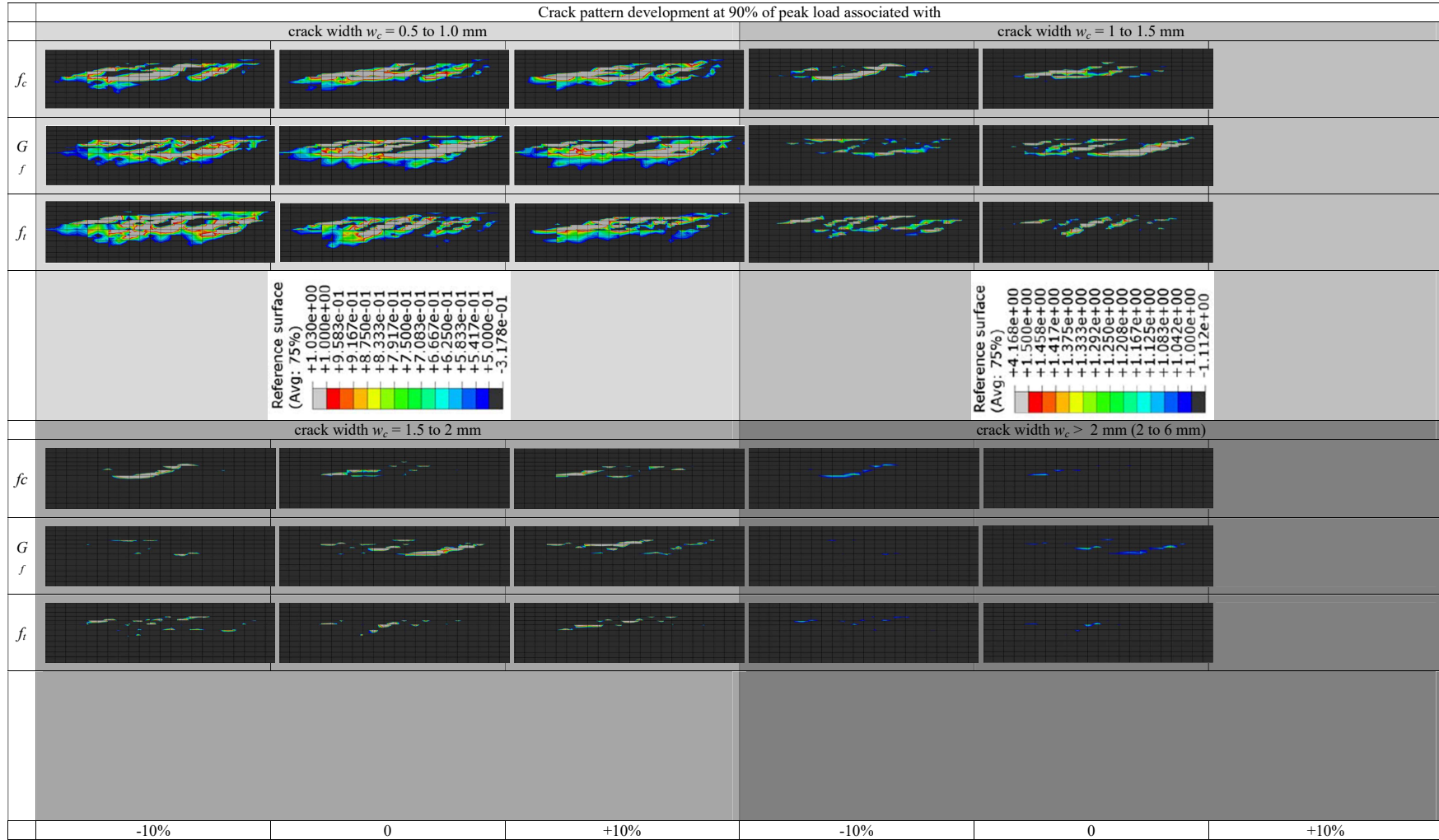


Figure 37. Crack pattern development at 90% of peak load associated with different crack width limits;

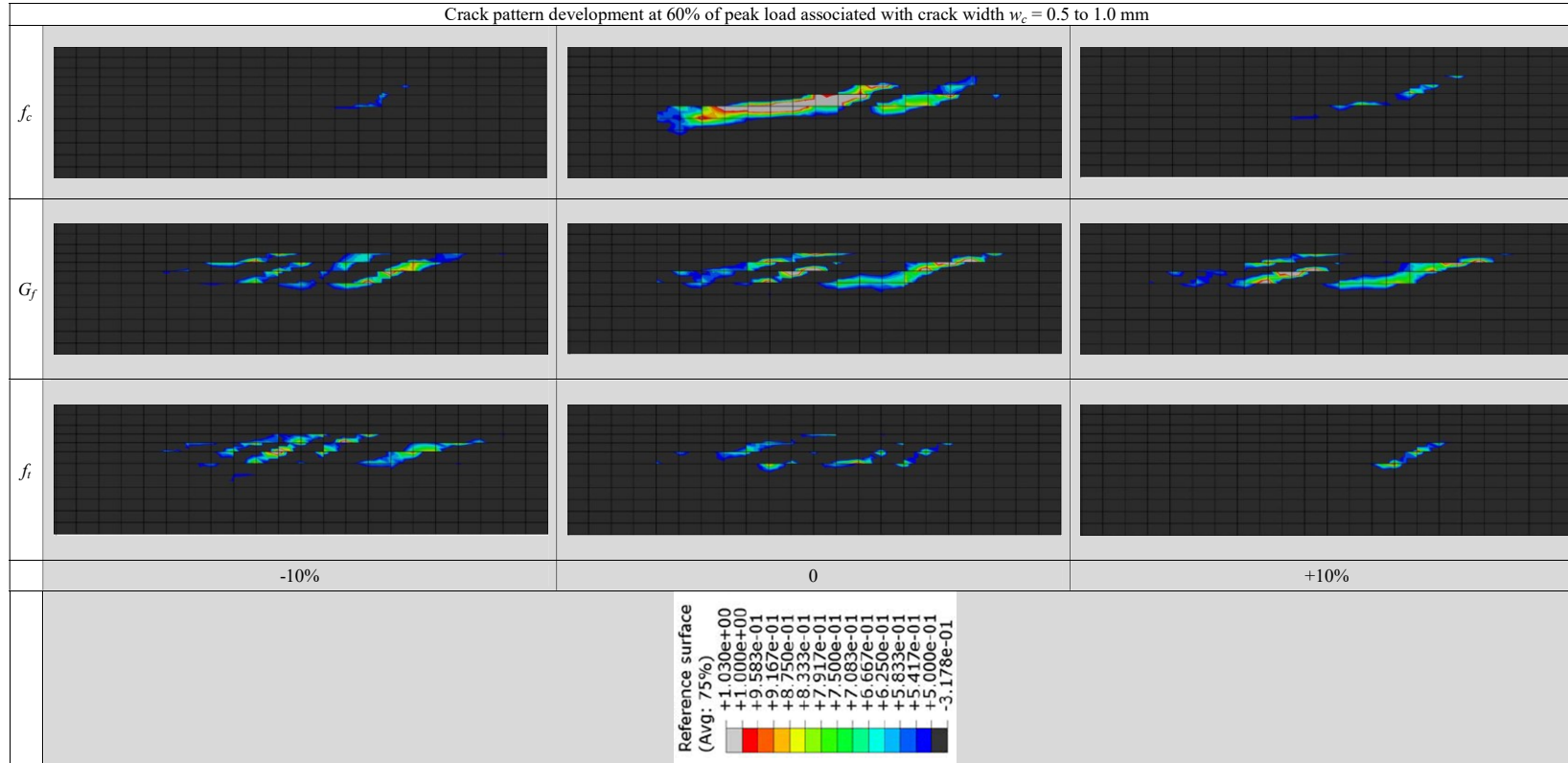


Figure 38. Crack pattern development at 60% of peak load associated with crack width $w_c = 0.5$ to 1.0 mm; notice that the comparison could be made only between crack pattern on the same row, because a change in the row provides a change in the leading parameter i.e. in the mechanical parameters values;

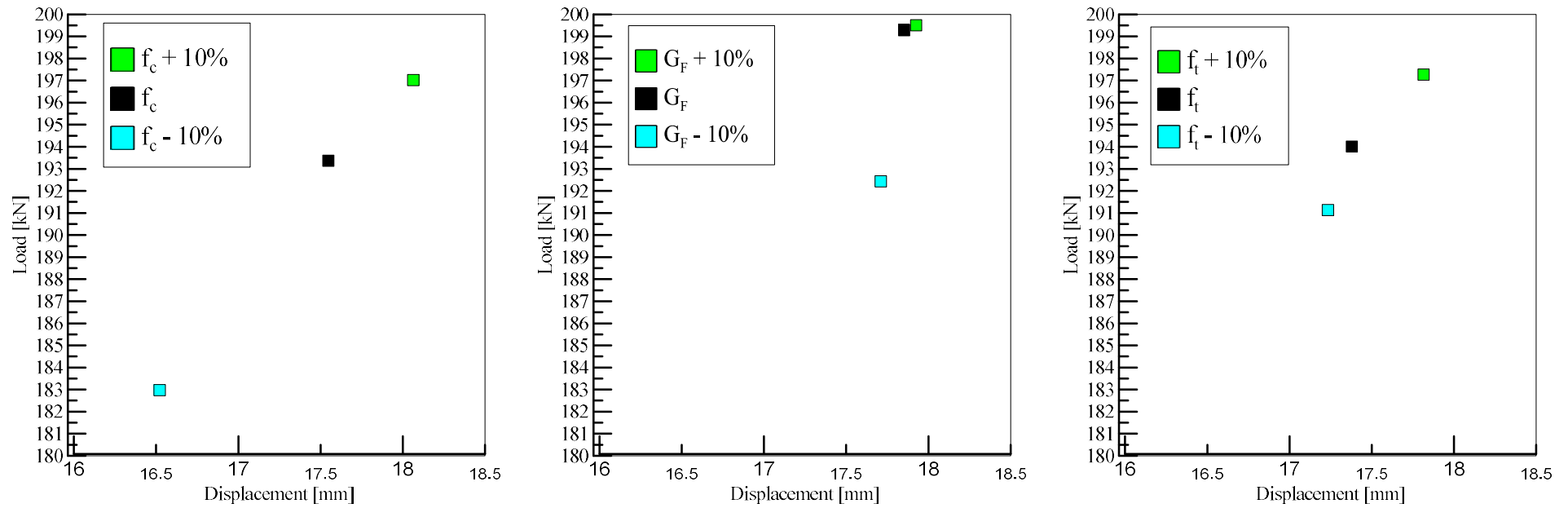


Figure 39. Sensitivity analysis at peak load, from left to right for compressive strength, fracture energy and tensile strength

By observing Figure 39, as a matter of fact the distance between the original point and another representative point (corresponding at a change of the leading parameter) is higher for the compressive strength than for the fracture energy.

This means that a little change in compressive strength provides an higher difference in term of peak load than a little change in fracture energy.

To have a numeric comparison for each couple of values (original-increased/decreased) the norm of the vector linking two points was evaluated. Of course, for the mechanical parameters that most influence the failure mechanism of the girder, we have to expect an higher norm of the vector.

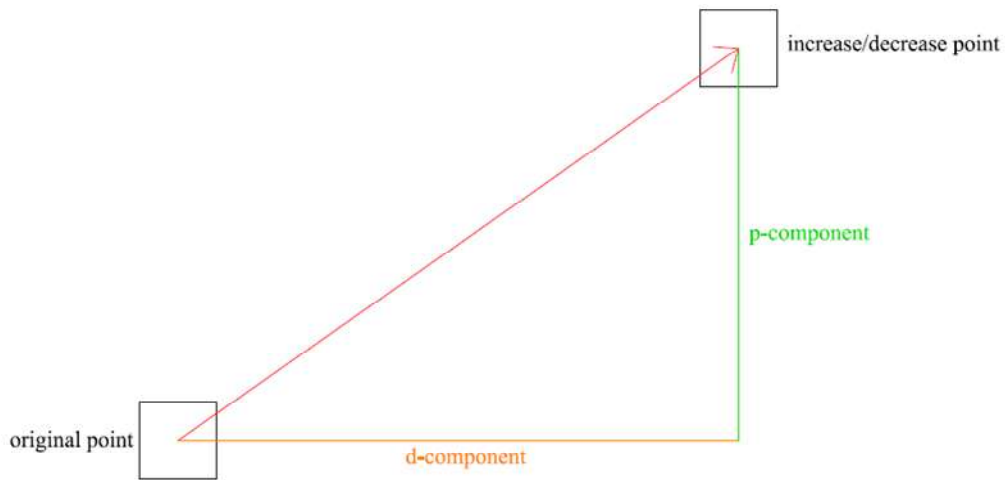


Figure 40. Vector linking two points

Known the 2 components of the vector linking 2 points, its norm (N_{link}) was evaluated:

$p_{component}$: absolute value of the difference between the load at the original point and the load at increase/decrease point;

$d_{component}$: absolute value of the difference between the displacement at the original point and the displacement at increase/decrease point;

$$N_{link} = \sqrt{(d_{component})^2 + (p_{component})^2}$$

Known that the different dimensions between the two components of the vector are not relevant, because we are interesting to evaluate a geometric quantity.

EVALUATION FOR INCREASE POINT

MATRIX	R_m	d_m	$d_{component}$	$p_{component}$	N_{link}
Original G_f	199.29	17.85	0.07	0.22	0.23
$G_f + 10\%$	199.51	17.93			
Original f_c	193.38	17.55	0.52	3.65	3.68
$f_c + 10\%$	197.02	18.06			
Original f_t	194.02	17.38	0.44	3.26	3.29
$f_t + 10\%$	197.28	17.81			

EVALUATION FOR DECREASE POINT

MATRIX	R_m	d_m	$d_{component}$	$p_{component}$	N_{link}
Original G_f	199.29	17.85	0.14	6.86	6.86
$G_f - 10\%$	192.44	17.71			
Original f_c	193.38	17.55	1.03	10.40	10.45
$f_c - 10\%$	182.98	16.52			
Original f_t	194.02	17.38	0.15	2.88	2.88
$f_t - 10\%$	191.14	17.23			

The graphical results previously obtained are supported by these quantitatively results; therefore it can be concluded that the mechanical parameter that most influence the failure mechanism of this girder is the compressive strength, because little changes in its value provide higher changes in the structural response rather than the changes in the structural response provided by other mechanical parameters.

6.1.3. Validation based on Target Correlation Matrix

An interestingly way to evaluate which is the best leading parameter in term of input mechanical parameters is proposed in this topic. As it was shown, FP was the exact method, and with it, all the mechanical parameters were correlated by means of Target Correlation Matrix. For each couple of variables (for example between compressive strength and tensile strength) the correlation between these two is ensured by a specific Pearson correlation coefficient (contained in the Target Correlation Matrix. When FBSP was used, only seven samples were selected from the N samples available in the context of FP; as seen, this selection is based on the fractile leading parameter values, in this way a change of leading parameter provides a change of the seven selected samples i.e. a change in the structural response see §6.1.4. Specifically, the correlation between the even mechanical parameter values (for each couple of variables) will be different from the correlation between the N mechanical parameters values for the same couple of variables used in the context of FP and also this correlation changes by changing the leading parameter. For this reason, it is interesting to evaluate which is the leading parameter using in the context of FBSP to reach a correlation between the seven selected samples closer to that of the N samples (which is the exact correlation). To achieve this aim, a simply but efficient Matlab script was developed. By loading in the code the seven mechanical parameters values for all the variable describing the problem, the code evaluates the Pearson correlation coefficient for each couple of variables and it builds the correlation matrix which will be the correlation matrix obtained by using FBSP with a specific leading parameter. In this way, denote as \mathbf{T} the exact target correlation matrix implemented in FReET and with \mathbf{T}_x the target correlation matrix obtained by using FBSP with x leading parameter, an error matrix could be evaluated, by using Eq.(48).

$$\mathbf{E} = \mathbf{T} - \mathbf{T}_x \tag{48}$$

To evaluate which is the error occurred by changing the leading parameter, the second-order-norm of matrix \mathbf{E} was calculated. The second-order-norm used in this work is the “spectral norm” of a matrix.

$$n_A = [\text{f}(\mathbf{A}^T \cdot \mathbf{A})]^{1/2} \tag{49}$$

Denoting \mathbf{A} as a generic matrix, the second-order-norm of \mathbf{A} , represented here as $n_{\mathbf{A}}$, was evaluated by using Eq.(49). In this expression f is a function that provides the maximum eigenvalue between all eigenvalues of the matrix in square brackets, which is equal to the scalar product between \mathbf{A} and its transposed matrix. To check the Matlab code, the N samples generated by FReET in the context of FP application, were loaded in this script; because of these samples has been generated by using the exact target correlation matrix (implemented in FReET), the evaluated norm by the script should be equal to zero. The script returned a norm equal to 0.0024 (i.e. 0.2% is the error committed, and it is only an approximation error..). The different norm evaluated by repeating this work, in the context of FBSP by using different leading parameters, are shown in Table 19. As one can seen from this table, if compressive strength was leading parameter, the evaluated norm error was lower than the same norm evaluated by using fracture energy or tensile strength leading parameter. This means that compressive strength leads to a correlation between the variables closer to the exact correlation.

Table 19. Error norm in target correlation matrix

FBSP			
Leading Parameter			
	Compressive strength	Fracture energy	Tensile strength
n (%)	25	92	52

In conclusion, three ways to correctly evaluated which is the best leading parameter were proposed. In the next paragraphs, the application of FBSP by using different leading parameters will be illustrated. The aim of this application will be making a comparison between the response curve obtained by FBSP with a generic leading parameter and the FP.

6.1.4. Validation based on FBSP

In this chapter, will be shown three different applications of FBSP by changing the leading parameter:

- FBSP by using compressive strength leading parameter (FBSPC, see §6.1.4.1);
- FBSP by using tensile strength leading parameter (FBSPPT, see §6.1.4.2);
- FBSP by using fracture energy leading parameter (FBSPG, see §6.1.4.3);

Aim of this topic, is the comparison between the PDF describing the structural response obtained by FP, with the three PDFs obtained by applying FBSP changing the leading parameter.

6.1.4.1. Compressive strength leading parameter

In this paragraph is reported FBSP application by using concrete compressive strength leading parameter. Known the probability density function of the compressive strength, its value assumed at the prescribed fractiles was calculated with the inverse of its PDF.

Table 20. Values of compressive strength at fractiles and corresponding sets

Fractiles	f_c [MPa]	Set
5%	53.4	212
15%	64.8	117
30%	72.5	13
50%	79.1	99
70%	84.5	87
85%	89.0	174
95%	93.5	46

Table 23 show the results obtained by the 7 NLFEA (one for each set). The design resistance was calculated by using Eq.(46) , in which mean value and standard deviation were calculated by the seven values of the peak loads reported in Table 23.

Table 21. Concrete and steel mechanical parameters associated to fractiles of compressive strength.

Set	f_c [MPa]	f_t [MPa]	G_f [N/mm]	E_c [MPa]	E_s [MPa]	f_{ys} [MPa]
212	53.4	2.6	0.139	3.11E+04	1.98E+05	1381.1
117	64.8	4.0	0.220	3.13E+04	2.00E+05	1371.2
13	72.5	3.3	0.146	3.31E+04	1.96E+05	1390
99	79.1	4.3	0.261	3.91E+04	2.02E+05	1430
87	84.5	4.7	0.217	3.65E+04	2.09E+05	1410.2
174	89.0	4.6	0.288	3.45E+04	2.08E+05	1385.6
46	93.5	3.4	0.174	3.89E+04	2.06E+05	1352.5

Table 22. Tendons mechanical parameters associated to the fractiles of compressive strength.

Set	E_t [MPa]	f_{yt} [MPa]	P [MN]
212	1.91E+05	1381.1	0.041
117	1.97E+05	1371.2	0.043
13	1.97E+05	1390	0.041
99	2.02E+05	1430	0.039
87	2.01E+05	1410.2	0.043
174	2.03E+05	1385.6	0.043
46	1.89E+05	1352.5	0.035

Table 23. NLFEA results of FBSP by using compressive strength as leading parameter

Simulation	Set	Peak Load [kN]
1	212	153.71
2	117	178.26
3	13	186.07
4	99	194.59
5	87	217.39
6	174	210.74
7	46	212.88

6.1.4.2. Tensile strength leading parameter

The FBSP shown in §6.1.4.1 was repeated changing the leading parameter from compressive strength to tensile strength.

Table 24. Tensile strength at fractiles.

Fractiles	f_t [MPa]
5 th	2.85
15 th	3.14
30 th	3.42
50 th	3.77
70 th	4.18
85 th	4.67
95 th	5.39

Table 25. Concrete and Steel mechanical parameters associated to the fractiles of tensile strength.

Set	f_c [MPa]	f_t [MPa]	G_f [N/mm]	E_c [MPa]	E_s [MPa]	f_{ys} [MPa]
69	67.45	2.86	0.154	3.50E+4	2.00E+5	618.28
7	67.06	3.14	0.144	3.29E+4	2.04E+5	602.14
139	69.33	3.42	0.145	3.06E+4	2.00E+5	599.08
176	74.74	3.77	0.201	3.53E+4	2.00E+5	631.33
288	82.11	4.18	0.215	3.58E+4	1.97E+5	598.17
249	88.44	4.67	0.456	3.96E+4	2.01E+5	602.36
89	104.18	5.38	0.265	4.03E+4	2.01E+5	636.59

Table 26. Tendons mechanical parameters associated to the fractiles of tensile strength.

Set	E_t [MPa]	f_{yt} [MPa]	P [MN]
69	1.96E+5	1392.8	0.0421
7	1.89E+5	1339.8	0.0402
139	1.85E+5	1360.8	0.0421
176	1.93E+5	1360.4	0.0408
288	1.92E+5	1365.3	0.0454
249	1.99E+5	1442.3	0.0437
89	1.91E+5	1398.0	0.0429

Table 27. Results with FBSP by using tensile strength as leading parameter.

Simulation	Set	Peak Load [kN]
1	69	162.39
2	7	169.18
3	139	176.30
4	176	198.26
5	288	198.50
6	249	221.49
7	89	232.83

6.1.4.3. Fracture energy leading parameter

Table 28. Fracture energy at fractiles.

Fractiles	G_F [N/mm]
5 th	0.126
15 th	0.152
30 th	0.177
50 th	0.208
70 th	0.245
85 th	0.289
95 th	0.354

Table 29. Concrete and Steel mechanical parameters associated to the fractiles of fracture energy.

Set	f_c [MPa]	f_t [MPa]	G_f [N/mm]	E_c [MPa]	E_s [MPa]	f_{ys} [MPa]
<i>118</i>	66.76	3.15	0.126	3.23E+4	2.04E+5	606.94
<i>135</i>	75.02	3.20	0.152	3.40E+4	1.97E+5	616.16
<i>84</i>	87.37	3.49	0.177	3.97E+4	2.00E+5	615.53
<i>31</i>	80.31	3.49	0.208	3.69E+4	2.03E+5	649.04
<i>181</i>	91.75	4.41	0.245	3.81E+4	1.98E+5	615.95
<i>244</i>	80.55	4.78	0.289	3.57E+4	1.93E+5	620.7
<i>266</i>	74.27	4.96	0.352	3.46E+4	2.08E+5	627.43

Table 30. Tendons mechanical parameters associated to the fractiles of tensile strength.

Set	E_t [MPa]	f_{yt} [MPa]	P [MN]
118	1.97E+5	1450.7	0.0421
135	1.98E+5	1415.0	0.0445
84	1.98E+5	1372.3	0.0412
31	1.95E+5	1394.9	0.0450
181	1.96E+5	1391.6	0.0410
244	1.94E+5	1450.9	0.0385
266	1.96E+5	1393.9	0.0382

Table 31. Design Resistance obtained with different methods.

	FBSPC	FBSPT	FP	FBSPG
R_d [kN]	132.30	127.38	133.39	145.41

6.1.4.3.1. Structural response evaluation

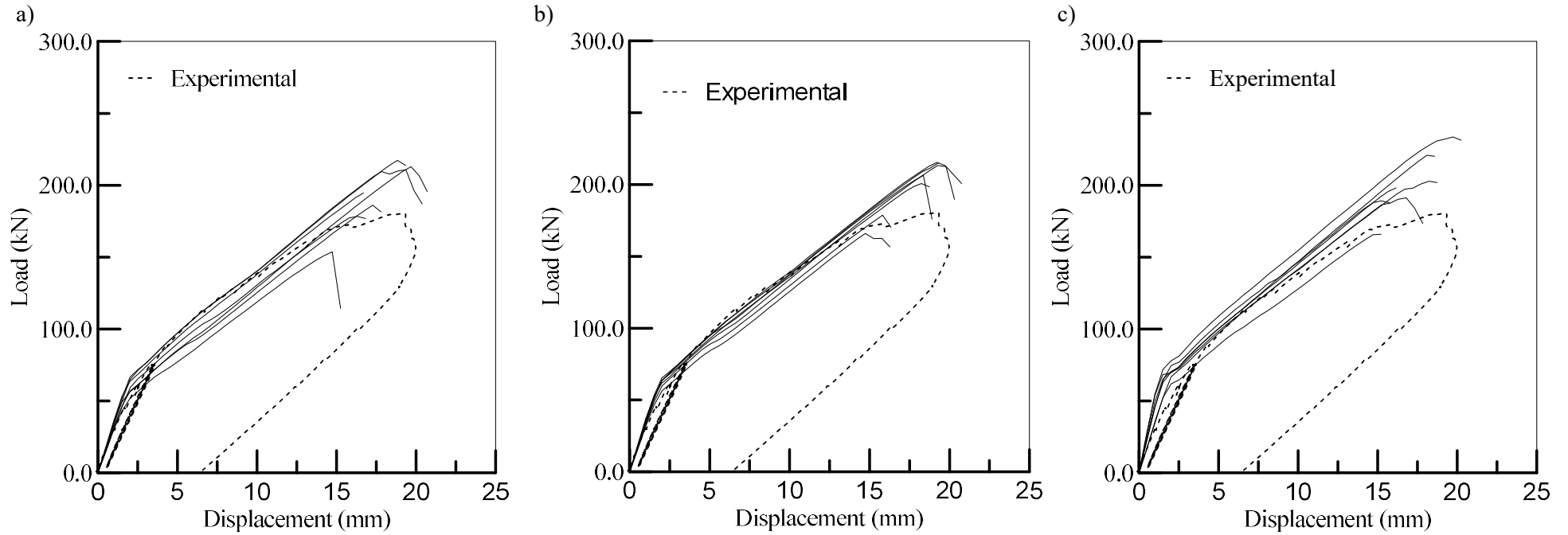


Figure 41. Structural response evaluation by using FBSP with different leading parameters: a) compressive strength, b) fracture energy, c) tensile strength;

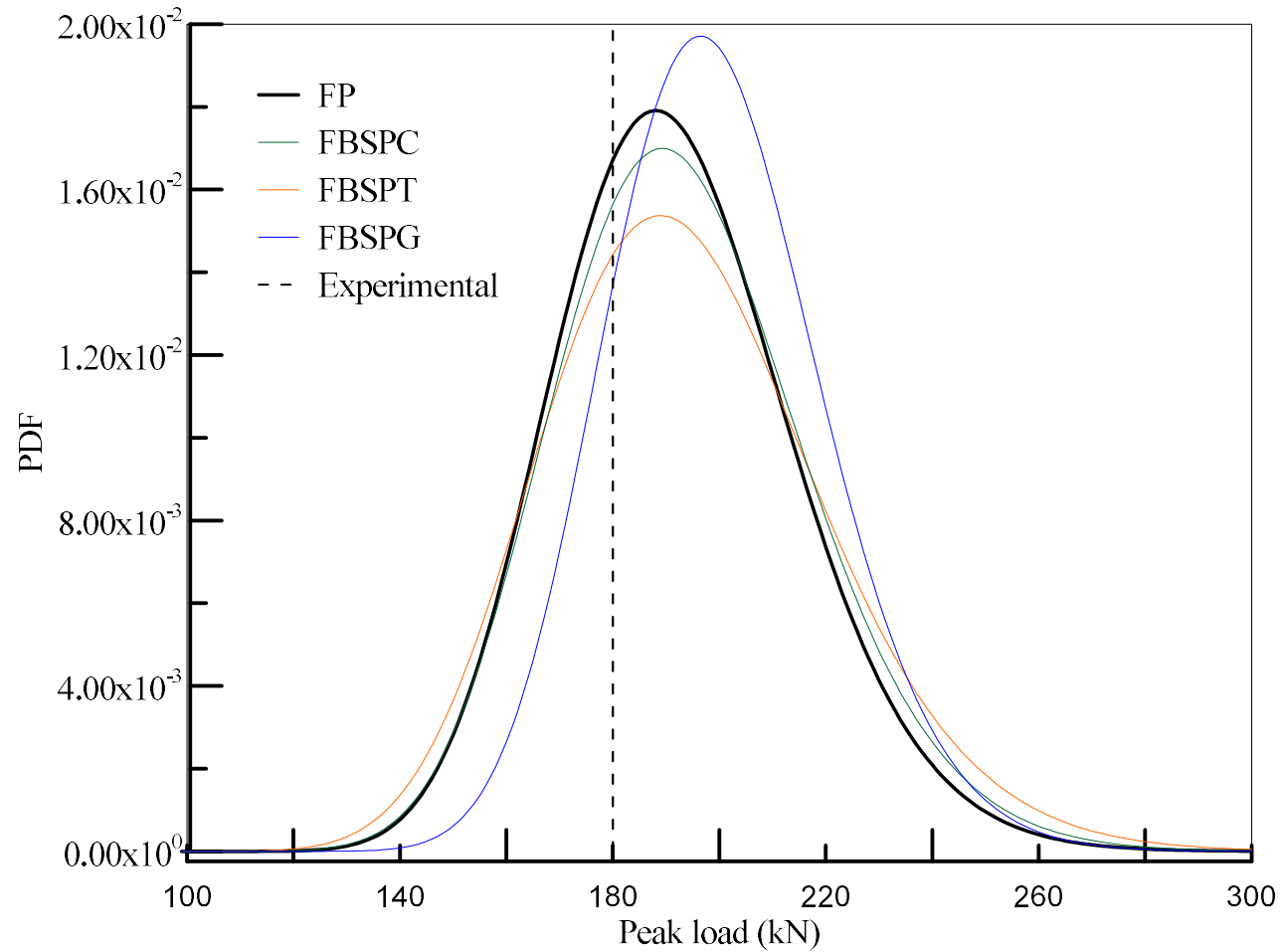


Figure 42. Different log-normal responses curves by using FBSP adopting different leading parameters: compressive strength (FBSPC), tensile strength (FBSPT) and fracture energy (FBSPG). There are also reported the log-normal response curve obtained by using FP approach and the mean load obtained from the experimental load test led on the analyzed T-shaped girder;

To determine which is the best leading parameter, in the context of this approach, a comparison of PDFs of the FBSP describing the structural response with the Log-Normal PDF, obtained by a fully probabilistic (FP) FReET simulation, is requested. On the other hand, for each seven analyses set, a Log-Normal distribution was evaluated and compared with the Log-Normal obtained by the FP method (from 301 peak loads).

As one can see from Figure 42, if tensile strength was leading parameter (FBSPT), the obtained log-normal response curve is located below the FP log-normal response curve (assumed here such as the exact solution). Otherwise, fracture energy leading parameter (FBSPG) provides an overestimation of the results (indeed the curve in this case is shifted on the right and it provides an high value of the mean value). Finally, the log-normal response curve obtained when compressive strength was selected leading parameter match better the FP log-normal response curve.

Hence, the FBSPC associated leading parameter f_c seems to be the appropriate one and capturing the correlation as defined for the full sample field

In Figure 42 it is also reported in term of vertical dashed line, the mean peak load obtained from the experimental test load led on the T-shaped analyzed girder. Making a comparison between this line and the mean peak load values obtained by the probabilistic approaches treated in this paragraph, it could be seen that both the FP and FBSP lead to a little overestimation of the mean peak load value. Indeed, all these curves are shifted on the right of the experimental line, while the centre of each one of these curves should be coincident with the dashed line. With the aim to pursue this aim, a stochastic optimization should be requested.

7. COMPARISON

In this topic, the shear design resistance for the discussed prestressed concrete girder, will be evaluated with the different safety methods discussed in §1.2 (PSF and ECOV) and by using FBSP with compressive strength leading parameter, which as illustrated, is the best leading parameter in the context of this girder. By summarizing, the design resistance was evaluated with:

Table 32. Summary of the adopted safety format methods

Safety Method	Analysis requested	Ultimate design load (R _d)
PSF	<i>one analysis</i> , with design values of mechanical parameters;	R _d is the ultimate load directly obtained by the only one analysis
ECOV	<i>two analyses</i> : - the first one with characteristic values of mechanical parameters; - the second one with mean values of mechanical parameters;	$V_r = \frac{1}{1.65} \ln\left(\frac{R_{u,m}}{R_{u,c}}\right)$ $\gamma_{rd} = e^{\alpha \cdot \beta \cdot V_r}$ $R_d = \frac{R_{u,m}}{\gamma_{rd} \cdot \gamma_r}$
FBSPC	<i>seven analyses</i> , with a sub-field samples set based on LHS method corresponding to the seven fractiles compressive strength values;*	$R_m = \frac{1}{7} \sum_{i=1}^7 (R_i)$ $\sigma = \sqrt{\frac{\sum_{i=1}^7 (R_m - R_i)^2}{7}}$ $V = \frac{\sigma}{R_m}$ $R_d = e^{R_m(1 - \alpha \cdot \beta \cdot V)}$

* Notice that by assuming a log-normal resistance, as shown in §5.3.2, R_i is the logarithm of the ultimated load obtained by each analysis.

By assuming the log-normal response curve obtained by FP such as the exact solution of the engineering problem and evaluating design resistance by using different Safety Formats illustrated in the above table, **Figure 43** has been drawn up.

COMPARISON

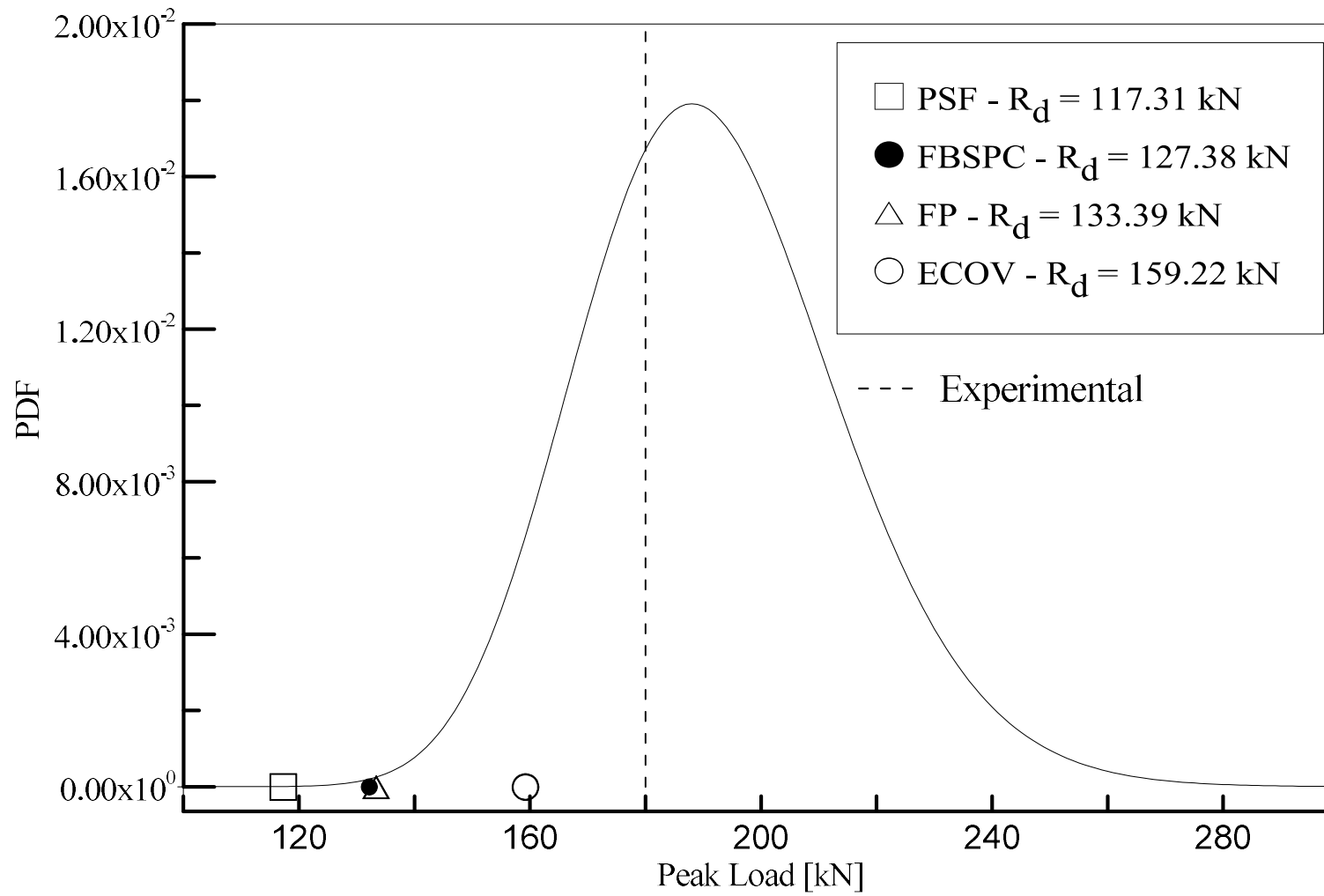


Figure 43. Design resistances obtained by using different safety formats

8. FBSP BASED ON MODEL CODE INFORMATION

In the absence of experimental data, the mechanical concrete parameters could be obtained by using correlations provided by codes. With the aim to evaluate the use of correlations reported in the Model Code 2010 (*fib*, 2013) in a probabilistic reliability analyses, a modified application of FBSP, called Fractiles Based Sampling Procedure based on Model Code information, denoted herein as FBSP_{MC} is proposed. The method is the same illustrated in §6 but in this case only the leading parameter and the mechanical parameters of steel and tendons were derived by FReET. The other concrete mechanical parameters are calculated from the leading parameter by using the Model Code 2010 (*fib*, 2013) correlations.

8.1. Compressive strength leading parameter

As shown in §6.1.4.1 the seven selected samples on the base of compressive strength values are: 45, 34, 293, 147, 57, 17 and 126. In the context of FBSP the other concrete mechanical parameters (tensile strength, fracture energy and elastic modulus) which are contained in each sample, derive by the target correlation matrix. In the context of FBSP_{MC}, these parameters were evaluated by using correlations between mechanical parameters provided by Model Code 2010 (*fib*, 2013):

Table 33. Model Code 2010 (*fib*,2013) correlations

Model Code Correlations	
Compressive strength (Leading Parameter)	f_{cm}
Tensile strength	$f_{ctm} = \left[2.12 \cdot \ln(1 + 0.1 \cdot (f_{cm})) \right]$
Fracture energy	$G_f = \frac{73 \cdot f_{cm}^{0.18}}{\sqrt{2}}$
Elastic modulus	$E_c = 21500 \cdot \left(\frac{f_{cm}}{10} \right)^{1/3}$

The estimate of the mechanical parameters reported in Table 33 was done for each set (for example the tensile strength correlation was applied seven times by using the seven different values of compressive strength). Notice that, as shown above, in this application only the concrete mechanical parameters were evaluated by using correlations; the other mechanical parameters (steel and tendons) are those obtained by FReET (the same which are in the sets in §6.1.4.1). In this way the new table of the mechanical parameters was obtained:

Table 34. Concrete mechanical parameters associated to fractiles of compressive strength by using Model Code 2010 correlations.

Set	f_c [MPa]	f_t [MPa]	G_f [N/mm]	E_c [MPa]
212	53.44	3.92	0.106	3.83E+04
117	64.79	4.27	0.109	4.64E+04
13	72.53	4.47	0.112	5.20E+04
99	79.08	4.64	0.113	5.67E+04
87	84.51	4.76	0.115	6.06E+04
174	88.98	4.86	0.116	6.38E+04
46	93.49	4.95	0.117	6.70E+04

The mechanical parameters of steel and tendons are not reported, because they are the same shown in §6.1.4.1 in the corresponding tables. With this new mechanical parameters, 7 NLFEA were led and the new design resistance was evaluated (exactly as shown for the FBSP).

Table 35. Results with FBSP_{MC}

Simulation	Peak Load [kN]
1	165.98
2	189.55
3	202.87
4	198.12
5	215.65
6	233.70
7	220.80
R_d	143.86

8.1.1. PDF of mechanical parameters comparison

Interestingly to show is the difference in term of probability density function (PDF), between mechanical parameter obtained by (a) FReET, (b) FBSP_{MC} and (c) experimental test. This could be made, by evaluating parameters of the probabilistic distribution for the three different approaches. In the context of FBSP_{MC}, this were made for the tensile strength and fracture energy (i.e. for the most important mechanical parameter for this girder, evaluated from the leading parameter by using Model Code correlations).

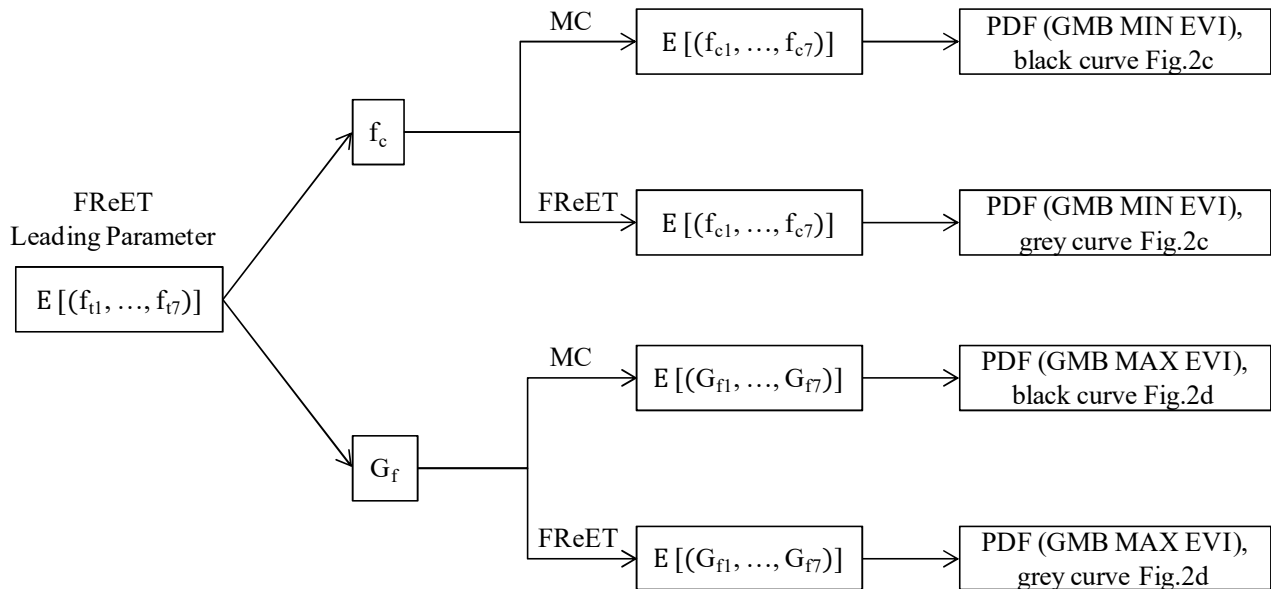


Figure 44. Flow-chart explanation for the mechanical parameters estimation by using FBSP_{MC} (MC in the figure) and FBSP (FReET in the figure), with tensile strength leading parameter.

Table 36. Mechanical parameters values with different approaches and compressive strength leading parameter

Sample	FBSP _{MC} [MPa]	FBSP [MPa]	EXPERIMENTAL [MPa]
Tensile Strength values			
1	3.92	3.5	
2	4.27	2.72	
3	4.47	2.92	
4	4.64	3.38	-
5	4.76	4.56	
6	4.86	5.63	
7	4.95	4.33	
Mean Value	4.55	3.83	3.9
σ	0.36	0.78	0.80
μ	0.28	0.61	0.63
α	4.39	3.48	3.54
Fracture Energy values			
1	105.64	139.15	
2	109.37	220.28	
3	111.61	146.11	
4	113.36	260.70	
5	114.72	217.38	
6	115.79	287.69	
7	116.83	174.43	
Mean Value	112.47	206.53	219.8
σ	3.94	56.35	72.09
μ	3.07	43.93	56.21
α	110.70	181.18	187.35

From the distribution parameters reported in Table 36, known the PDF (GMB max EVI), plotting the three curves in the same graph, the differences are immediate.

As one can see from Figure 45, FReET values of the tensile strength match better the experimental values of tensile strength, while the Model Code curve is far from these curves.

8.2. Tensile strength leading parameter

Table 37. Reworked correlations by using tensile strength as leading parameter

Reworked Model Code Correlations	
Tensile strength (Leading Parameter)	f_{ctm}
Compressive strength	$f_{cm} = \frac{f_{ctm}}{e^{2.12} - 1} \cdot 0.1$
Fracture energy	$G_f = \frac{73 \cdot f_{cm}^{0.18}}{\sqrt{2}}$
Elastic modulus	$E_c = 21500 \cdot \left(\frac{f_{cm}}{10}\right)^{1/3}$

The application shown in §8.1 was repeated changing the leading parameter. Correlations provided by Model Code 2010 (*fib, 2013*) are function of compressive strength. For this application, the same correlations were explicated in term of tensile strength. This means that with the “new obtained correlations”, each mechanical parameter could be evaluated known the value of tensile strength. Table 37 show the “new obtained correlations”; in reality, as it can be seen from this table, the difference is only for the correlation between tensile strength and compressive strength.

Table 38. Concrete mechanical parameters associated to fractiles of tensile strength by using Model Code 2010 correlations.

Set	f_t [MPa]	f_c [MPa]	G_f [N/mm]	E_c [MPa]
69	2.85	28.43	94.30	2.04E+04
7	3.14	33.97	97.36	2.43E+04
139	3.42	40.27	100.39	2.89E+04
176	3.77	49.14	104.06	3.52E+04
288	4.18	61.92	108.48	4.44E+04
249	4.67	80.66	113.76	5.78E+04
89	5.39	117.32	121.70	8.41E+04

Also in this case, the mechanical parameters of steel and tendons are not reported, because they are the same shown in §6.1.4.2 in the corresponding tables. The results obtained by the new 7 NLFEA are shown in Table 39.

Table 39. Results with FBSPT *modified*

Simulation	Peak Load [kN]
1	119.92
2	126.50
3	142.11
4	163.31
5	177.75
6	205.31
7	250.76
R_d	73.25

8.2.1. PDF of mechanical parameters comparison

Table 40. Mechanical parameters values with different approaches and tensile strength leading parameter

Sample	MC [MPa]	FReET [MPa]	EXPERIMENTAL [MPa]
Compressive Strength values			
1	28.43	67.45	
2	33.97	67.06	
3	40.27	69.33	
4	49.14	74.74	-
5	61.92	82.11	
6	80.66	88.44	
7	117.32	104.18	
Mean Value	58.82	76.69	77
σ	31.33	14.14	12.63
μ	24.42	11.02	9.85
α	44.72	70.32	71.32
Fracture Energy values			
1	94.30	154.15	
2	97.36	143.90	
3	100.39	144.65	
4	104.06	201.07	-
5	108.48	214.55	
6	113.76	456.42	
7	121.70	265.36	
Mean Value	105.72	225.73	219.8
σ	9.65	110.99	72.09
μ	7.53	86.54	56.21
α	101.38	175.78	187.35

As shown in §8.1.1 will be now repeated for the parameters evaluated by using Model Code 2010 (fib,2013) correlation with tensile strength leading parameter; therefore, PDF of compressive strength and fracture energy were checked, see Figure 45.

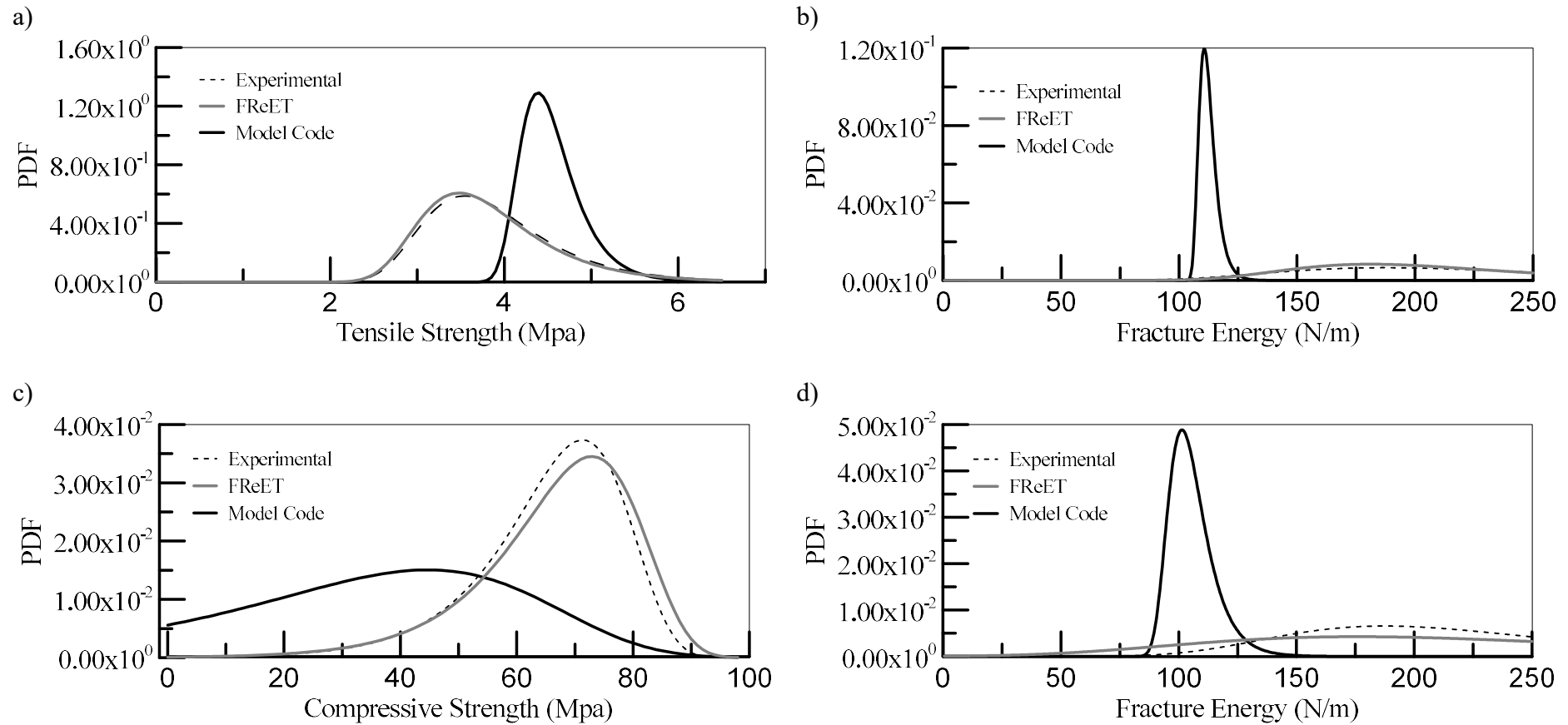


Figure 45. Probability Density Functions for different mechanical parameters in which the probabilistic distribution parameters were obtained from experimental tests (experimental in the legend), FBSP (by using Target Correlation Matrix, FReET in the legend) and FBSP_{MC} (mechanical parameters evaluated from the leading parameter by using Model Code correlations, Model Code in the legend): (a) and (b) show the results when compressive strength was leading parameter, (c) and (d) show the results when tensile strength was leading parameter;

8.3. Fracture energy leading parameter

As shown in the previous chapters, herein the concrete mechanical parameters should be evaluated by using correlations starting from fracture energy value. This approach was not possible because a problem of inconsistency has been recognized. Indeed, by inverting the correlation shown in the MC, with the aim to evaluate compressive strength values starting by fracture energy values, unrealistic values of compressive strength were obtained.

Table 41. Re-worked correlations to evaluate compressive strength by using fracture energy

$G_f = \frac{73 \cdot f_{cm}^{0.18}}{\sqrt{2}}$	exact correlation
$f_{cm} = \left(\frac{\sqrt{2} \cdot G_f}{73} \right)^{\frac{1}{0.18}}$	reversing correlation

This aspect could be easily understood by observing Figure 46. This figure shows that if fracture energy was evaluated by compressive strength, using the exact correlation proposed by MC, the obtained fracture energy values were different from the experimental (as shown in Figure 45) but plausible. Otherwise, when compressive strength was evaluated by fracture energy by adopting the reversing correlation, the obtained values of compressive strength were unrealistic and physically not possible. This means that these correlations should be re-evaluated because they are inconsistent.

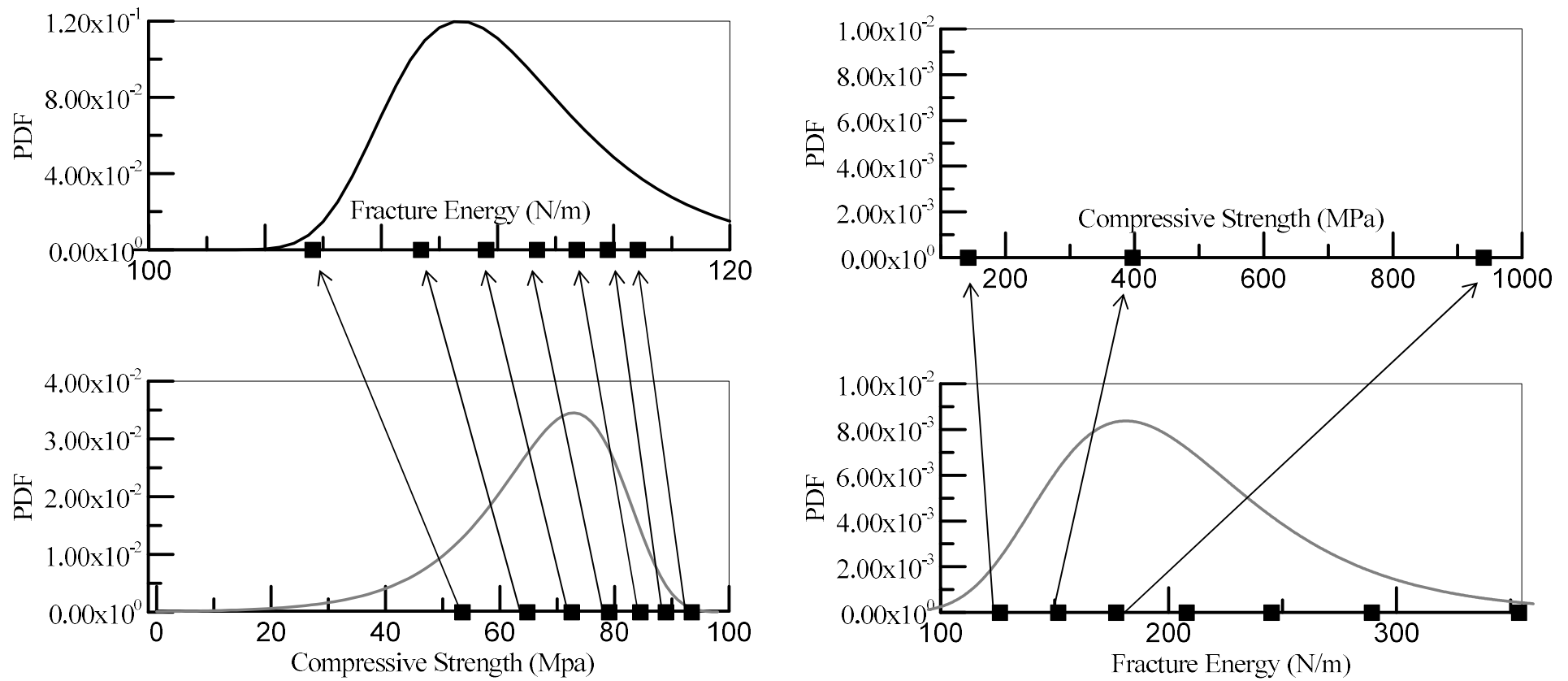


Figure 46. Model Code 2010 (*fib*,2013) correlation, from f_c to G_f (a); Reformulating Model Code 2010 (*fib*,2013) correlation, from G_f to f_c (b). The first correlation (a) leads to results which are different from experimental ones (see **Figure 45.b**) but realistic; the second correlation (b) leads to unrealistic values of compressive strength.

9. APPENDIX: PROBABILISTIC STRUCTURAL RESPONSES OF DIFFERENT RC PANELS

In the previous chapters, the possibility to evaluate the structural response of a structural element *via* probabilistic analyses has been illustrated. Specifically, the dependence of FBSP by the failure mechanism of the analyzed structural element was many times cited but never exactly demonstrated. In this chapter, a probabilistic study on different reinforced concrete panels is proposed; specifically, FP by using LHS sampling procedure and FBSP with different leading parameters were led on each panel. Aim of this topic will be shown if a change of the failure mechanism could provide a change of the mechanical parameter governing the structural response. To achieve this goal, three different panels, with similar geometric characteristic but substantial differences in term of steel reinforcement have been investigated.

These three panels (**Table 42**) were extrapolated from a large database available in the literature [25]. Indeed, over the past 30 years, an element-based approach was developed to study reinforced concrete structures (see PARC). The conceptual basis of this approach is that the behavior of any whole structure can be predicted by integrating what can be learned from experiments about its parts (elements). At the Univ. of Houston a Universal Panel Tester capable of testing full-size elements (1,398 m x 1,398 m x 0.178 m) has been built. From the experimental behavior of such elements analytical models could be further evaluated. These analytical models can be integrated into finite element programs to compute and predict the responses of whole structures or subassemblages.

Table 42. Main geometric and reinforcement properties

Panel	Thick. [mm]	Steel in <i>l</i> direction		Steel in <i>t</i> direction		α
		Rebars	ρ_l	Rebars	ρ_t	
CA2	178	No. 4 at 188 mm	0.0077	No. 4 at 188 mm	0.0077	45
CA4	203	No. 8 at 188 mm	0.027	No. 8 at 188 mm	0.027	45
CB4	203	No. 8 at 188 mm	0.027	No. 4 at 188 mm	0.0067	45

No. 4: 129 mm²
No. 8: 510 mm²

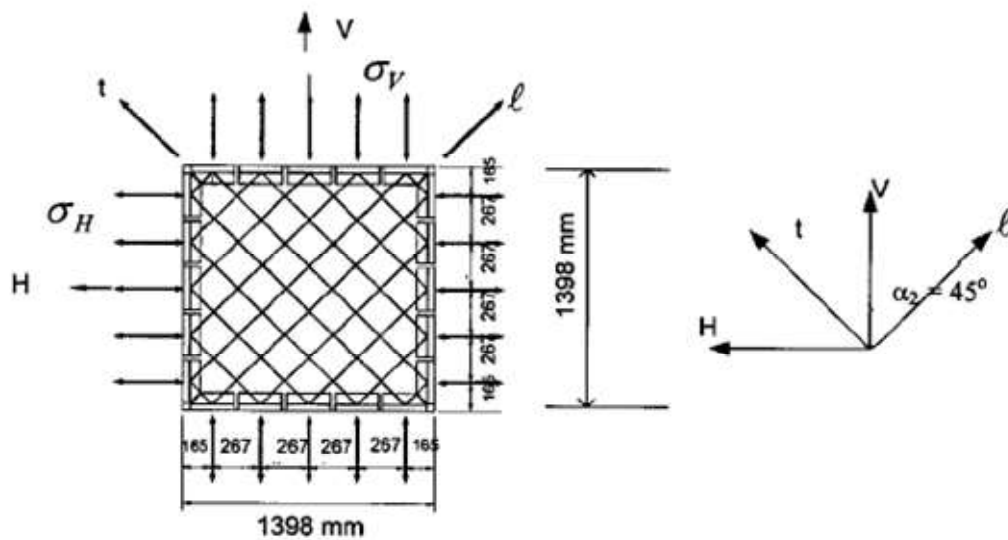


Figure 47. Example of analyzed Panel – CA serie

Specifically, the original study inherently these panels focused on the prediction of the panel's behavior under cyclic loadings. The elements were subjected to reversed cyclic principal stresses in the horizontal and vertical directions: the two stresses were maintained equal in magnitude and opposite in direction to obtain a state of pure shear stress (see **Figure 48**). NLFEA analysis was carried out using a single 4-node membrane element with reduced integration (defined M3D4R in [3]). To simulate the same loading condition, an external frame was modeled using truss elements in [7]. At the frame's end, the cyclic displacement time history was imposed.

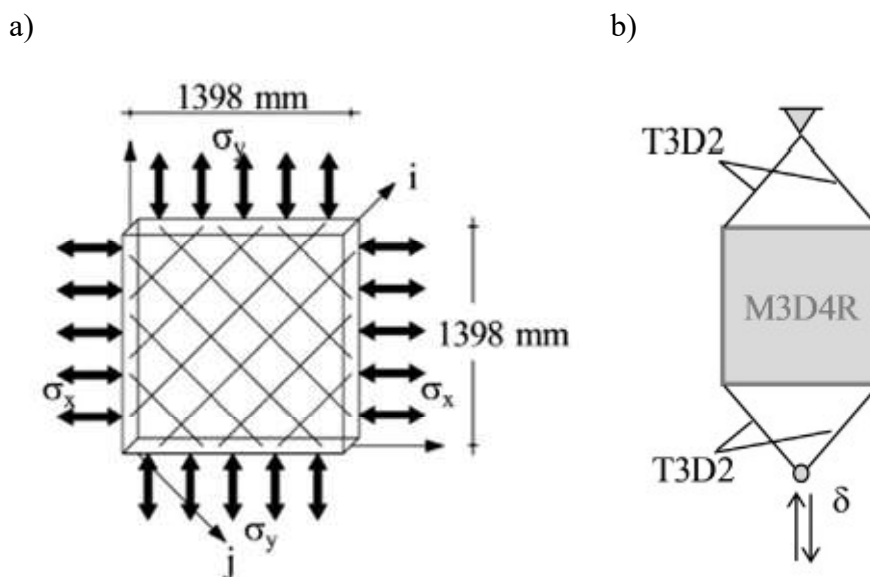
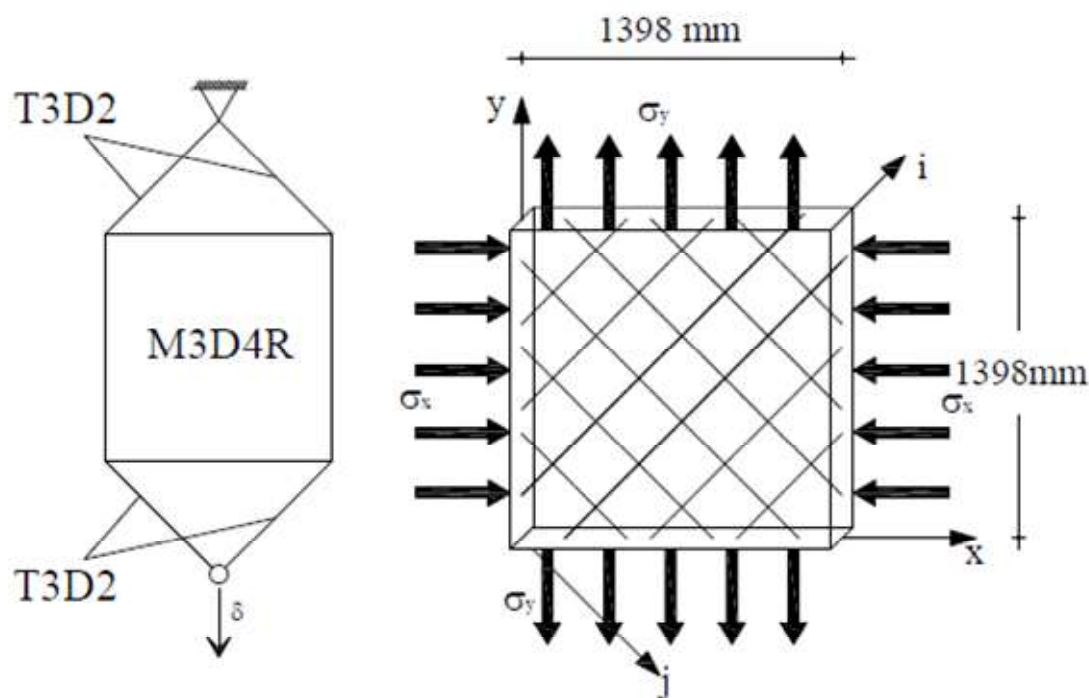


Figure 48. a) tensional state under cyclic loadings; b) NLFEA SET-UP under cyclic loadings

Since in this new study, there is no interest to evaluate the behavior of the panel under cyclic loadings, the same mesh of the panels have been adopted but at the frame's end a monotonic displacement time history was imposed (moving the node only down):



Furthermore, because of probabilistic mechanical properties of the material constituting these three panels were not known, the following approach has been adopted:

1. Check of the subroutine used for the NLFEA and failure mechanism prediction, making a comparison with the experimental curves by using mechanical properties reported in [25];
2. Failure mechanism prediction by using mean mechanical properties of the girder analyzed in §4, see **Table 1**;
3. FP and FBSP for each panel, by using probabilistic samples just seen in §5;

On the other words, as already widely shown for the T-shaped prestressed girder in the previous chapters, has been herein repeated for each panel, by assuming that these panels were made of the same concrete constituting the girder. In this case, when probabilistic analyses will be approached (see above point 3), there is no interest to match the experimental curve; this approach represents a parametric analysis useful to understand what could happen to the parameters governing the structural response, by changing the panel (i.e. the failure mechanism).

9.1. Model and failure mechanism prediction with real experimental mechanical parameters

By observing panels reported in **Table 42**, in first approximation and without considerations about the mechanical properties, a failure mechanism prediction based on reinforcement bars properties could be state:

- CA2: due to a low mechanical percentage of armor in each of the two directions, a failure mechanism provided by the yielding of the steel could unfold;
- CA4: because of an high mechanical percentage of armor in each of the two directions, a failure mechanism provided by the crashing of the concrete could unfold;
- CB4: for this panel, the armor is not symmetric; the different value of the tensile occurs in each one direction, provide a force (equal to the difference between the two mentioned tensile) which could be absorbed by the concrete, by means the aggregate interlocking phenomenon. However, the low mechanical percentage of armor in t direction, could be provide also a steel failure mechanism.

Table 43. Real experimental mechanical properties

Panel	f_c [MPa]	f_t [MPa]	G_F [N/mm]	E_c [MPa]	E_s [MPa]	f_{ys} [MPa]
CA2	45.0	2.5	0.145	3.45E+4	2.00E+5	424.1
CA4	45.0	2.5	0.145	3.45E+4	2.00E+5	453.4
CB4	47.0	2.13	0.147	3.45E+4	2.00E+5	424.1

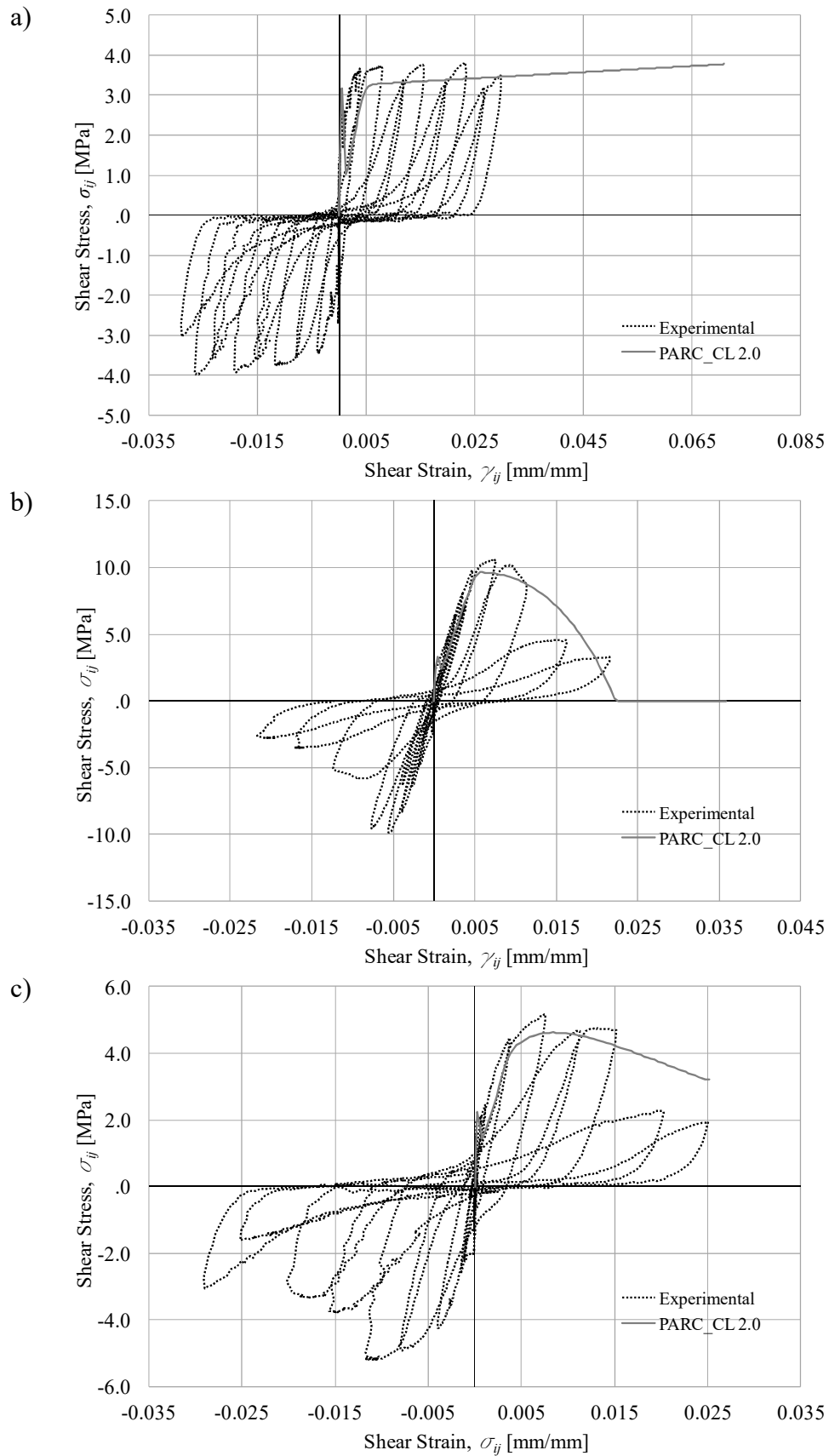


Figure 49. Comparison with experimental by using real mechanical parameters data: a) CA2 b) CA4 c) CB4

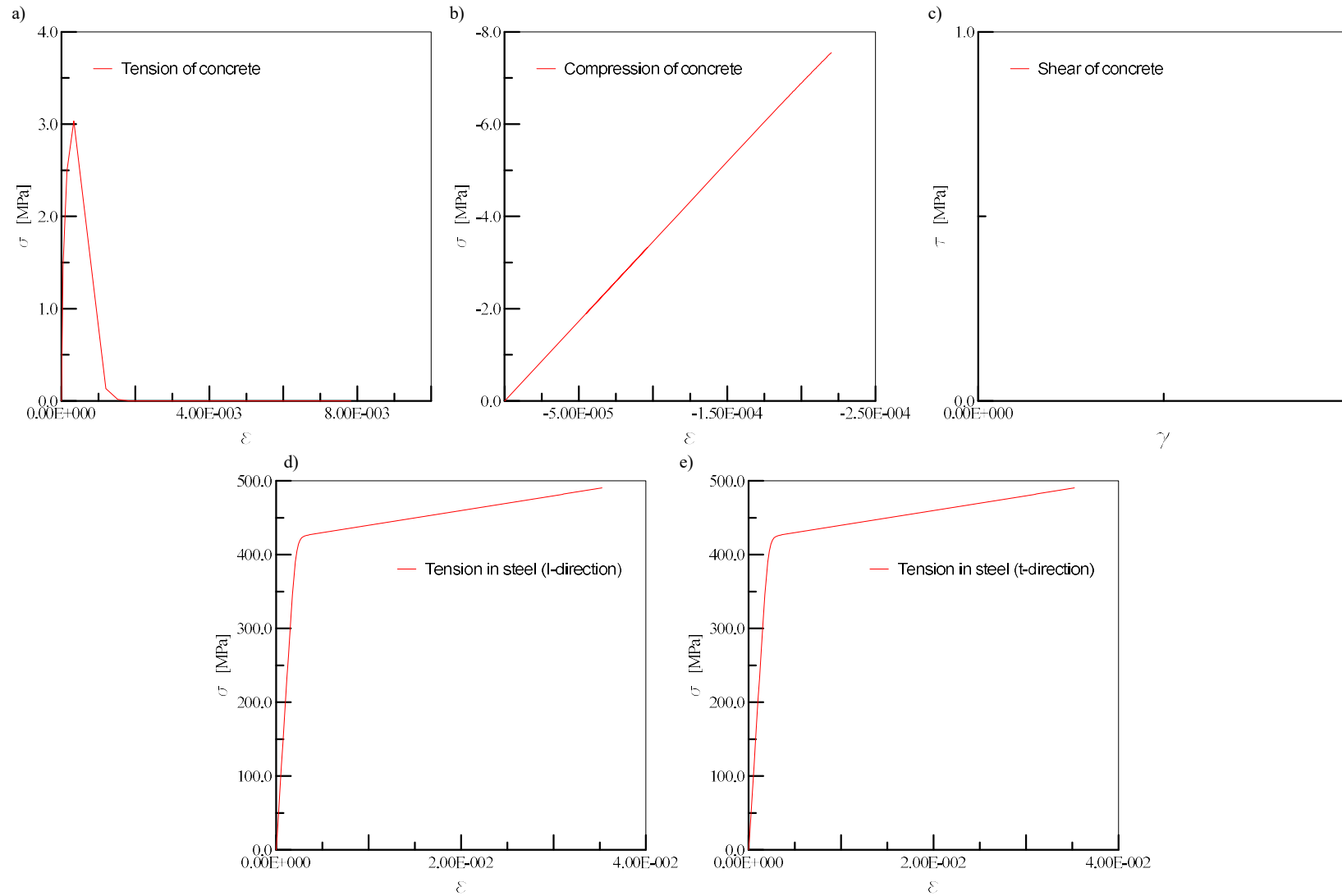


Figure 50. Panel CA2 with real experimental mechanical parameters: State of stress in the Gauss Point integration for concrete and steel

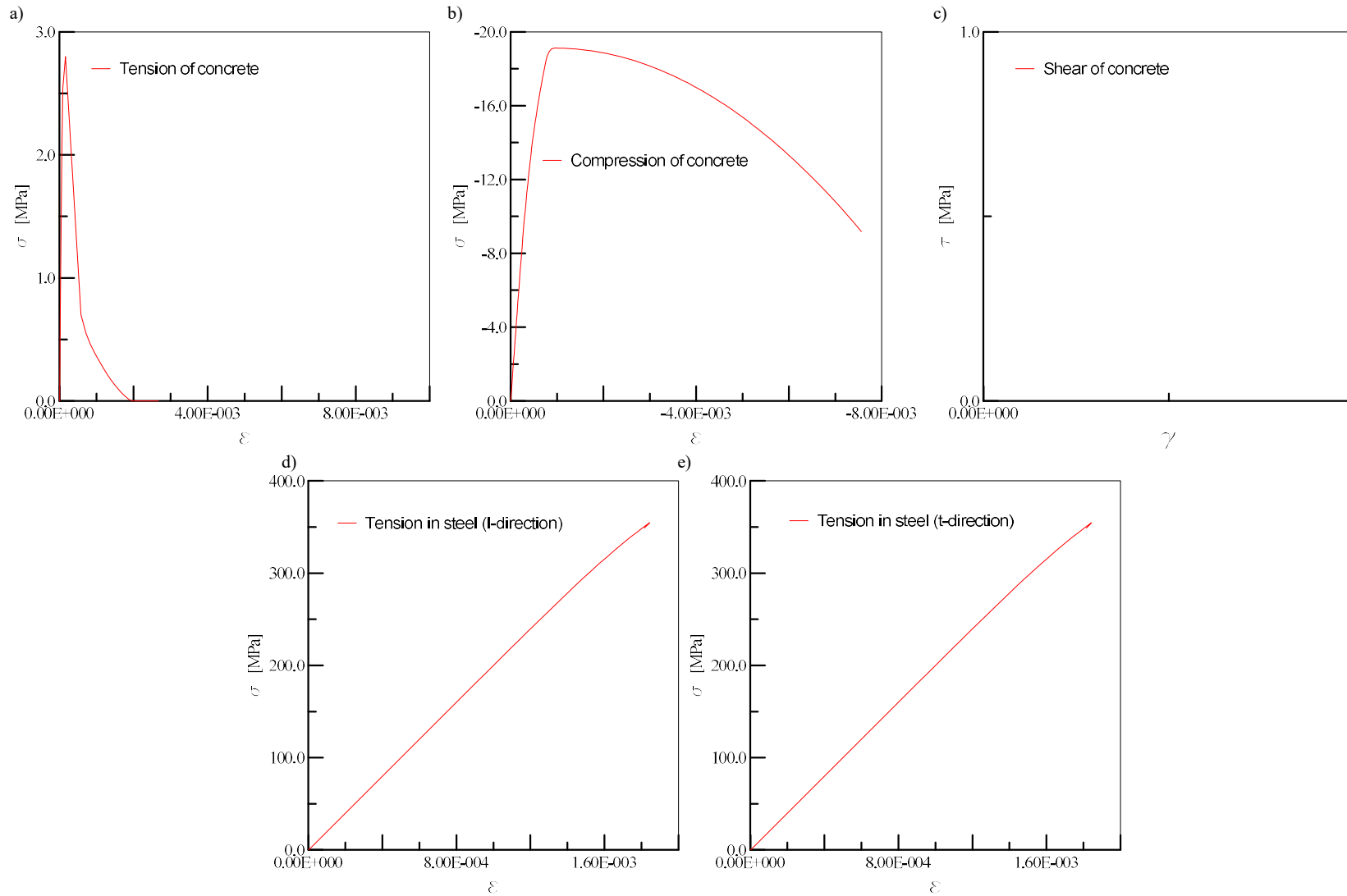


Figure 51. Panel CA4 with real experimental mechanical parameters: State of stress in the Gauss Point integration for concrete and steel

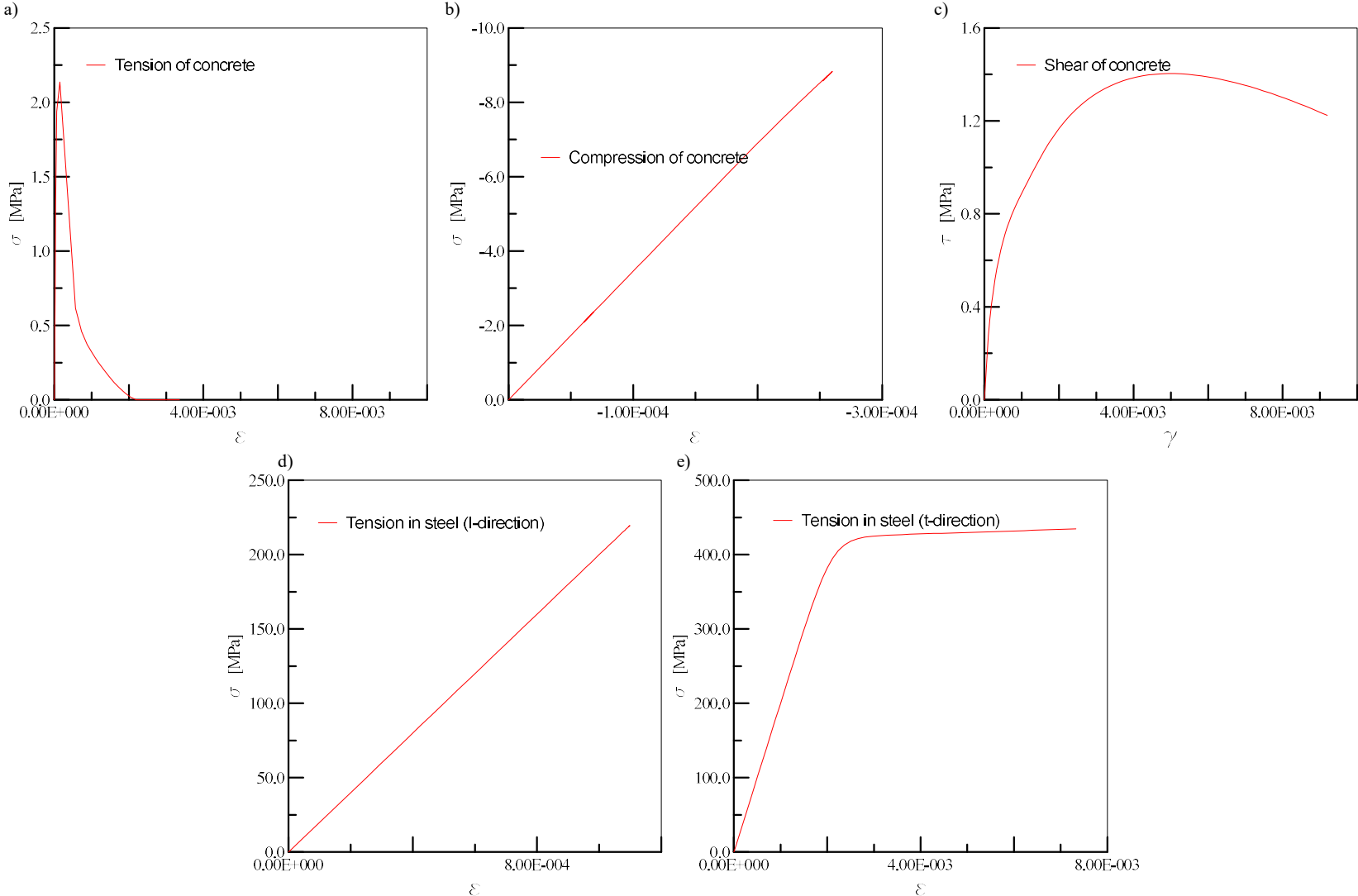


Figure 52. Panel CB4 with real experimental mechanical parameters: State of stress in the Gauss Point integration for concrete and steel

9.2. Failure mechanism prediction with new mechanical parameters values

The knowledge of the failure mechanism of the analyzed structural element is something of very important, specially in the context of FBSP. To predict it, a NLFEA with mean mechanical parameters values was carried out for each panel. As it has been just shown, this prediction, useful for the next probabilistic study, was led by assuming the same concrete of the previous analyzed girder, because of probabilistic mechanical parameters values were not known for the concrete constituting these panels.

The failure mechanism prediction was drawn up by plotting the state of stress in the only one gauss point of the adopted mesh. Stresses were separately evaluated:

- concrete:

1. Tension;
2. Compression;
3. Shear stress (due to aggregate-interlocking);

- steel:

1. Tension;

Panel	Failure mechanism	Reference
CA2	Ultimate strain of steel (even if the ultimate strain is not reached, the ultimate increment of the analysis is assumed at $\gamma=3E-2$, which is the shear deformation assumed in the analysis led with the mean mechanical parameters values where the steel reached the ultimate deformation, assumed equal to $15E-3$)	Figure 54: (d),(e)
CA4	Crushing of the concrete due to the achievement of the compressive strength; notice that due to the reduction of compressive strength when biaxial stress state occurs, the ultimate value of compression stress is less than the compressive strength used as input (77 MPa),;	Figure 55: (b)
CB4	Crushing of concrete due to aggregate interlocking;	Figure 56: (c)

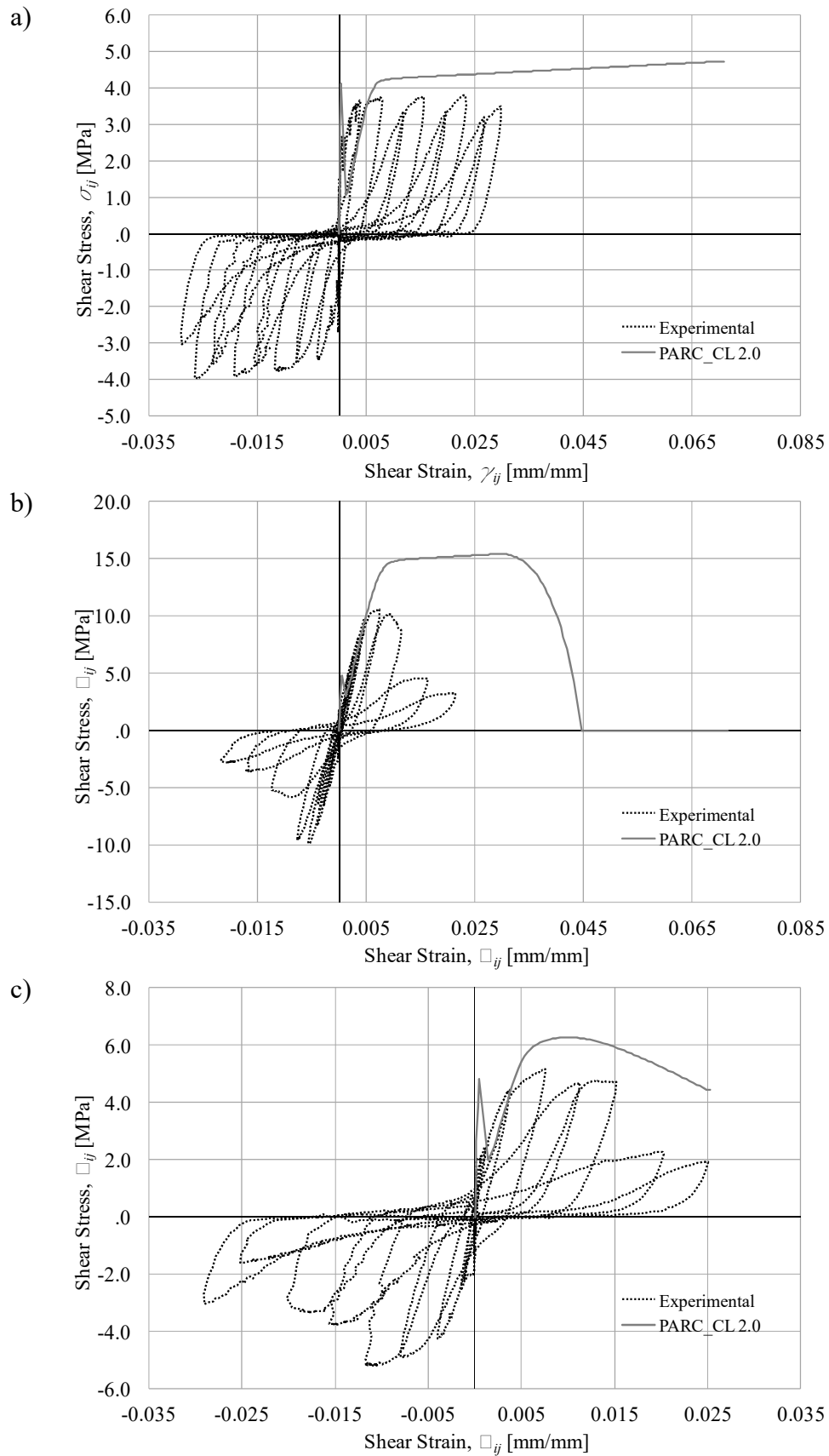


Figure 53. Comparison with experimental by using new mechanical parameters data: a) CA2 b) CA4 c) CB4

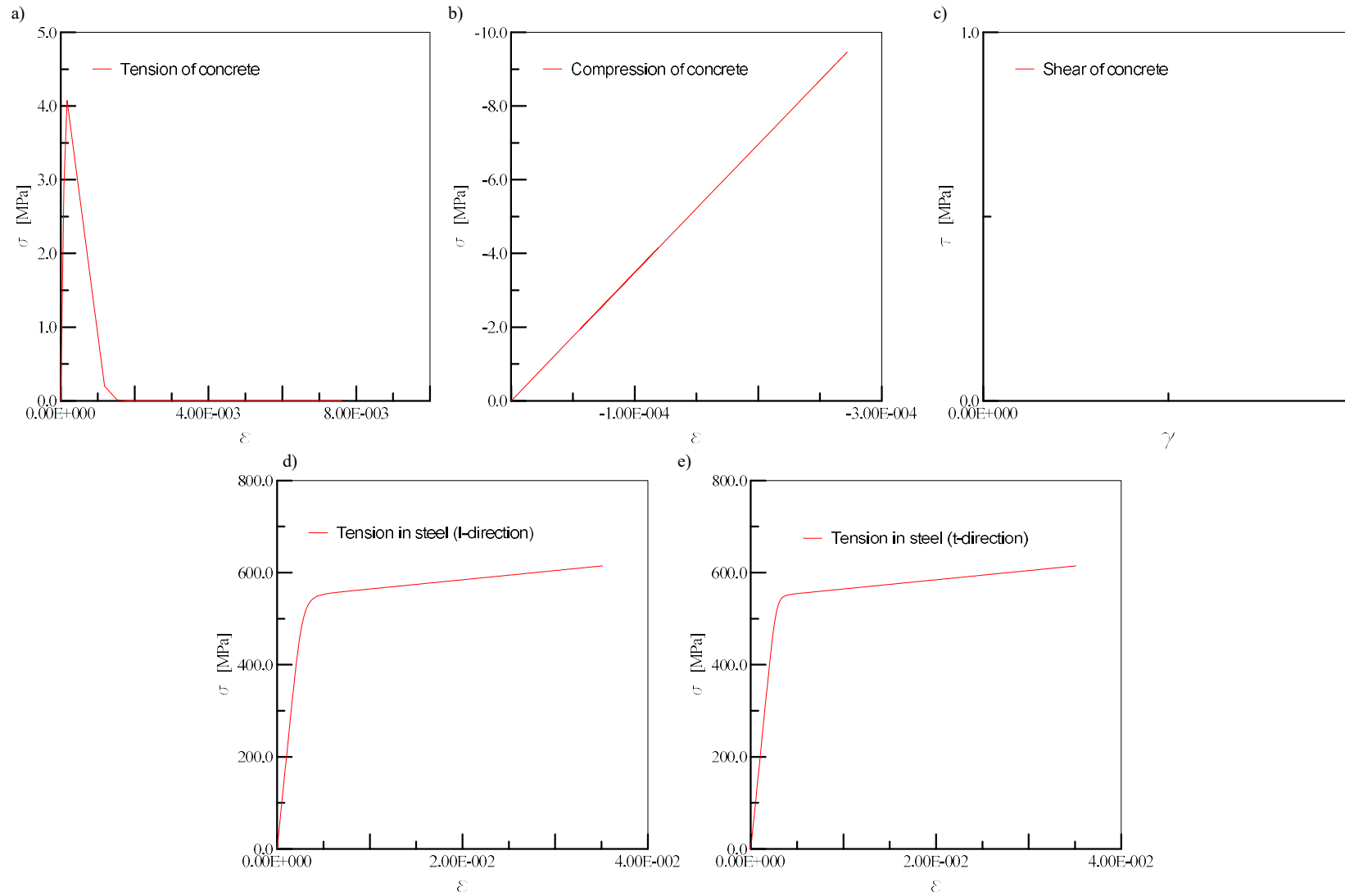


Figure 54. Panel CA2: State of stress in the Gauss Point integration for concrete and steel

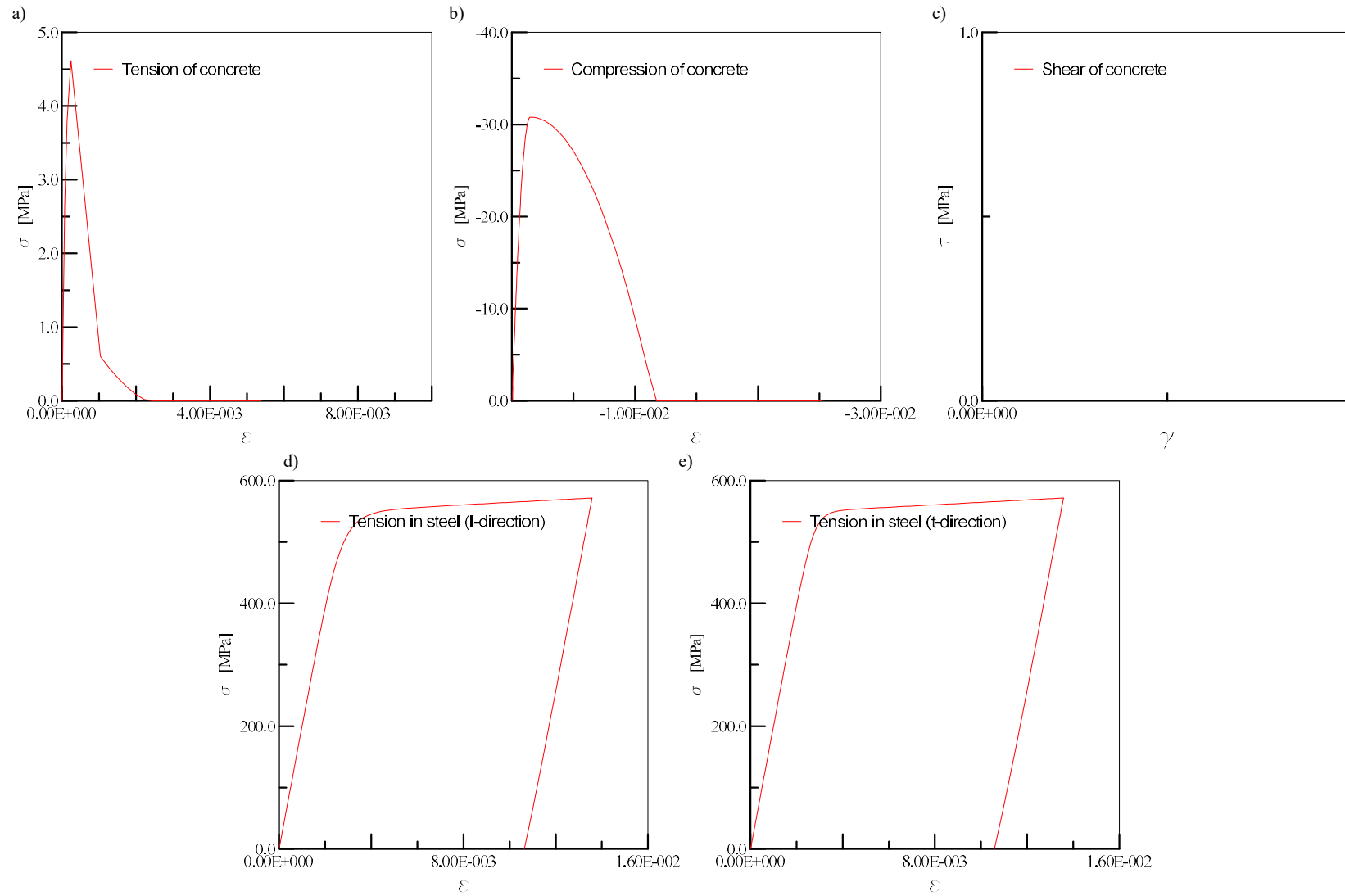


Figure 55. Panel CA4: State of stress in the Gauss Point integration for concrete and steel

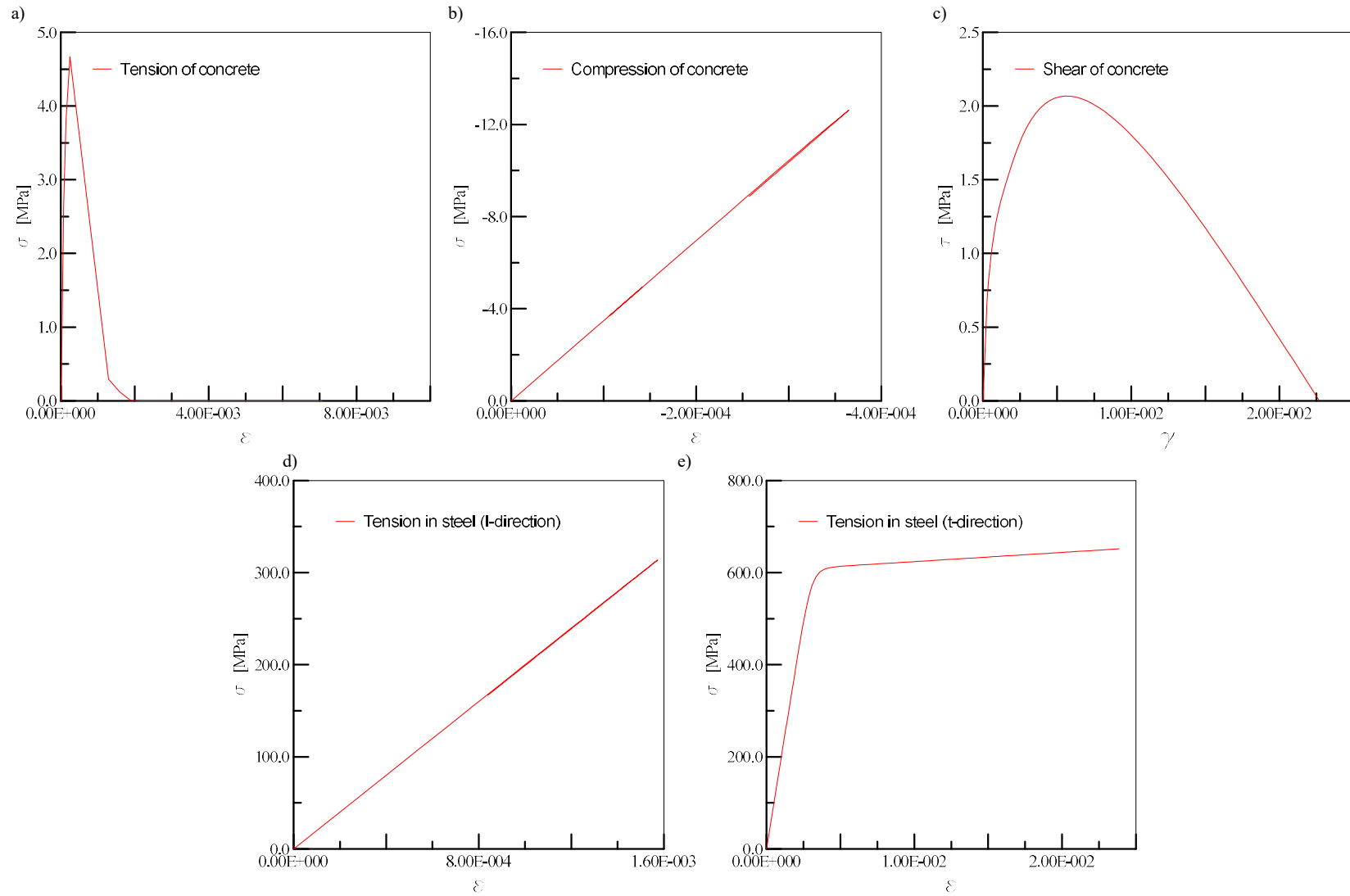


Figure 56. Panel CB4: State of stress in the Gauss Point integration for concrete and steel

9.3. Probabilistic structural responses

In this chapter, the probabilistic structural response of each panel described above, will be evaluated. The probabilistic framework developed for each panel is shown below:

- Fully Probabilistic, by leading a number equal to 300 NLFEA corresponding to the N_{set} generated by FReET software, representing the concrete of the previous analyzed girder;
- Fractiles Based Sampling Procedure, by using compressive strength, tensile strength, fracture energy and yielding of steel leading parameters;

Aim of this topic will be observing the different FP responses (specifically in term of mean and covariance values) obtained by changing the panel. Then, useful for the context of FBSP, will be evaluated which is the best leading parameter (by using the validation based on FBSP, i.e. by observing which is the probabilistic curve obtained by FBSP that match better the FP curve). Finally, the same work will be repeated for the CB4 panel, by using different crack model.

9.3.1. Fully Probabilistic

FP structural responses in term of $\tau - \gamma$, are reported in:

- (a) Panel CA2: **Figure 58**;
- (b) Panel CA4: **Figure 60**;
- (c) Panel CB4: **Figure 62**;

PDFs obtained by FP structural responses are shown in **Figure 57**. By observing this figure, some important considerations could be made:

- (a) The minimum covariance was obtained for the CA2 panel, indeed the failure mechanism of this panel should be governed by the yielding of steel;
- (b) The CB4 panel shows a covariance greater than the CA2 panel, but not with a very high value. This panel fail due to aggregate interlocking which as one can see, leads to a lower covariance than the failure mechanism provide by crashing of the concrete.
- (c) The highest covariance was obtained by the CA4 panel; therefore, crushing of concrete leads to a fail of this panel.

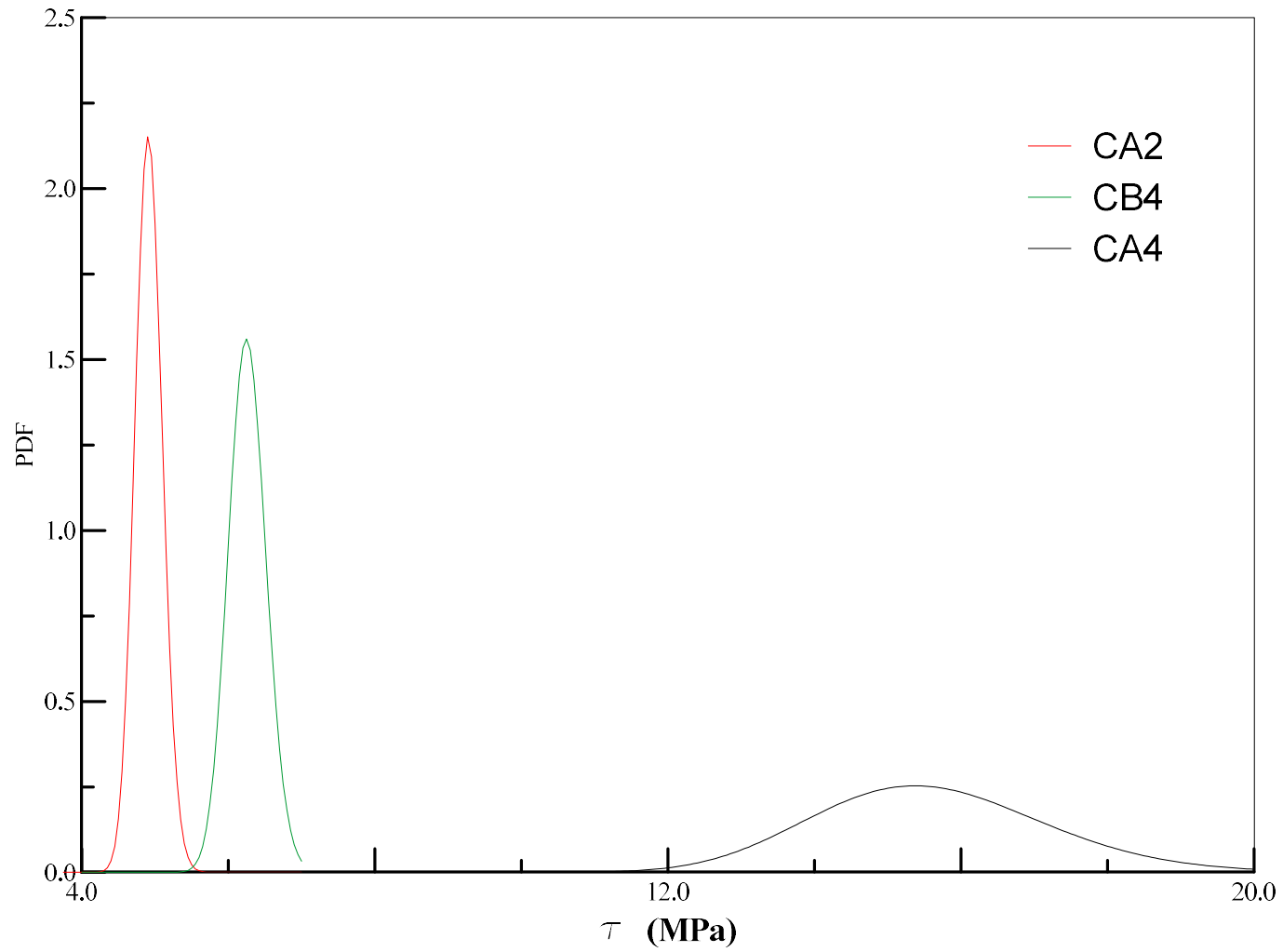


Figure 57. Fully Probabilistic structural responses

9.3.2. Fractiles Based Sampling Procedure

The application of FBSP is already shown in §6. Herein this method was applied for these mechanical parameters:

Compressive strength: FBSPC

Tensile strength: FBSPT

Fracture energy: FBSPG

Yielding stress of steel: FBSPY (only for CA2 and CA4 panel)

The design resistance has been evaluated for each leading parameter by using Eq.(46).

9.3.2.1. CA2 panel

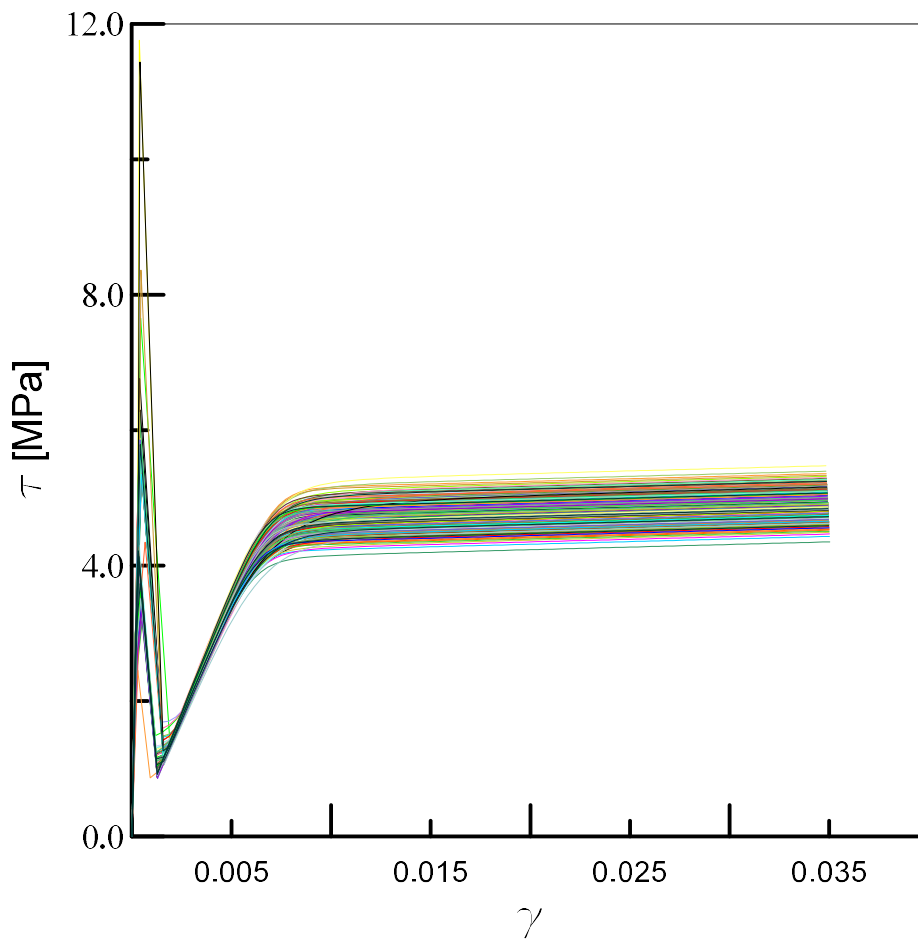


Figure 58. FP curves for the CA2 panel

Table 44. Ideal Design Resistance obtained with different methods.

	FPSPY	FBSPC	FP	FBSPT	FBSPG
τ_d [MPa]	4.24	4.29	4.38	4.56	4.69

Where the reference value are the shear stresses at $\gamma=3E-2$, which is the shear deformation assumed in the analysis led with the mean mechanical parameters value where the steel reached the ultimate deformation, assumed equal to $15E-3$.

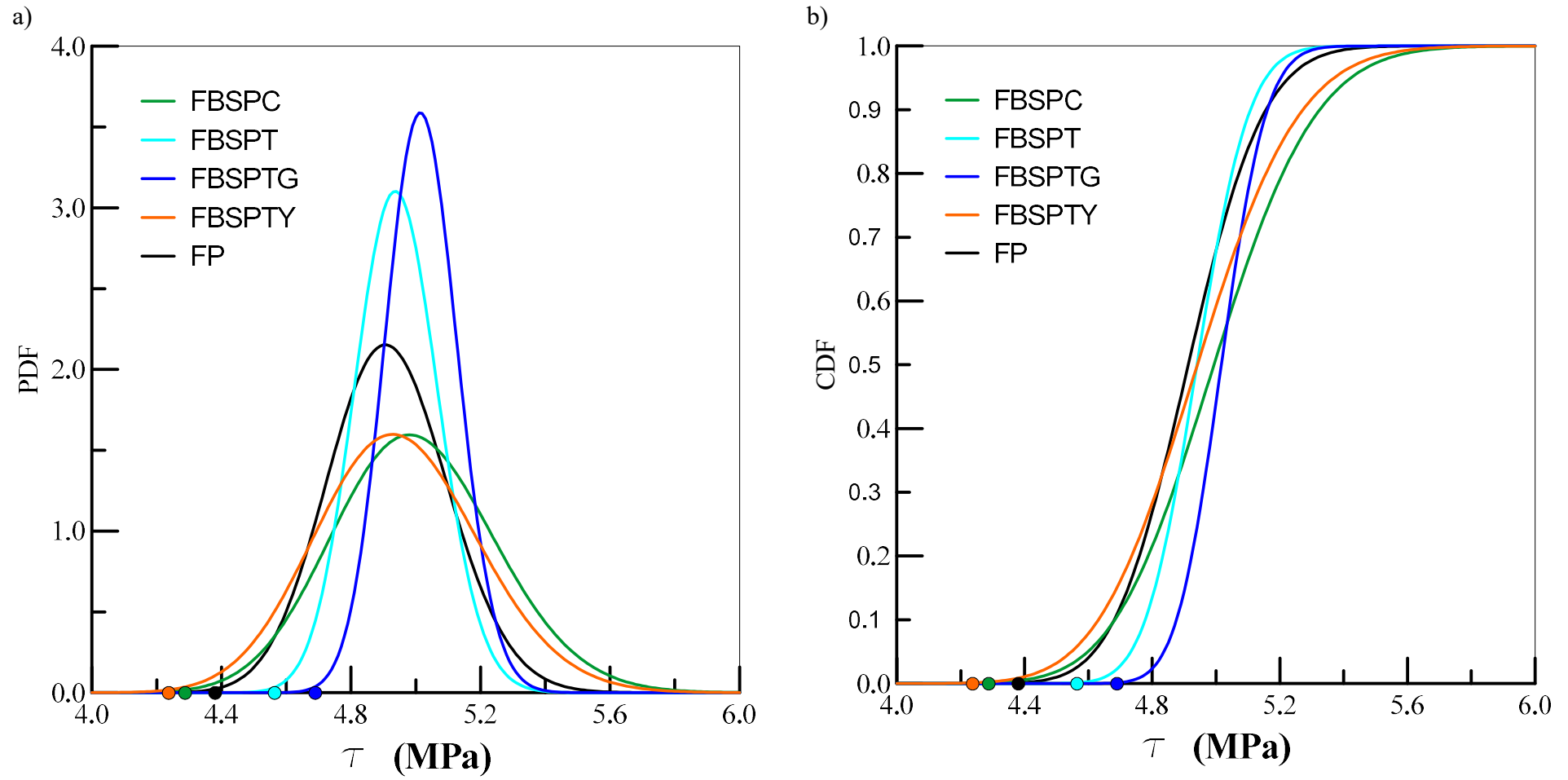


Figure 59. Panel CA2: Comparison between FP and FBSP by using different leading parameters; a) PDF b) CDF

9.3.2.2. CA4 panel

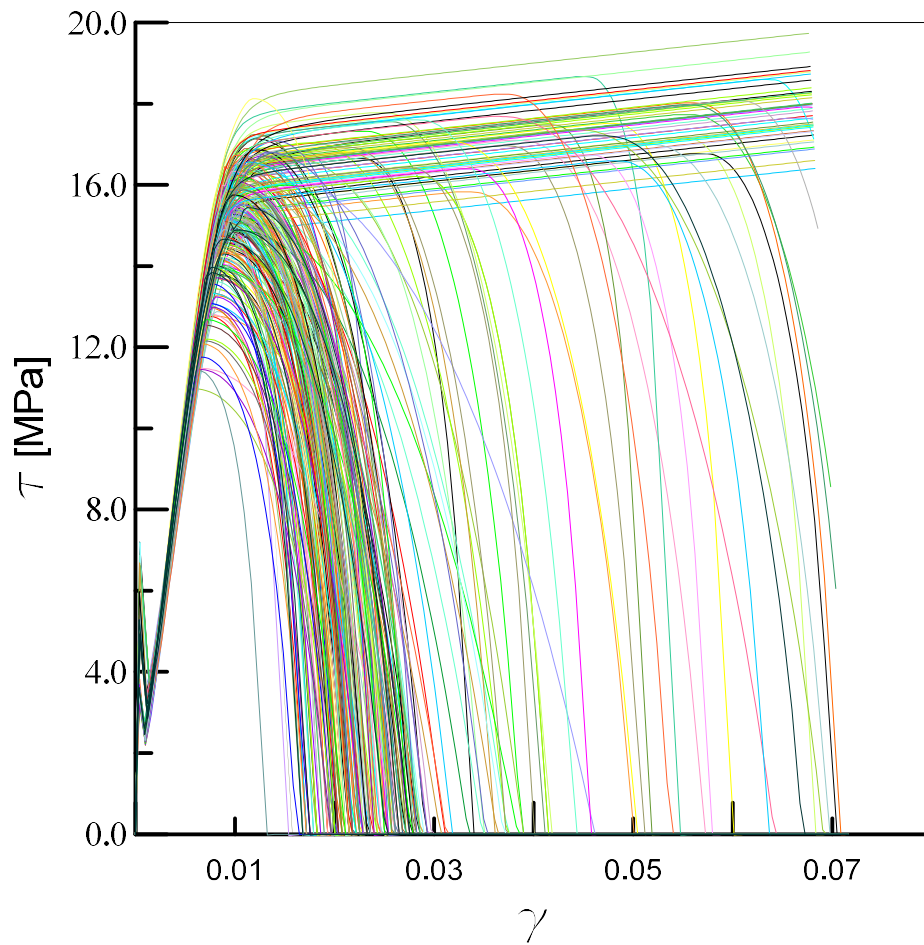


Figure 60. FP curves for the CA4 panel

Table 45. Ideal Design Resistance obtained with different methods.

	FSPSC	FBSPTY	FP	FBSPT	FBSPG
τ_d [MPa]	9.49	11.12	11.39	11.80	12.89

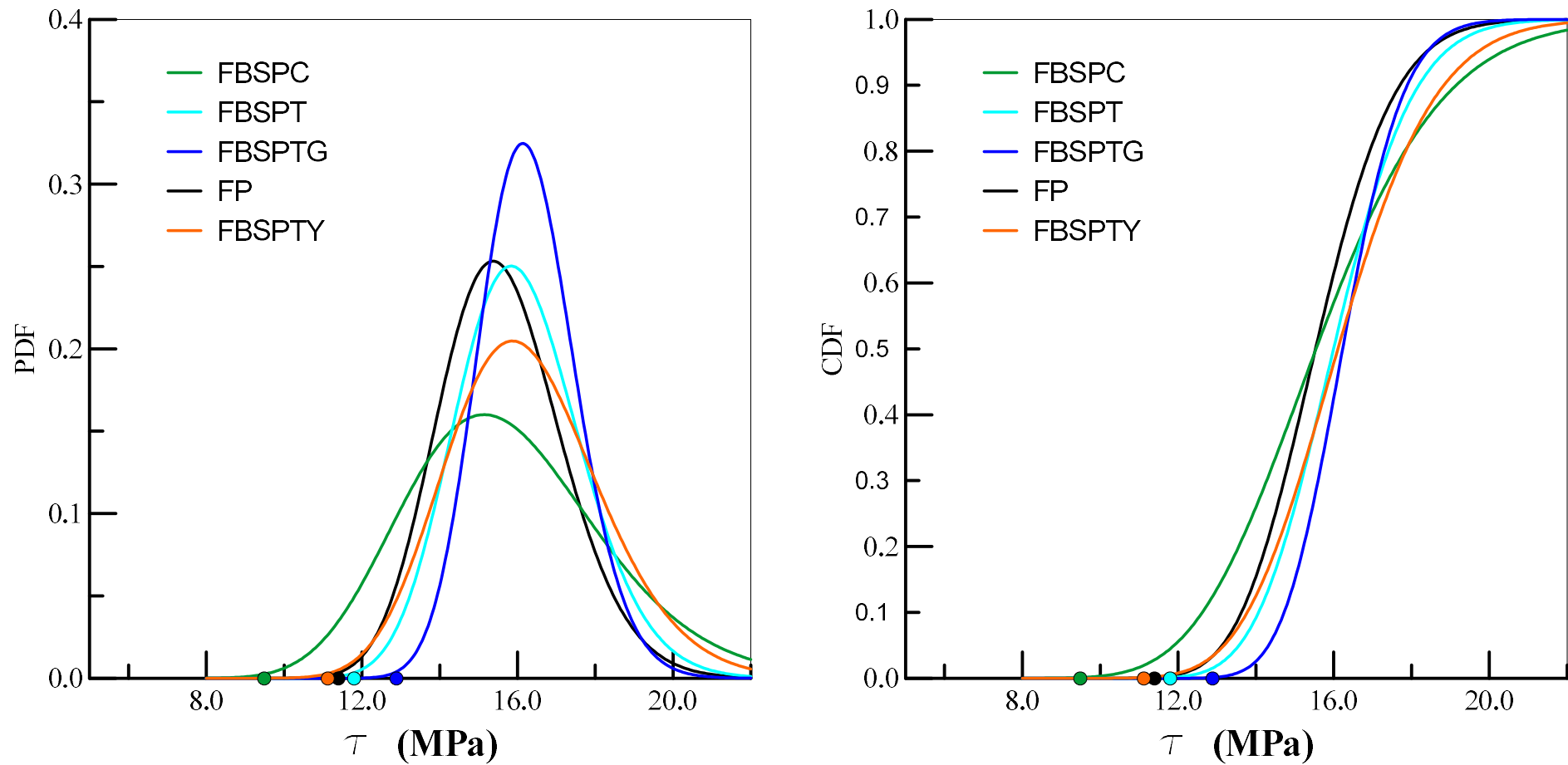


Figure 61. Panel CA4: Comparison between FP and FBSP by using different leading parameters; a) PDF b) CDF

9.3.2.3. CB4 panel

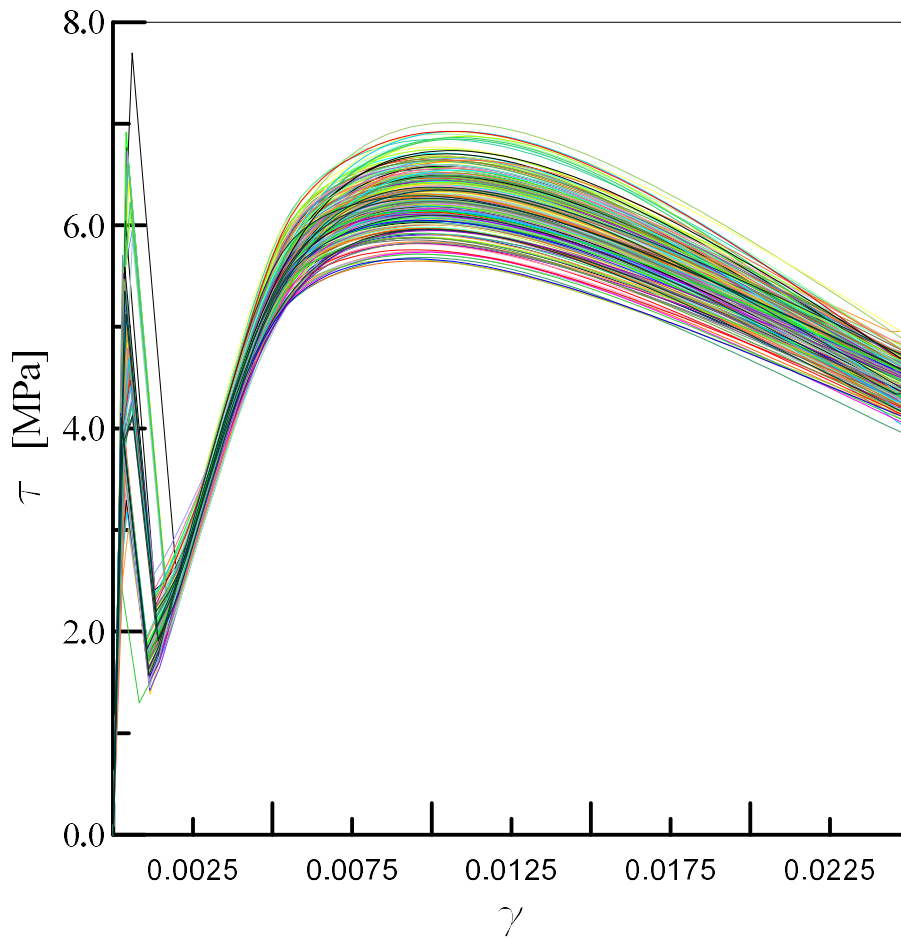


Figure 62. FP curves for the CB4 panel

Table 46. Ideal Design Resistance obtained with different methods.

	FPSPC	FBSPT	FP	FBSPG
τ_d [MPa]	5.26	5.52	5.53	5.90

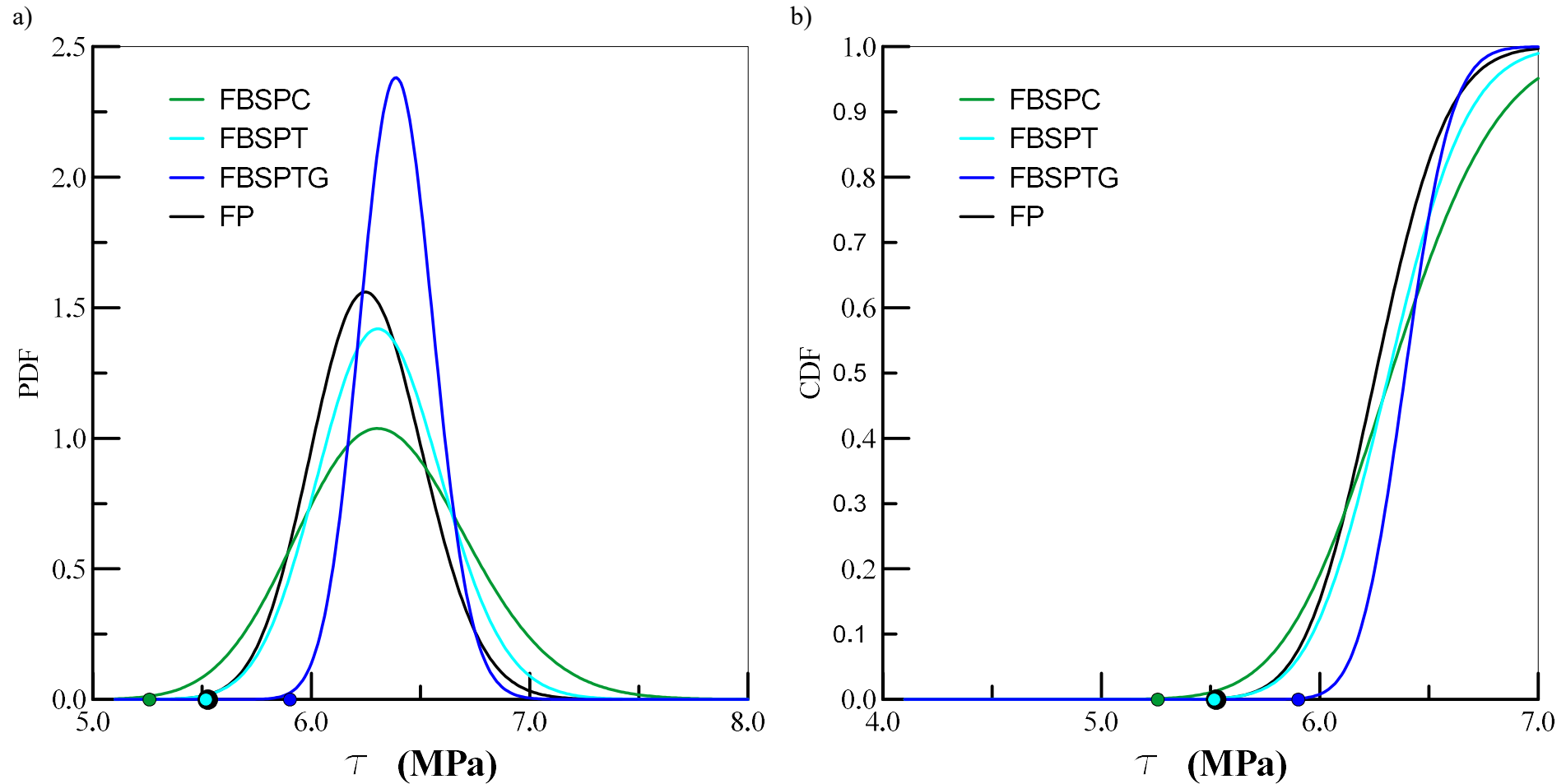


Figure 63. Panel CB4: Comparison between FP and FBSP by using different leading parameters; a) PDF b) CDF

9.3.3. Probabilistic structural responses by using different aggregate interlocking models

In order to demonstrate how the aggregate interlock formulation can change the panel’s behavior in terms of shear stress-strain curve, the CB4 panel has been analyzed with the use of the PARC_CL 2.0 in which different formulations for aggregate interlock have been implemented. Particular attention has been given to these 2 models:

1. The modified *Gambarova’s formulation*, explained in §3.1;
2. *aggregate size based shear retention factor*: the shear stiffness diminishes with the crack opening. It is assumed that aggregate interlock equals zero for crack opening width values higher than half the maximum aggregate size, d_{max} . The linear decay of the shear retention is defined in Eq.(50):

$$G_{cr} = \beta_{aggreg} \cdot G \tag{50}$$

where

$$\beta_{aggreg} = 1 - (2 / d_{max}) \cdot \varepsilon_n \cdot a_m$$

being ε_n the crack strain values (which are the plastic part of the maximum principal strain values).

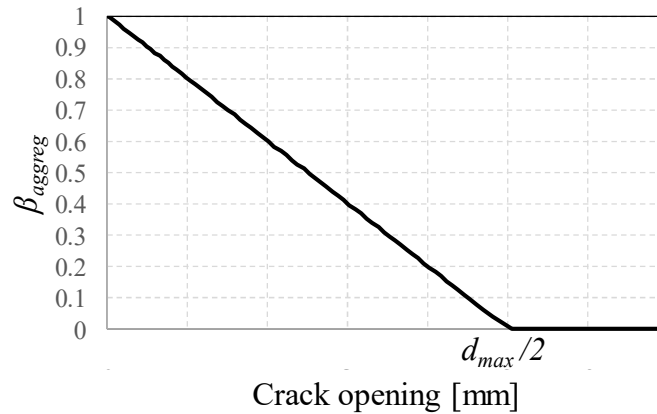


Figure 64. Variation of the aggregate size based shear retention factor with the crack opening.

Differently to the aggregate interlock formulation proposed by Gambarova and implemented in the PARC_CL 2.0 model, the aggregate size based shear retention factor depend only to the crack opening w and not to the crack sliding v . Furthermore, as shown in **Figure 65**, only the NLFEA with the Gambarova’s formulation is able to catch thereal envelope of the shear stress-strain curve.

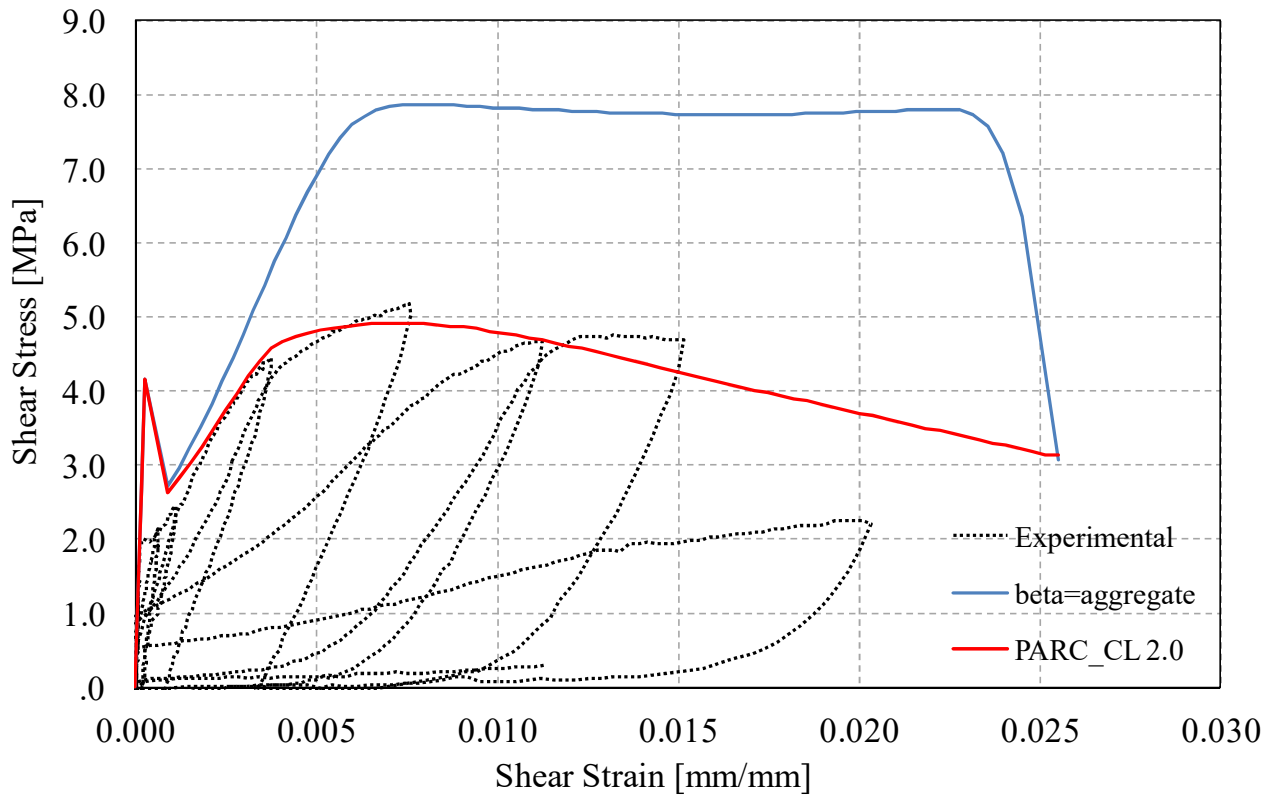


Figure 65. Shear-stress versus shear-strain curves for panel CB4 in the ij -system: comparison between experimental results and PARC_CL 2.0 results obtain with different aggregate interlock formulations.

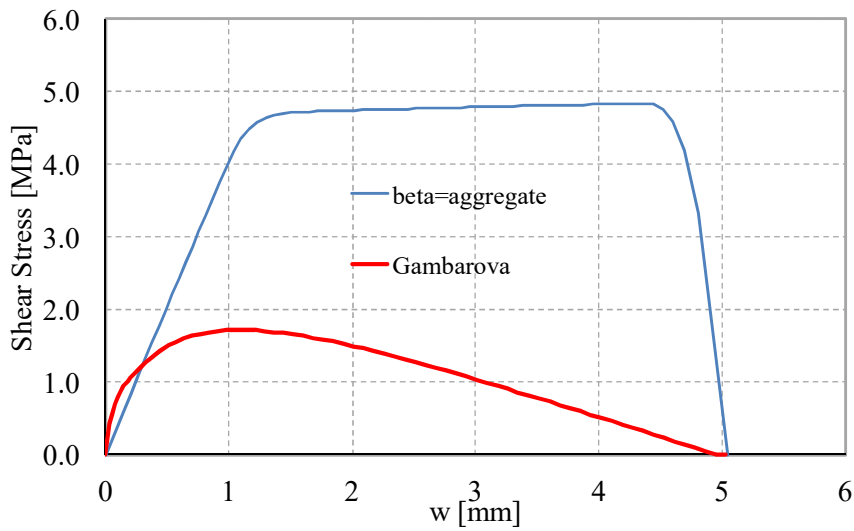


Figure 66. Shear stress vs crack opening for panel CB4 and different constitutive laws.

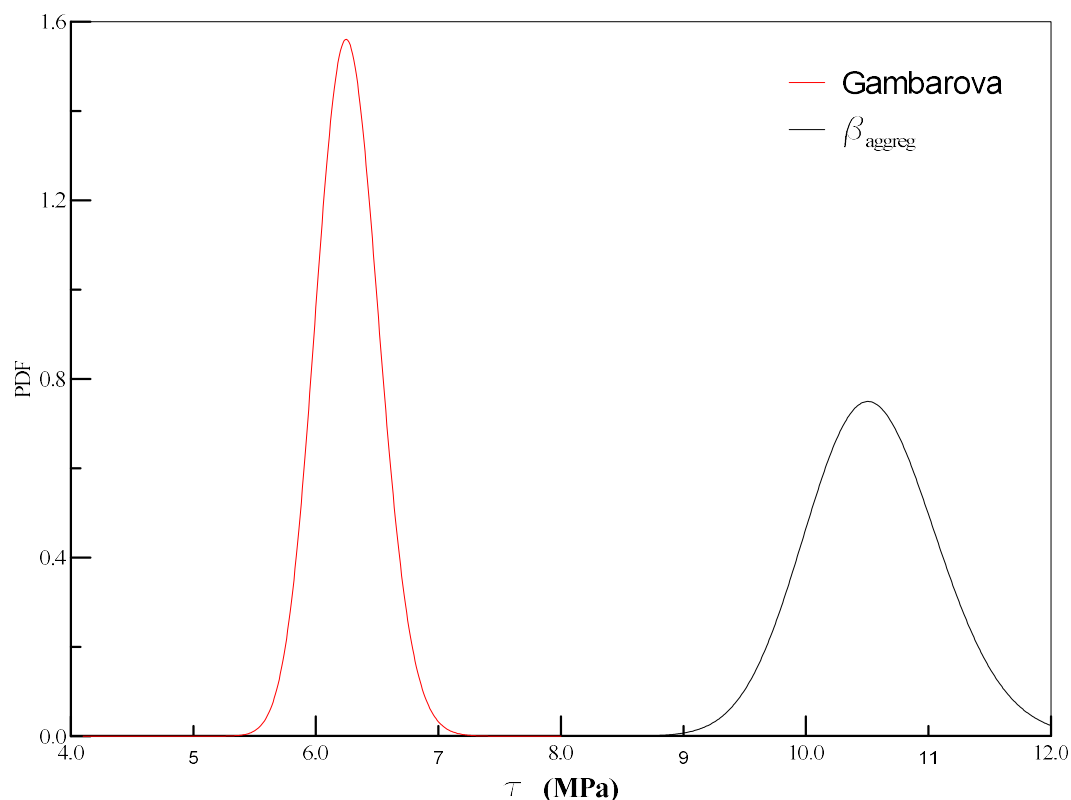


Figure 67. Probabilistic structural responses of the CB4 panel, by using different aggregate-interlock model

As one can see from **Figure 67** the response of the CB4 using β_{aggreg} model leads both to an higher covariance and mean value, rather than the same curve obtained by using Gambarova's formulation. For this reason, the design resistance obtained with Gambarova's formulation is more conservative and realistic.

On the other hand, as shown in **Figure 68**, the change of the aggregate-interlocking model, provides a change of the leading parameter. By using Gambarova's formulation, the leading parameter is the tensile strength while with the other one model the leading parameter seems to be compressive strength. This could be justified by observing **Figure 66**: with the Gambarova's formulation, the shear stress is dependent by the crack opening (which is dependent by the tensile strength by means of the stiffness) from the start to the end of the analysis. Otherwise, with the β_{aggreg} model, the shear stress is dependent by the crack opening only for the initial values of crack opening; after this moment an horizontal plateau can be observed. This could mean that with the Gambarova's formulation there is an higher dependence by the crack opening (i.e. by the tensile strength) rather than with the β_{aggreg} model.

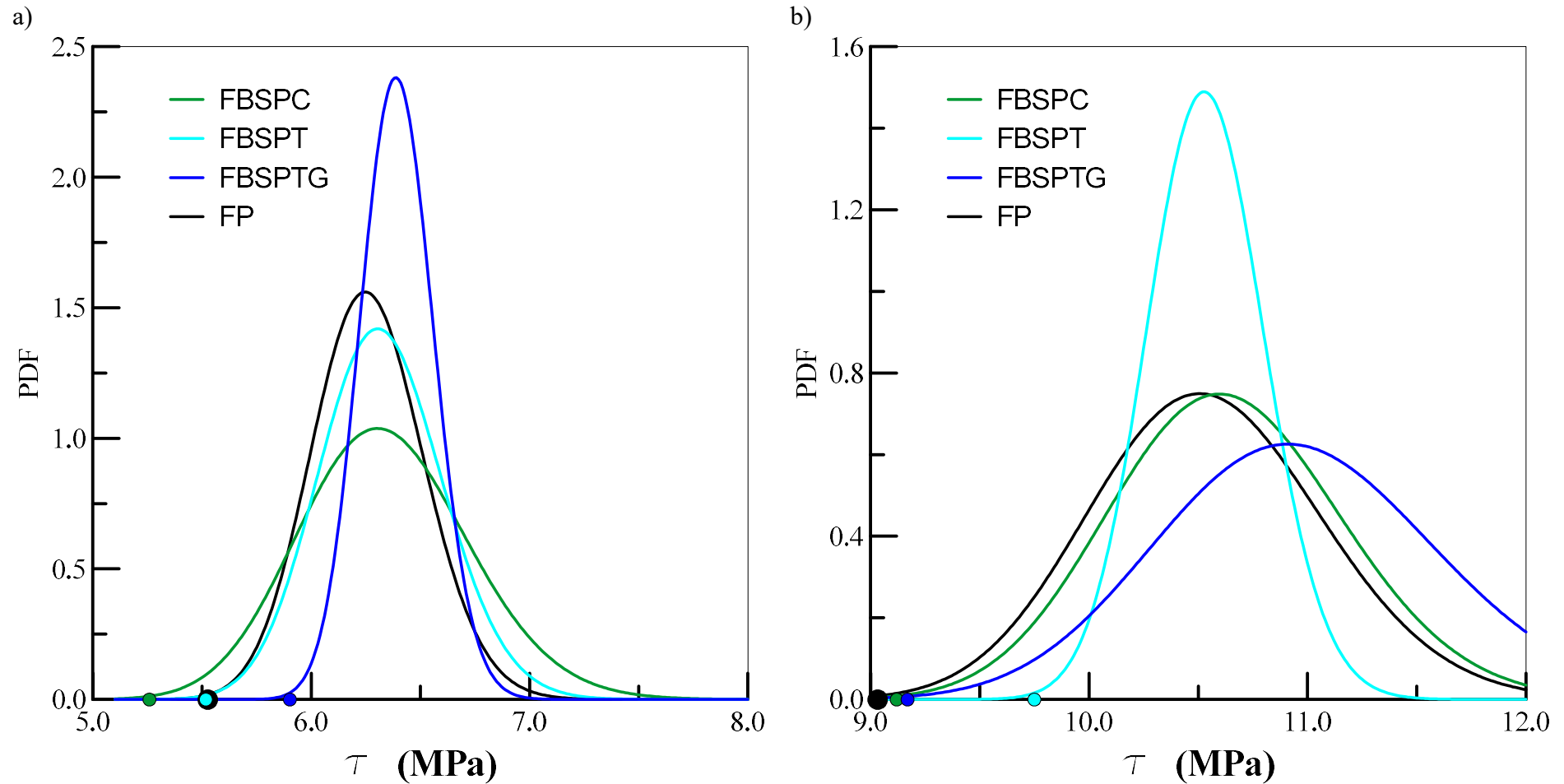


Figure 68. Different structural responses by using FBSP with different leading parameters and comparison with FB response, for the same panel (CB4) using different aggregate-interlocking model: a) Gambarova; b) Aggregate sized based shear retention factor

10. CONCLUSION

In this Master Thesis, a new probabilistic method to evaluate the design resistance of a structural element has been proposed. For the analyzed T-shaped prestressed girder, FBSP leads to a design resistance higher than the PSF one which is more conservative, but lower than the design resistance obtained by FP. This aspect shows that this new method is certainly conservative, while the other probabilistic simplified method proposed by codes (ECOV) leads to an overestimation of the design resistance. For this particular problem, by making a comparison with the FP safety format could be concluded that:

- a) FBSPT leads to an underestimate of the design resistance;
- b) FBSPG leads to an overestimate of the design resistance;
- c) FBSPC leads to a design resistance more close to the FP design resistance;

Particular attention should be given to the computational effort of this evaluation. The FBSP with only seven non-linear analyses, is able to reach almost the same design resistance obtained by FP which requires a greater number of analyses. However with this method an increase of designer's responsibility occurs. Specifically, it is important to highlight that the obtained result could not be generalized yet to all the structural problem occurring in the practical applications. Indeed the leading parameter is not a prefixed parameter but depends by the failure mechanism of the analyzed structural element and also by the adopted model to describe the physical problem.

This aspect, has been partially shown in this Master Thesis by means of the study about the probabilistic responses of different RC panels. In particular, from the latter study could be demonstrated that:

- 1) Panel CA2: The prediction is a shear failure mechanism provided by the achievement of the yielding stress of the steel. According to this fact, FBSP by using f_{ys} leading parameter, leads to a design resistance close to the FP. The fact that also FBSPC leads to a design resistance close to the FP, even if compressive strength should not be a parameter governing the response of this panel, could be provided by the low covariance assumed by f_{ys} . On the other hand, by changing the 7 samples, the values of f_{ys} are almost the same.

2) Panel CA4: the prediction is a shear failure mechanism provided by crushing of concrete due to the achievement of the compressive strength; for this reason, the mechanical parameter governing the response of this panel should be compressive strength. However, design resistance closer to the FP have been obtained by using (a) yielding of steel and (b) tensile strength leading parameters. Otherwise FBSPC leads to a design resistance far from the FP even if conservative. This apparently fail of the method could be justified with this observations:

- (a) As one can see from the FP τ - γ curves, with some samples (corresponding to high values of the concrete properties), the failure occurs after the yielding of steel;
- (b) PARC_CL 2.0 provides a reduction of the compressive strength to take into account the biaxial stress state; this reduction is made by adopting a coefficient β (see PARC) which is also dependent by tensile strength.

3) Panel CB4: the prediction is a shear failure mechanism provided by crushing of concrete due to aggregate-interlocking, like the analyzed prestressed girder; in this case tensile strength seems to be the leading parameter while compressive strength leads to a lower value of the design resistance. As seen, the opposite behavior is shown from the girder. This could be justified by the presence of the precompression force which could lead to an increase of compressive strength dependence (because of the loss of prestressing force).

For this panel is also shown that by analyzing the same structural element using a different model for the aggregate-interlock, there is a change of the leading parameter and also of the design resistance. The use of Gambarova's formulation (implemented in PARC) leads to a conservative design resistance; furthermore this formulation is able to catch the experimental results better than the others aggregate-interlock formulations.

The FBSP in its standard version requires the knowledge of all the experimental PDF of the basic variables describing the problem. These curves for the concrete mechanical parameters are difficult to obtain; in this case, an alternative version of FBSP has been proposed. The FBSP based on Model Code information (FBSP_{MC}) leads to inappropriate design resistance and shows that correlations provided by codes are inconsistent. In particular, the inverse use of these correlations is not recommendable. Specifically:

- a) FBSPC_{MC} leads to an overestimate of the design resistance;
- b) FBSP_{MC} leads to unrealistic design resistance (very low due to high covariance);
- c) FBSPG_{MC} cannot be applied;

From all this aspect it is important to conclude and highlight that a designer should have both a detailed description of the structure which should be designed and the adopted model to describe it. In particular, to correctly apply FBSP, the failure mechanism of the structural element and also the mechanical properties mainly influencing the type of this failure mechanism should be known, otherwise the FP is recommended.

Although in this research topics were treated in an extensive way, further studies should be led. In particular:

- 1) The same study should be repeated by changing the input PDFs of the mechanical parameters, to evaluate effects of these in the design resistance evaluation;
- 2) Probabilistic analysis of the CA4 panel without the reduction of compressive strength due to the presence of biaxial stress state;
- 3) Probabilistic analysis of the CB4 panel by using different aggregate-interlock models;
- 4) Analysis of the same T-shaped girder treated in this Master Thesis, without precompression force, to evaluate if it provides effect on the failure mechanism;
- 5) Investigation of more structural elements to obtain a wide range of results and try to generalize the FBSP;

11. REFERENCES

- [1] A. Strauss , S. Hoffmann , R. Wendner & K. Bergmeister (2009) Structural assessment and reliability analysis for existing engineering structures, applications for real structures, *Structure and Infrastructure Engineering: Maintenance, Management, Life-Cycle Design and Performance*, 5:4, 277-286.
- [2] A. Strauss, T. Zimmermann*, D. Lehký, D. Novák, Z. Keršner. (2014), Stochastic fracture-mechanical parameters for the performance-based design of concrete structures. *Structural Concrete*
- [3] Abaqus 6.12. User's and theory manuals; 2012 <<http://www.3ds.com/>> [1 June 2016].
- [4] Bažant, Z. P., Becq-Giraudon, E.: Statistical prediction of fracture parameters of concrete and implications for choice of testing standard. *Cement and Concrete Research*, 2002, vol. 32, pp. 529–556.
- [5] Belletti B, Esposito R, Walraven J. Shear capacity of normal, lightweight, and high-strength concrete beams according to ModelCode 2010. II: experimental results versus nonlinear finite element program results. *ASCE J Struct Eng* 2013
- [6] Belletti B, Scolari M., Vecchi F. , 'NLFEA of reinforced concrete shear walls under cyclic loading by means of PARC_CL2.0 crack model', 21-23 November 2016, fib Symposium, Cape Town.
- [7] Belletti B, Scolari M., Vecchi F., PARC_CL 2.0 crack model for NLFEA of reinforced concrete structures under cyclic loadings, *Computers and Structures* (2017)
- [8] Belletti, B., Damoni, C., den Uijl JA, Hendriks, MAM, Walraven, JC. Shear resistance evaluation of prestressed concrete bridge beams: fib Model Code 2010 guidelines for level IV approximations. *Struct Concr* 2013
- [9] C. C. Hurd. 1985. A note on early Monte Carlo computations and scientific meetings. *Annals of the History of Computing* 7:141–155.
- [10] Cervenka, V., Cervenka, J., Pukl, R. (2007). Safety assessment in fracture analysis of concrete structures. *Proceedings of the 6th International Conference on Fracture Mechanics of Concrete and Concrete Structures, Volume 2, Pages 1043-1049.*
- [11] Comité Euro-International du Béton and Fédération Internationale de la Précontrainte (CEB-FIP). (1993). CEB-FIP Model Code 1990 (MC90), Bulletin d'information 213 and 214, Thomas Telford, London
- [12] EN 1990, Eurocode 0: Basis of structural design
- [13] EN 1990, Eurocode 2: Design of concrete structures
- [14] Fib – International Federation for Structural Concrete, (2013). *fib Model Code for Concrete Structures 2010*. Berlin: Verlag Ernst & Sohn.
- [15] Gambarova, P. G. (1983), "Sulla trasmissione del taglio in elementi bidimensionali piani di c.a. fessurati.", *Proc., Giornate AICAP*, 141–156 (in Italian).
- [16] Gomes A. , Appleton J., "Nonlinear cyclic stress-strain relationship of reinforcing bars including buckling", *Engng. Struct.* 19(10) 1997 822-826
- [17] Hasofer AM, Lind NC. Exact and invariant second-moment code format. *J Eng Mech ASCE* 1974;100(EM1)(1):111–21.
- [18] He W., Wu Y-F., Liew K.M. (2008), "A fracture energy based constitutive model for the analysis of reinforced concrete structures under cyclic loading. *Computational methods in applied mechanics engineering*", 197 pp. 4745–4762.
- [19] Hendriks MAN, Uijl JA, De Boer A, Feenstra PH, Belletti B, Damoni C. Guidelines for nonlinear finite element analyses of concrete structures. *Rijkswaterstaat Technisch Document (RTD), Rijkswaterstaat Centre for Infrastructure, RTD 2012;1016:2012.*
- [20] Huntington DE, Lyrantzis CS. Improvements to and limitations of Latin Hypercube Sampling. *Probab Eng Mech* 1998;13(4):245–53.
- [21] Iman RC, Conover WJ. A distribution free approach to inducing rank correlation among input variables. *Commun Stat* 1982;B11:311–34.
- [22] Iman, R. C., and Conover, W. J. _1980_. "Small sample sensitivity analysis techniques for computer models with an application to risk assessment." *Commun. Stat: Theory Meth.*, A9_17_, 1749–1842.

REFERENCES

- [23] Keramat M, Kielbasa R. Efficient average quality index of estimation of integrated circuits by modified Latin Hypercube Sampling Monte Carlo (MLHSMC). In: Proc of IEEE symp on circuits and systems, Hong Kong; 1997.
- [24] Madsen HO, Krenk S, Lind N. Methods of structural safety. Englewood Cliffs: Prentice Hall; 1986.
- [25] Mansour M., Thomas T. C. Hsu², Behavior of Reinforced Concrete Elements under Cyclic Shear. I: Experiments, Journal of Structural Engineering (2005)
- [26] Menegotto M., and Pinto, P.E. (1973). "Method of analysis for cyclically loaded R.C. plane frames including changes in geometry and non-elastic behaviour of elements under combined normal force and bending, Symposium on the Resistance and Ultimate Deformability of Structures Acted on by Well Defined Repeated Loads", International Association for Bridge and Structural Engineering, (ABSE) Lisbon, Portugal.
- [27] N. Metropolis and S. Ulam. 1949. The Monte Carlo method. *Journal of the American Statistical association* 44:335-341.
- [28] Nakamura, H., Higai, T., "Compressive Fracture Energy and Fracture Zone Length of Concrete", Benson P. Shing (editor), ASCE, 2001, 471-487.
- [29] Nakamura, H., Higai, T., "Compressive Fracture Energy and Fracture Zone Length of Concrete", Benson P. Shing (editor), ASCE, 2001, 471-487.
- [30] Nova' k, D., Teply' , B. and Kers'ner, Z., (1998). The role of Latin hypercube sampling method in reliability engineering, in Proceedings of ICOSSAR- 97, Kyoto, Japan, 1998, pp. 403 – 409.
- [31] Novák, D. &Lehký, D. (2006). "ANN Inverse Analysis Based on Stochastic Small-Sample Training Set Simulation", *Engineering Applications of Artificial Intelligence*, Vol. 19, 731-740.
- [32] Novák, D., Rusina, R., and Vořechovský, M. _2003_. "Small-sample statistical analysis—Software FREET." *Proc., 9th Int. Conf. on Applications of Statistics and Probability in Civil Engineering (ICASP9)*, Rotterdam Millpress, San Francisco, Calif., 91–96.
- [33] Novák, D., Vořechovský, M. and Teplý, B. (2014) FReET: Software for the statistical and reliability analysis of engineering problems and FReET-D: Degradation module. *Advances in Engineering Software*, 72, pp. 179-192.
- [34] Novak, D., Vorechovsky, M., Teply, B., (2007). Software for the statistical and reliability analysis of engineering problems and FReET-D: Degradation module. *Advances in Engineering Software (Elsevier)*, 72, 179-192.
- [35] Novák, D., Vořechovský, M., Lehký, D., Bergmeister, K., Pukl, R. & _ervenka, V. (2007). "Stochastic nonlinear analysis of concrete structures - Part I: From simulation of experiment and parameters identification to reliability assessment." In *10th Int. Conf. on Applications of Statistics and Probability in Civil Engineering – ICASP10*, Tokyo, Japan.
- [36] Owen AB. Controlling correlations in Latin Hypercube Samples. *J Am Stat Assoc (Theory and methods)* 1994;89(428):1517–22.
- [37] Roy A., Robuschi S., Hendriks M.A.N., Belletti B. 2016. Safety assessment of existing reinforced concrete beams using probabilistic methods at different levels. *Key Engineering Materials Volume 711, Pages 958-965 - 8th International Conference on Concrete under Severe Conditions - Environment and Loading*, Lecco, Italy, 12-14 September.
- [38] Strauss, A., Bergmeister, K., Hoffmann, S., Pukl, R. and Novak, D., Advanced life-cycle analysis of existing concrete bridges. *ASCE Journal of Materials in Civil Engineering*, 2007.
- [39] Strauss, A., Krug, B., Slowik, O., Novak, D., (2017). Combined shear and flexure performance of prestressing concrete T-shaped beams: Experiment and deterministic modeling. *Structural Concrete*, 1-20.
- [40] Vecchio F.J. and Collins M.P. (1993), "Compression Response of Cracked Reinforced Concrete", *ASCE Journal of Structural Engineering*, 119(12):3590-3610.
- [41] Vor'echovsky' M, Novak D. Correlation control in small sample Monte Carlo type simulations I: A Simulated Annealing approach. *Probab Eng Mech* 2009;24(3):452–62.
- [42] Vor'echovsky' M. Hierarchical Subset Latin Hypercube Sampling for correlated random vectors. In: Topping and Tsompanakis (Eds.), *Proceedings of the first international conference on soft computing*

REFERENCES

technology in civil, structural and environmental engineering, held in Madeira, Portugal. Civil-Comp Proceedings: 92. Stirlingshire, Scotland: Civil-Comp Press; 2009. 17 pages, CD-ROM.

REFERENCES
